Nonsmooth Bifurcations and the Role of Density Dependence in a Chaotic Infectious Disease Model

Ryan Patrick Hughes

Thesis submitted to the Faculty of the
Virginia Polytechnic Institute and State University
in partial fulfillment of the requirements for the degree of

Master of Science
in
Mathematics

Lauren M. Childs, Chair
Julie C. Blackwood
Mihaela S. Ciupe

December 13, 2019
Blacksburg, Virginia

Keywords: Bifurcation, Local Asymptotic Stability, Liapunov Exponent, Chaos

Nonsmooth Bifurcations and the Role of Density Dependence in a Chaotic Infectious Disease Model

Ryan Patrick Hughes

(ACADEMIC ABSTRACT)

Discrete dynamical systems can exhibit rich and interesting dynamics at lower dimensions (and co-dimensions) than that of ODE models [1]. Classically, the minimal dimension to observe chaotic behavior in an ODE model is three; whereas it can be achieved in a one-dimensional discrete map [1, 2]. It is often the choice of mathematical biologists to use discrete systems as it fills many roles such as sparse data, incorporation of life cycle stages and noisy measurements [3]. This work is analyzes a discrete time model of an infected salmon population [4]. It provides an in-depth analysis of non-smooth bifurcations for alternate functional forms for density dependence in the growth function of a given model. These demonstrate interesting structures and chaotic behaviors with biologically feasible interpretations such as intrinsic growth rate and probability of death. The choice of density dependence function, as well as parameterization, leads to whether chaos occurs or not.

Nonsmooth Bifurcations and the Role of Density Dependence in a Chaotic Infectious Disease Model

Ryan Patrick Hughes

(GENERAL AUDIENCE ABSTRACT)

Often times biological processes do not happen in a continuous streamlined chain of events. We observe discrete life stages, ages, and morphological differences. Similarly, data is generally collected in discrete (and often fixed) time intervals. This work focuses on the role that population density has on the behavior of these systems. We dive into a case study for a viral infection in a salmon population. We show chaotic behavior can be observed as low as a single dimension model and discuss the biological implications. Additionally, we show that the choice of density dependence in a given infectious disease model directly impacts disease dynamics and can allow or prohibit chaotic behavior.

Dedication

To Chaos...

Acknowledgments

I would like to take the time here to thank the three women on my committee: Lauren Childs, Stanca Ciupe and Julie Blackwood. Each of the three have provided insightful and critical comments to make this thesis a better research body, aided with clarity of my presentation/writing, and general editing of mathematical topics. Without their support this thesis would not be where it is. I would also like to thank Leah Johnson for the extremely useful comment about the colorblind scale for my heatmaps which I've included here. Additionally, I would like to thank everyone in the joint lab meeting who listened to my defense and gave helpful feedback.

I would like to thank my parents, friends, and family for continuing to support me through graduate school. I would like to thank Lauren Berman for continually supporting me as I wrote this thesis; her support was invaluable.

Lastly, I would like to take the time to again thank Lauren Childs. Lauren worked tirelessly on providing critical comments every step of the way; whether it be code, writing or presenting. She took the time to meet with me (some weeks even three times) to discuss current topics and future directions. I am *extremely* appreciative of the time and effort she has put in to helping me prepare this thesis. I am also appreciative of everything she has helped me with beyond the scope of this thesis, much of which will help me in my career in the near future.

Contents

List of Figures

List of Tables

Chapter 1

Introduction and Preliminaries

1.1 Discrete Models in Biology

1.1.1 Introduction

Mathematical modeling is a critical concept with a variety of applications that have allowed us to predict weather, sports games, biological processes; and much more [1]. Mathematicians previously were bound to closed form analytic expressions for ordinary and discrete dynamical systems (or weak families of solutions for partial differential equations); the advancement in computing has led to numerical and heuristic approaches about systems previously untouchable [3, 4, 5, 6]. Additionally, extensive work has been put into solving for closed form/analytic expressions with software (Mathematica/Maple/Matlab).

Discrete models arise naturally in biology, namely in cases when there is a lack of data, or rather a lack of continuous data. For example, one area of active research involves the use of discrete models for dynamical systems in which continuous data is unavailable or unrealistic. In addition to lack of continuous data, discrete models are also natural for situations in which organisms have fixed life stages or cycles. Rarely do organism undergo morphological changes in a continuous stream of events. On the other hand, due to cost factors or experimental complications, data is sometimes collected as infrequently as once a year depending on the situation [7, 8, 9].

1.1.2 Classical Examples

In many introductory ordinary differential equations or mathematical biology classes the continuous logistic growth model is a vital tool for modeling population dynamics. It the continuous form, it follows a sigmoidal shape and accounts for density dependence by limiting

the growth of the population to a carrying capacity, often denoted K which represents the maximum population biologically feasible or allowable for a particular environment [10, 11]. The population also has it's on intrinsic growth rate, often denoted r which represents how the population grows on its own.

The discrete version of the logistic growth model, often referred to as the logistic map for short, rather than bounding the population by a given carrying capacity, examines the population as a function of the population at previous time steps (iterations). Often, the carrying capacity is normalized to be 1. Below we introduce the map and highlight key historical results pertaining to it.

The logistic map is particularly interesting from a mathematical perspective as it exhibits chaotic behavior. Moreover, this occurs for a one-dimensional system as opposed to three dimensional continuous systems that exhibit chaotic behavior [2, 12, 13]. We define chaos rigorously in later sections (Section 1.2.3).

For now, we introduce the logistic map as:

$$x_{n+1} = f(x_n) = rx_n(1 - x_n), \tag{1.1}$$

where x_n is the population, $x_n \in (0, 1)$ and r is the intrinsic (per capita) growth rate. Typically we assume that $r \in [0, 4]$ as $r > 4$ leads to negative values of x_n which is not biologically relevant. An example of a stable scenario, $r = 1.4$, and a chaotic scenario, $r = 3.9$, are shown in Figure 1.1.

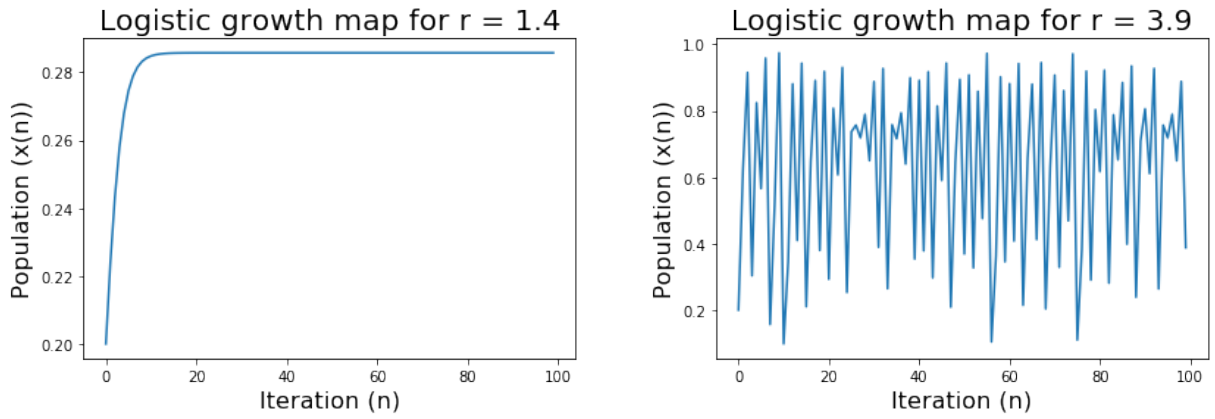

(a) A stable fixed point.

(b) A chaotic scenario.

Figure 1.1: The discrete logistic growth map over 100 iterations for $r = 1.4$ and $r = 3.9$. The former was shown to be an example of the map tending to a single stable fixed point and the latter of the map exhibiting chaotic behavior.

For the logistic map, we compute the fixed point and its stability directly. Knowing that a

fixed point is given by $x_{n+1} = x_n - x^*$ we obtain:

$$x^* = rx^*(1 - x^*), \tag{1.2}$$

The trivial solution that satisfies Equation 1.2 is given by $x^* = 0$. The nontrivial solution can be solved via:

$$\begin{aligned} & x^* = rx^*(1 - x^*) \\ \iff & 1 = r - rx^* \\ \iff & x^* = \frac{r-1}{r}, \end{aligned} \tag{1.3}$$

which is entirely dependent on the growth parameter r.

Local asymptotic stability is an important measure of end behavior in both discrete and continuous dynamical systems [14]. We compute this directly for the logistic map by analyzing

$$f'(x^*) = r(1 - 2x^*).$$

The stability of the trivial fixed point is given as:

$$f'(0) = r,$$

which we know is stable if:

$$\begin{aligned} \iff & |f'(0)| < 1 \\ \iff & |r| < 1. \end{aligned}$$

However, the intrinsic growth rate is assumed to be non-negative, which leads us with the condition that the trivial fixed point is stable if:

$$0 \leq r < 1. \tag{1.4}$$

Now, for the nontrivial fixed point, we see that stability criterion follows from:

$$\begin{aligned} \iff & \left| f'\left(\frac{r-1}{r}\right) \right| < 1 \\ \iff & \left| r\left(1 - 2 \cdot \frac{r-1}{r}\right) \right| < 1 \\ \iff & |2 - r| < 1 \\ \iff & 1 < r < 3. \end{aligned} \tag{1.5}$$

Hence, at $r = 1$, the fixed points $x^* = 0$ and $x^* = \frac{r-1}{r}$ swap stability through a transcritical bifurcation. This has been extensively studied with a variety of applications and important

theoretical contributions [2, 12, 13, 14, 15, 6]. The transcritical bifurcation for the logistic map is demonstrated numerically in Figure 1.2. In particular, the transcritical bifurcation observed in the logistic map shows that the stable (solid) branch of the trivial fixed point along the x-axis lose stability at $r = 1$ and become unstable (dashed line along the x-axis). The nontrivial fixed point is given by the convex curve which is locally asymptotically stable in the region provided by Equation 1.5.

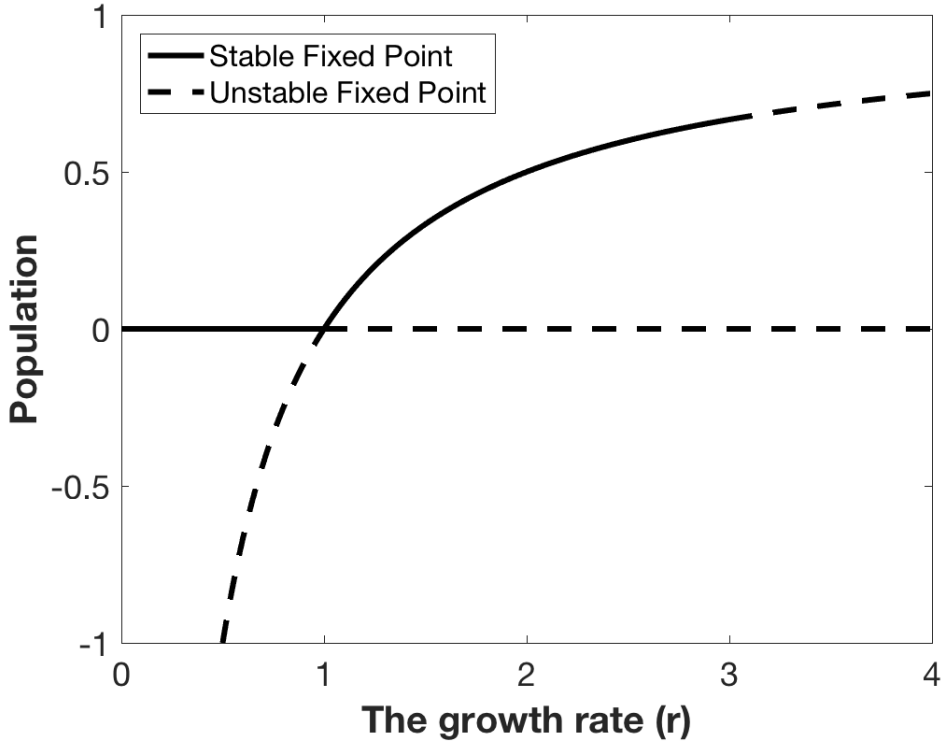

Figure 1.2: Stability of the nontrivial fixed point of the logistic map. We observe a transcritical bifurcation for the single bifurcation parameter r as its varied between $r \in [0, 4]$.

A much more in depth analysis and definition of bifurcations will be provided in Section 1.2. Additionally Chapters 4 and 5 provides in depth numerical examples for a specific infectious disease model introduced in Chapter 3.

1.2 Bifurcation Analysis

1.2.1 Bifurcation Definition

A common problem of ordinary differential equations (ODEs) is analyzing the behavior of:

$$\frac{d\vec{x}}{dt} = \vec{F}(\vec{x}, \vec{\alpha}) \tag{1.6}$$

where $\vec{\alpha}$ is a vector of parameters for the system. Classically, bifurcation analysis involved fixing n number of parameters and varying $m < n$ other parameters, to gain a high level understanding of qualitative changes in dynamical behavior. The process is similar for discrete dynamical systems. However as mentioned previously, interesting behavior can happen in one-dimensional systems [2].

1.2.2 Bifurcations in the Logistic Map

We recall from earlier that the logistic map given by

$$x_{n+1} = rx_n(1 - x_n), \tag{1.7}$$

has been shown to have fixed points at $x^* = 0$ and $x^* = 1 - \frac{1}{r}$. In Section 1.1.2, we derived stability conditions for each of the fixed points and produced a plot that exhibits the stability of each as we vary the single bifurcation parameter r. In this section, we numerically examine long term dynamics that demonstrate chaotic behavior for various values of r.

In Figure 1.3, we simulate the dynamics of the logistic growth map for 1000 time steps and plot the last 500 time steps for $r \in [0, 4]$. Effectively we are analyzing the long term behavior for this model. We see the stable branch at $x = 0$ turn upward (i.e. the stable branch of $\frac{r-1}{r}$), and per Figure 1.2, we know this fixed point loses stability at $r = 3$. We observe a two-cycle (the two branches) until around $r = 3.5$ where we observe period doubling (a two-cycle becomes a four-cycle) which appears to cascade into chaotic behavior. Chaos is formally defined as sensitivity of initial conditions, i.e. two close initial conditions can spend arbitrarily long times apart and close together and mathematically characterized below in Section 1.2.3 [8, 2, 12, 15, 16, 17].

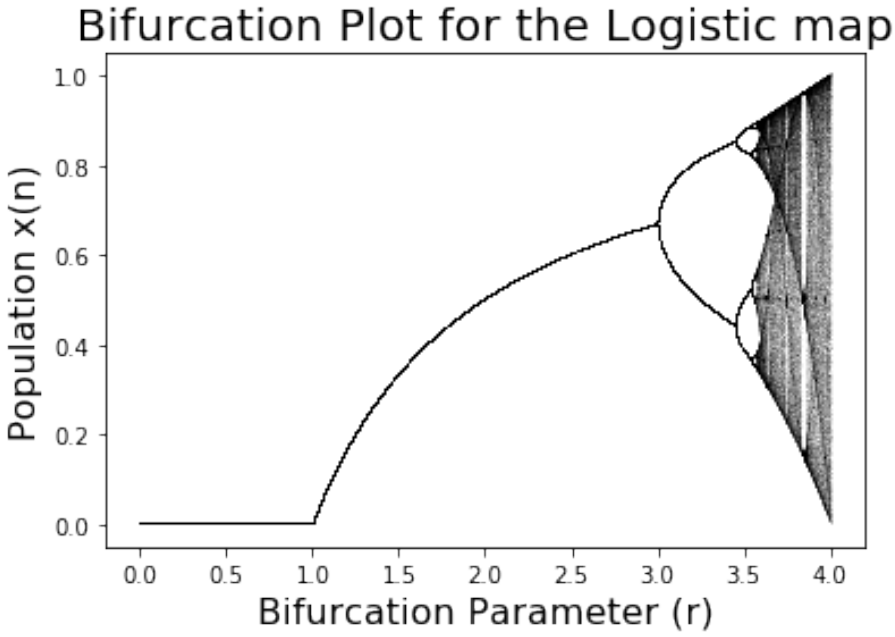

Figure 1.3: The bifurcation plot for the logistic growth map with r as the bifurcation parameter. This exhibits period doubling and cascades into what appears to be chaotic behavior.

1.2.3 Chaos and Liapunov Exponents

Liapunov exponents are a metric for analyzing behavior of a dynamical system. In particular, it has been shown that the Liapunov exponent can provide insight to true chaos in a dynamical system [8].

We take the definition of chaos from [8] as $f(\vec{x}_{t+1})$ or $\frac{d\vec{x}}{dt}$, produces bounded solutions for which $\forall x_0 \in \mathcal{D}(f)$, end behavior is not eventually periodic. For clarity, $\mathcal{D}(f)$ is the domain of the system and $f(\vec{x}_{t+1})$ and $\frac{d\vec{x}}{dt}$ represent discrete and continuous systems respectively.

Eventually periodic points obey the following conditions:

$$\exists p \neq 0, N \in \mathbb{Z} \text{ s.t. } f^{t+p}(x_0) = f^t(x_0), \ \forall t \geq N. \tag{1.8}$$

Hence if a map *does not* have points which are eventually periodic we cannot guarantee if two sequential points in time will be arbitrarily close or arbitrarily far away [8].

Next, we say a map $f : \mathcal{D}(f) \mapsto I$ has sensitive initial conditions if for a given initial condition x_0, $\exists \delta > 0$, $\exists \epsilon > 0$, and image (or solution) $y_0 \in I$ such that:

$$\begin{aligned} &|x_0 - y_0| < \epsilon \\ \implies &|f^k(x_0) - f^k(y_0)| > \delta, \end{aligned} \tag{1.9}$$

for some $k \in \mathbb{Z}$ [8]. The Liapunov exponent provides a method to calculate the sensitivity of initial conditions without analyzing the end behavior at every given point in time after transients are eliminated. We denote the Liapunov exponent for a given initial condition x_0 by $\lambda(x_0)$. The mathematical intuition behind Liapunov exponents is that it measures exponential separation of a function being applied to two close initial conditions (characterized above).

We define formally define the Liapunov exponent as:

$$\lambda(x_0) = \lim_{t\to\infty} \frac{1}{t} \left| \frac{df^t(x)}{dx}\Big|_{x=x_0} \right|,$$

where t denotes the iteration number of the map f. Now, observe that since $\frac{df^t(x_0)}{dx} = f'(x_0)f'(x_1)...f'(x_{t-1})$, we can use this to simplify the expression for the Liapunov exponent to be:

$$\lambda(x_0) = \frac{1}{t} \sum_{k=0}^{t-1} \ln |f'(x_k)|. \tag{1.10}$$

Thus we can formally say that if $\lambda(x_0) > 0$, there exists a sensitive initial condition $x_0 \in \mathcal{D}(f)$ which satisfy the definition of Equation 1.9. Although this does not prove every initial condition is sensitive (and thus behavior is chaotic) it sheds light on results observed numerically. With both of these concepts in mind, often times the Liapunov exponent can be bounded above or below for all initial conditions to show behavior is truly chaotic. We discuss this in Section 1.2.4.

The Liapunov Exponent for the Logistic Map

We calculate the Liapunov exponent for a fixed initial condition for the logistic growth map and observe how it changes based on the intrinsic growth rate r in the model. Recall that the logistic map is given by:

$$x_{n+1} = rx_n(1 - x_n),$$

from Equation 1.1 where r is the intrinsic growth rate. We saw in Figure 1.3 dynamical behavior that appears to be chaotic when $r > 3.8$. In Figure 1.4, we recreate the plot from [8], with $x_0 = 0.1$ and calculate the Liapunov exponent for $r \in [3, 4)$ for the logistic map.

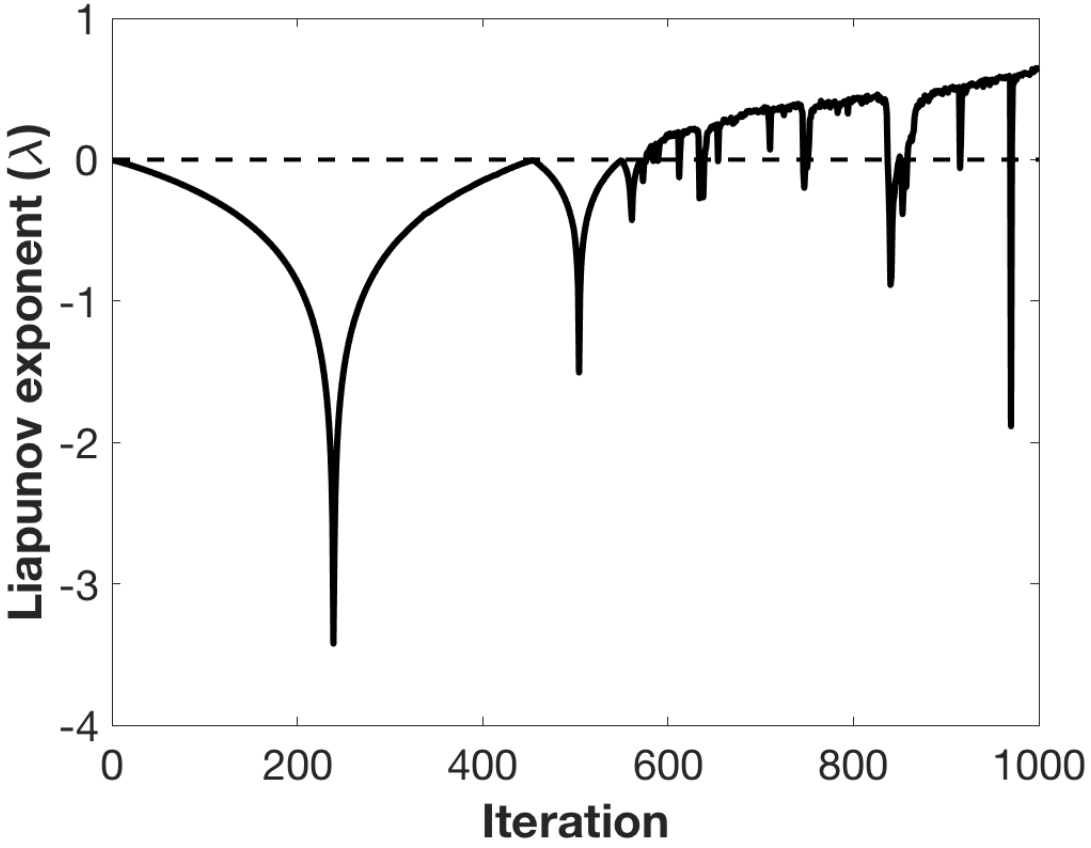

Figure 1.4: The Liapunov exponent for the logistic map for a fixed initial condition of $x_0 = 0.1$. The dashed line represents the horizontal axis, $x = 0$, which is the threshold for chaotic behavior as determined by the Liapunov exponent.

In particular, we take $r \in [3, 4)$ for 1000 iterations. We also note that the dotted line in Figure 1.4 refers to the horizontal axis of 0, i.e. above which the metric indicates chaotic behavior is occurring. We see that as the iteration number increases, potential chaotic behavior ensues, some periodic behavior observed for certain values of r (i.e. where $\lambda < 0$).

Although this particular example characterizes potential chaotic behavior for a fixed initial condition of $x_0 = 0.1$, we can say that the logistic map does exhibit chaotic behavior for $r > 3.56995$ [2, 12, 13]. Note that calculating the Liapunov exponent numerically for a fixed initial condition does not imply chaos, but can be indicative it is occurring.

1.2.4 Liapunov Exponents for Systems of Equations

In Section 1.2.3, we defined the Liapunov exponent as means to measure the sensitivity to initial conditions. This gave a metric for chaotic behavior. In the case of a single equation we saw that the Liapunov exponent is given by:

$$\lambda(x_0) = \frac{1}{t}\sum_{k=0}^{t-1} \ln|f'(x_k)|.$$

We can define the Liapunov exponent similarly for a system of discrete equations. We use the Jacobian and the spectral radius (largest eigenvalue in magnitude) to characterize this. For example, the two-dimensional system given by:

$$\begin{aligned} x_{t+1} &= f(x_t, y_t), \\ y_{t+1} &= g(x_t, y_t), \end{aligned}$$

has the Jacobian characterized by:

$$J(x,y) = \begin{bmatrix} \frac{\partial f}{\partial x} & \frac{\partial f}{\partial y} \\ \frac{\partial g}{\partial x} & \frac{\partial g}{\partial y} \end{bmatrix}.$$

Then we recall that the spectral radius, for a given fixed point (x^*, y^*) is given by:

$$\rho\big(J(x^*, y^*)\big) = \max_i |\lambda_i|,$$

where λ_i are the eigenvalues of the Jacobian evaluated at any point.

In the more general case of arbitrarily large systems, we take $J \in \mathbb{R}^{n\times n}$, and an initial condition to be given by: $(\vec{x}_0)$. The Liapunov exponent is for a system of discrete equations [8] is given by:

$$\lambda(\vec{x}_0) = \lim_{t\to\infty} \frac{1}{t} \ln\left[\rho\left(\prod_{k=0}^{t-1} J(\vec{x}_0)\right)\right]. \tag{1.11}$$

It is important to note here that in Equation 1.11, $x_0 \neq x^*$, i.e. we are evaluating the Jacobian at an initial condition (rather than the traditional fixed point analysis).

For example, in the case of the two-dimensional system, we see that the Liapunov exponent is given by:

$$\lambda(\vec{x}_0) = \lim_{t\to\infty} \frac{1}{t} \ln\left[\rho\left(\begin{bmatrix} f_x(x_t,y_t) & f_y(x_t,y_t) \\ g_x(x_t,y_t) & g_y(x_t,y_t) \end{bmatrix} \ldots \begin{bmatrix} f_x(x_0,y_0) & f_y(x_0,y_0) \\ g_x(x_0,y_0) & g_y(x_0,y_0) \end{bmatrix}\right)\right] \tag{1.12}$$

where $f_{x,y}(x_t, y_t)$ and $g_{x,y}(x_t, y_t)$ are the respective partial derivatives evaluated at the current time step.

1.2.5 Bounds on the Liapunov Exponent for Systems

It is not always analytically feasible or possible to calculate the Liapunov exponent for an initial condition depending on the characteristics of the system. It has been shown that any matrix norm induced by a vector norm is an upper bound for the spectral radius [5]. We provide two common norms here as they will be useful in later sections for providing bounds on the spectral radius of various systems.

Mathematically, we know that for any matrix norm that bounds the spectral radius can be expressed as:

$$\rho(J) \leq ||J||, \tag{1.13}$$

where $||\cdot||$ is defined below [5]. Two particular norms of interest are the L_1 and L_∞ norms. They are defined as:

$$||J||_1 = \sup_{1\leq j\leq n} \sum_{i=1}^{m} |a_{ij}|, \tag{1.14}$$

$$||J||_\infty = \sup_{1\leq i\leq n} \sum_{j=1}^{n} |a_{ij}|. \tag{1.15}$$

First, note the similarity of definitions for each of the norms, though the indices in the sum and supremum are critical in providing the exact definitions. Additionally, we use the supremum here, though in the biological world we are loose and can substitute this with the maximum (as in general they are not necessarily the same) [5].

1.3 The Basic Reproductive Number

A key point of interest in dynamical systems analysis is examining which parameters influence qualitative changes in behavior of a system. In the realm of infectious disease modeling, a metric known as the basic reproductive number (often denoted R_0) can be calculated in terms of other parameters [18]. R_0 represents the average number of infected cases a single average infectious individual will generate throughout their infectious period in a fully susceptible population. In other words, it is a metric for whether and how quickly an infectious disease can spread throughout a population [18, 19, 20, 21, 4, 22].

The threshold of $R_0 = 1$ is a tipping point at which an infection begins to spread as opposed to $R_0 < 1$ in which the infection will die out. Mathematically, $R_0 < 1$ is typically associated with the Disease Free Equilibrium (denoted DFE), or the system in the absence of infection, being locally asymptotically stable. On the contrary, $R_0 > 1$ is associated with the DFE being unstable [18, 19, 20, 21, 4, 22]. In more complicated systems, which exhibit bistability, an endemic state can persist even while the DFE is stable. Often times in models with

multiple compartments it is not immediately clear how to solve for a closed form expression for R_0 from the stability analysis.

1.3.1 Next Generation Matrix Method in ODEs

The Next Generation Matrix Method is one method for calculating the basic reproductive number [20, 23]. The Next Generation Matrix Method works by segmenting the entire population of individuals into compartments by infection status.

Here, we review the Next Generation Matrix Method with a system of ordinary differential equations. We denote X as the compartments of the model that are infected and Y as the compartments of the model not infected. We write the following equation as:

$$\frac{dX}{dt} = \mathcal{F}(X,Y) - \mathcal{G}(X,Y),$$
$$\frac{dY}{dt} = \mathcal{H}(X,Y)$$

where $\mathcal{F}(X,Y)$ is the entrance of new infections to the system, and $\mathcal{G}(X,Y)$ is all transitions apart from new infections. We take $\mathcal{H}(X,Y)$ as all transitions of non-infecteds in the model. Note that the DFE is given by $(\vec{0},\overline{Y})$ where $\overline{Y} \in \mathbb{R}^n$ in general. Thus $F(\vec{0},\overline{Y}) = G(\vec{0},\overline{Y}) = \vec{0}$ [20, 23]. Thus, we can see that:

$$D\mathcal{F}\big|_{(\vec{0},\overline{Y})} = \left[\frac{\partial \mathcal{F}}{\partial X} \quad \frac{\partial \mathcal{F}}{\partial Y}\right]\Bigg|_{(\vec{0},\overline{Y})},$$
$$D\mathcal{G}\big|_{(\vec{0},\overline{Y})} = \left[\frac{\partial \mathcal{G}}{\partial X} \quad \frac{\partial \mathcal{G}}{\partial Y}\right]\Bigg|_{(\vec{0},\overline{Y})},$$

where $D\mathcal{F}\big|_{(\vec{0},\overline{Y})}$ and $D\mathcal{G}\big|_{(\vec{0},\overline{Y})}$ denote the Jacobians of $\mathcal{F}(X,Y)$ and $G(X,Y)$ evaluated at the Disease Free Equilibrium. The Next Generation Matrix Method shows taking the matrices

$$\tilde{F} = D\mathcal{F}\big|_{(\vec{0},\overline{Y})},$$
$$\tilde{G} = D\mathcal{G}\big|_{(\vec{0},\overline{Y})},$$

the basic reproductive number R_0 is given by the spectral radius, i.e. largest (in magnitude) eigenvalue of $\tilde{F}\tilde{G}^{-1}$ [4, 24]. Hence,

$$R_0 = \rho(\tilde{F}\tilde{G}^{-1})$$

where ρ denotes the spectral radius [20, 23].

1.3.2 Next Generation Matrix Method for Discrete Systems with Stable Cycles

Here, we review the theory of the next generation method originating from an underlying k-cycle.

We use a system of discrete differential equations of the form:

$$\vec{x}(t+1) = G(\vec{x}(t)),$$

where

$$x(t) = \Big[x_1(t), x_2(t)...x_n(t)\Big] \in \mathbb{R}_+^n,$$
$$G : \mathbb{R}_+^n \mapsto \mathbb{R}_+^n \text{ is in } \mathcal{C}^1(\mathbb{R}_+^n).$$

We assume that the first $m \in (0, n]$ variables refer to our infected states and the rest, $n-m$ variables, are the non-infected states [4]. We group the states such that:

$$\begin{aligned} X_0(t+1) &= G_0\big[x_1(t), x_2(t), ...x_m(t)\big], \\ X_1(t+1) &= G_1\big[x_{m+1}(t), x_{m+2}(t), ...x_n(t)\big]. \end{aligned} \tag{1.16}$$

We let $G_0(X_0(t), X_1(t)) = \mathcal{F}(t) + \mathcal{T}(t)$ where $\mathcal{F}$ is the vector of new infections that survive $(F_j, \forall j \in [1, k])$ and $\mathcal{T}$ is the vector of all other such transitions $(T_j,\ \forall j \in [1, k])$. We do not go into the forms of G_1, as they do not impact our analyses.

As with the Next Generation Matrix Method for ODEs [20, 23], we use the DFE and analyze its associated stability. We assume the DFE exhibits a stable period-k cycle given by:

$$z = \{z_{1\infty}, z_{2\infty}, ...z_{k\infty}\}, \tag{1.17}$$

where $k \geq 1$. We linearize the system $x(t+1) = G(x(t))$ by taking:

$$Y(t+1) = \Big(DG(0, z_{k\infty}) \cdot DG(0, z_{k-1\infty}) \cdots DG(0, z_{1\infty})\Big) Y(t) \tag{1.18}$$

where $DG(\cdot, \cdot) \in \mathbb{R}^{n \times n}$ is the Jacobian of G_0, G_1. The Jacobian matrices take the form:

$$DG(0, z_{j\infty}) = \begin{bmatrix} F_j + T_j & O \\ A_j & C_j \end{bmatrix}, \tag{1.19}$$

where $j \in \{1, 2..., k\}$, F_j, and T_j are non-negative matrices from evaluating the Jacobian with respect to one point in the k-cycle of the DFE. Here, O is the zero matrix. Although A_j is non-zero, it plays no role in the eigenvalue calculation (i.e. since $DG(0, z_{k\infty})$ is upper

triangular). In the bottom right corner, C_j is associated with other eigenvalues of the system [4]. Thus we are left with the system from Equation 1.18 taking the form:

$$Y(t+1) = \begin{bmatrix} (F_k + T_k)(F_{k-1} + T_{k-1})...(F_1 + T_1) & O \\ A & C_k C_{k-1} ... C_1 \end{bmatrix} Y(t). \tag{1.20}$$

At the DFE, the k-cycle is locally asymptotically stable, so $\rho(C_k C_{k-1} ... C_1) < 1$. Hence the additional eigenvalues associated with $\prod_i C_i$ do not impact the stability of the DFE and do not appear in R_0.

In order to form a succinct expression for the basic reproductive number we first define:

$$\begin{aligned} \tilde{\mathcal{T}} &= T_k T_{k-1} ... T_1, \\ \tilde{\mathcal{F}} &= (F_k + T_k)(F_{k-1} + T_{k-1})...(F_1 + T_1) - \tilde{\mathcal{T}}. \end{aligned}$$

Thus,

$$\tilde{\mathcal{F}} + \tilde{\mathcal{T}} = (F_k + T_k)(F_{k-1} + T_{k-1})...(F_1 + T_1).$$

As some individuals may die (from the infection or naturally), it is assumed that $\rho(T_k \cdot T_{k-1} \cdot ... \cdot T_1) < 1$. Additionally, by construction $\tilde{\mathcal{F}}$ and $\tilde{\mathcal{T}}$ are entry-wise non-negative, so we observe that:

$$(I - \tilde{\mathcal{T}})^{-1} = I + \tilde{\mathcal{T}} + \tilde{\mathcal{T}}^2 + ... + \tilde{\mathcal{T}}^n,$$

where $I \in \mathbb{R}^{n \times n}$ is the identity matrix and $(\cdot)^{-1}$ denotes the matrix inverse. Hence, the matrix $(I - \tilde{\mathcal{T}})^{-1}$ is also entry-wise non-negative. Thus, $\tilde{\mathcal{F}}(I - \tilde{\mathcal{T}})^{-1}$ is also entry-wise non-negative. It's largest eigenvalue in magnitude gives the expected number of new infections for a given period k-cycle. So we take the formal definition from [4] of the basic reproductive number as:

$$R_0 = \rho\big(\tilde{\mathcal{F}}(I - \tilde{\mathcal{T}})^{-1}\big). \tag{1.21}$$

1.4 Summary

Throughout this chapter we have introduced critical foundation concepts of mathematical epidemiology such as the basic reproductive number, disease free equilibrium, and the next generation matrix method. These concepts have been used frequently throughout the literature [4, 18, 19, 20, 21, 22]. Additionally, we demonstrated how each of these concepts can lead to answering of basic mathematical (and biological questions) about population models such as the logistic growth map. In particular, we can demonstrate that a model becomes chaotic for a range of parameters as well as make actionable biological decisions from this. In the following Chapter, we introduce the biological concept of density dependence and mathematically characterize it in order to lay the groundwork for Chapters 3, 4 and 5.

Chapter 2

Density Dependence

Density dependence is when the current population size at a given time step influences the dynamics of the entire population at the next time step. Specifically, the role of population size and proportion to carrying capacity are key factors in things such as growth (on the individual and population level) as well as trends in group behavior such as feeding patterns, mating, and death [3]. Populations tending toward extinction often exhibit biological behavior and population dynamics differently than those in a stable regime. For example if a single individual is infected with some disease in a population of three it will likely have much more drastic effects on a population of one thousand [3]. In general, the population of three individuals has a higher probability of heading to extinction sooner than the population of one thousand.

In order to understand the role of density dependence for a particular population or organism, extensive work has been performed to correctly choose forms to incorporate density dependence [7, 17, 3, 25, 26, 27, 28, 29, 30]. Below, we introduce several classical functional forms in the context of density dependence.

2.1 Generic Form

Density dependence is often incorporated mathematically in the following manner:

$$N_{t+1} = N_t f(N_t),$$

where N_t is the population at time t and $f(N_t)$ is a function describing density dependence often backed from biological data [3]. For shorthand we refer to the function $f(N)$ where N would be synonymous to N_t. However, in the situation that we use a particular functional form in a specific biological model, we do not use the short hand and stick with N_t as the population(s) at a given time step are truly crucial to the understanding of the problem. This notation is historically consistent with literature, in particular [3].

We consider $f(N) \in [0,1]$ as it is the restriction of growth due to density at a given time step. Beyond the basic requirement that $f(N_t) \in [0,1]$, open questions remain pertaining to why particular functional forms induce specific dynamical behaviors in a model.

Generally, we require that as population size tends toward zero, individuals play a larger role (for a fixed number) than in a larger population. Hence, we are interested in the function space such that $f(N) \in [0,1]$, $f(N)$ is decreasing (perhaps monotonically), and nonlinearly. In the following section, we discuss several examples of functional forms.

2.2 Classical Forms

Functional forms are carefully chosen to best represent the population modeled and incorporate the correct form of density dependence. Particularly, functional form choices are made such that biological data or theory reinforce the mathematical behavior they exhibit [3]. This section serves to shed light and clarify historical choices on such forms.

In addition to algebraic simplicity, the models aim to exhibit rational qualitative behavior of density dependence. Specifically, the functional forms in Table 2.1 (reproduced from [3]) exhibit behavior exemplified by density dependence playing a larger role at smaller population size, and a smaller role at larger population size. This idea similar to biological 'negative feedback' is a helpful characterization for thinking of populations close to extinction. Individuals play a critical role in the sustainability of a population when N nears 0 as opposed to when N is arbitrarily large.

Table 2.1: Functional Forms to Incorporate Density Dependence.

Function number	$f(N)$	Sign of $\frac{df^2}{dN^2}$	Reference
$f_1(N)$	N^{-b}	+	[27]
$f_2(N)$	e^{-bN}	+	[7, 12, 17, 25, 26]
$f_3(N)$	$\frac{1}{1+aN}$	+	[8, 30]
$f_4(N)$	e^{-aN^b}	+,-	[3]
$f_5(N)$	$\frac{1}{1+(aN)^b}$	+,-	[31]
$f_6(N)$	$\frac{1}{(1+aN)^b}$	+	[32, 33]
$f_7(N)$	$\frac{1}{(1+e^{bN-a})}$	+,-	[9, 28, 29]

Below, we give the plot of each functional forms and introduce one key form that becomes evident in Chapter 4. In particular, we note that the functional forms $f_1(N) = N^{-b}$ and $f_7(N) = \frac{1}{1+e^{bN-a}} \neq 1$ when $N = 0$. In order to normalize these functions so that they are 1

when $N = 0$, we perform the following:

$$\begin{aligned} 1 &= \frac{1}{c + e^{bN-a}} \\ \implies c + e^{bN-a} &= 1 \\ \implies c &= 1 - e^{-a}, \end{aligned} \tag{2.1}$$

for $f_7(N)$. In order to normalize $f_1(N)$ so that it does not blow up to infinity, we fix $f_1(0) = 1$ as it is discretized.

Although not included in Table 2.1 for historical reference, this 'normalized' version of $f_7(N)$ will be used moving forward and is reflected as such.

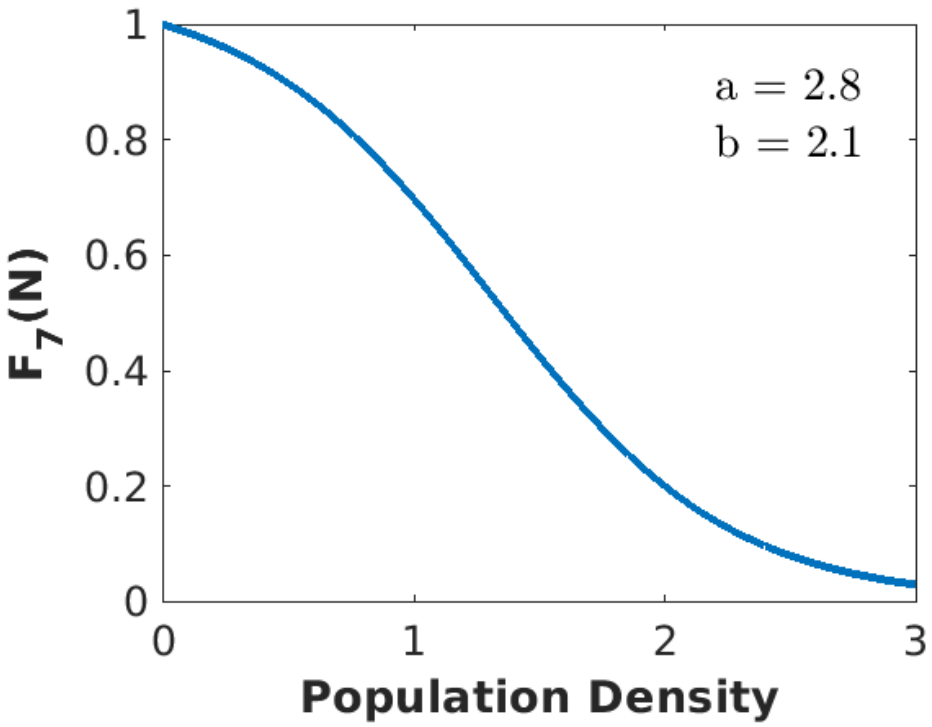

Figure 2.1: A plot of $f_7(N)$ for population density. The values of a and b were chosen to highlight the 'desired' properties of $f_7(N)$ such as concavity and monotonicity. We see shortly that these values are not backed by literature and drastically change the behavior.

This particular functional form takes two input parameters (a, b) (and technically c which is dependent on a) and is bounded by $0 \leq f(N) \leq 1$. We see that as population density increases, the function decreases (i.e. plays a smaller role). Note the converse is also true, as population density decreases, the function increases (i.e. plays a larger role). We also see now that the normalized version of $f_7(N) = 1$ when $N = 0$. Although c does depend on a

with respect to Equation2.1, we omit it's value from the plot as the true driving parameters are a and b.

We propose the use of this particular functional form for a case study in Chapter 4. Other relevant functional forms included in Table 2.1 exhibit the same qualitative behavior in Figure 2.4. We discuss the differences below.

Although we choose particular functional forms of interest, it is important to recognize the role that they play in a model. We assume that the particular choice of $f(N)$ is responsible for describing how the population will be impacted by density dependence at the time step, bounded by the current population N_t. Additionally, as mentioned in Figure 2.1 the current choice of a and b were to demonstrate the concavity and monotonicity of the given functional form. We keep those values here, then quickly shift gears and revert to historical choices of values below in Section 2.3.

We can define the 'simplest' population model from [3] as given by:

$$N_{t+1} = N_t f(N_t) = \frac{N_t}{c + e^{bN_t - a}} \tag{2.2}$$

where a, b are again, the scaling parameters to adjust the model to a given population. Note that there is no reproduction term considered in this model. This example model is derived for $f_7(N)$ purely to demonstrate some key roles discussed shortly below, though in general it could be derived for any of the given functional forms.

Previously in Figure 2.1 we saw the role that the particular form had on a population with respect to the population size. The plot below shows how the population changes as a function of both density and previous size. Although this may be the 'simplest' population density model possible for the particular functional form given previously in Figure 2.1, it demonstrates the drastic differences in the curves simply by adding a factor of N_t in the numerator.

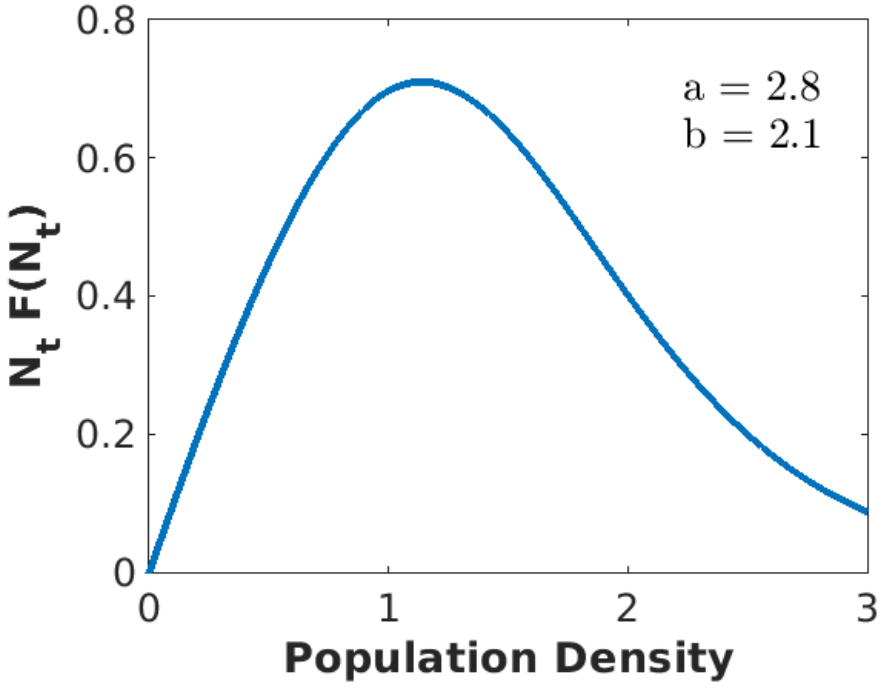

Figure 2.2: The simple population model for the given functional form of $f_7(N)$. The model was reproduced from [3] and exhbits how drastically the curve can change by adding an additional factor of N_t to it.

Now that we have introduced the normalized form of a key functional form of interest, we begin to address how each functional form behaves. In Section 2.3 we discuss results pertaining to each of the functional forms for different choices of the scaling parameters a and b.

2.3 Comparison of Forms

The table below is reproduced, in part, from [3]; it highlights key functional forms to incorporate density dependence in a population model. The concavity of a function bounded by $[0, 1]$ is of importance as it tells us behavior of how the function tends to zero. Similar to Table 2.1, we add an additional two columns of the fitted parameter choices for a and b.

Table 2.2: The functional forms from [3], again where $c = 1 - e^{-a}$ is the scaling parameter derived previously.

Function number	$f(N)$	Sign of $\frac{df^2}{dN^2}$	Fitted a	Fitted b	Reference
$f_1(N)$	N^{-b}	+	**X**	1.496×10^{-7}	[27]
$\mathbf{f_2(N)}$	$\mathbf{e^{-bN}}$	+	**X**	**0.1**	[7, 12, 17, 25, 26]
$f_3(N)$	$\frac{1}{1+aN}$	+	9.578×10^4	**X**	[8, 30]
$f_4(N)$	e^{-aN^b}	+,-	2.353	8.936×10^{-8}	[3]
$f_5(N)$	$\frac{1}{1+(aN)^b}$	+,-	1.9949	1.6668×10^{-9}	[31]
$f_6(N)$	$\frac{1}{(1+aN)^b}$	+	10	10	[32, 33]
$f_7(N)$	$\frac{1}{(c+e^{bN-a})}$	+,-	8.9473×10^{-7}	0.1	[9, 28, 29]

In this thesis, we substitute each of these functional forms into an infectious disease model pertaining to salmon. The ISAv model, introduced in Chapter 3, uses a Ricker recruitment function ($f_2(N)$) to incorporate density dependence for the particular population of salmon it studies. In order to accurately compare each of the functional forms, we fit each of the functions to the 'baseline' function $f_2(N) = e^{-bN}$ (with $b = 0.1$ taken from the literature, particularly [3, 17]).

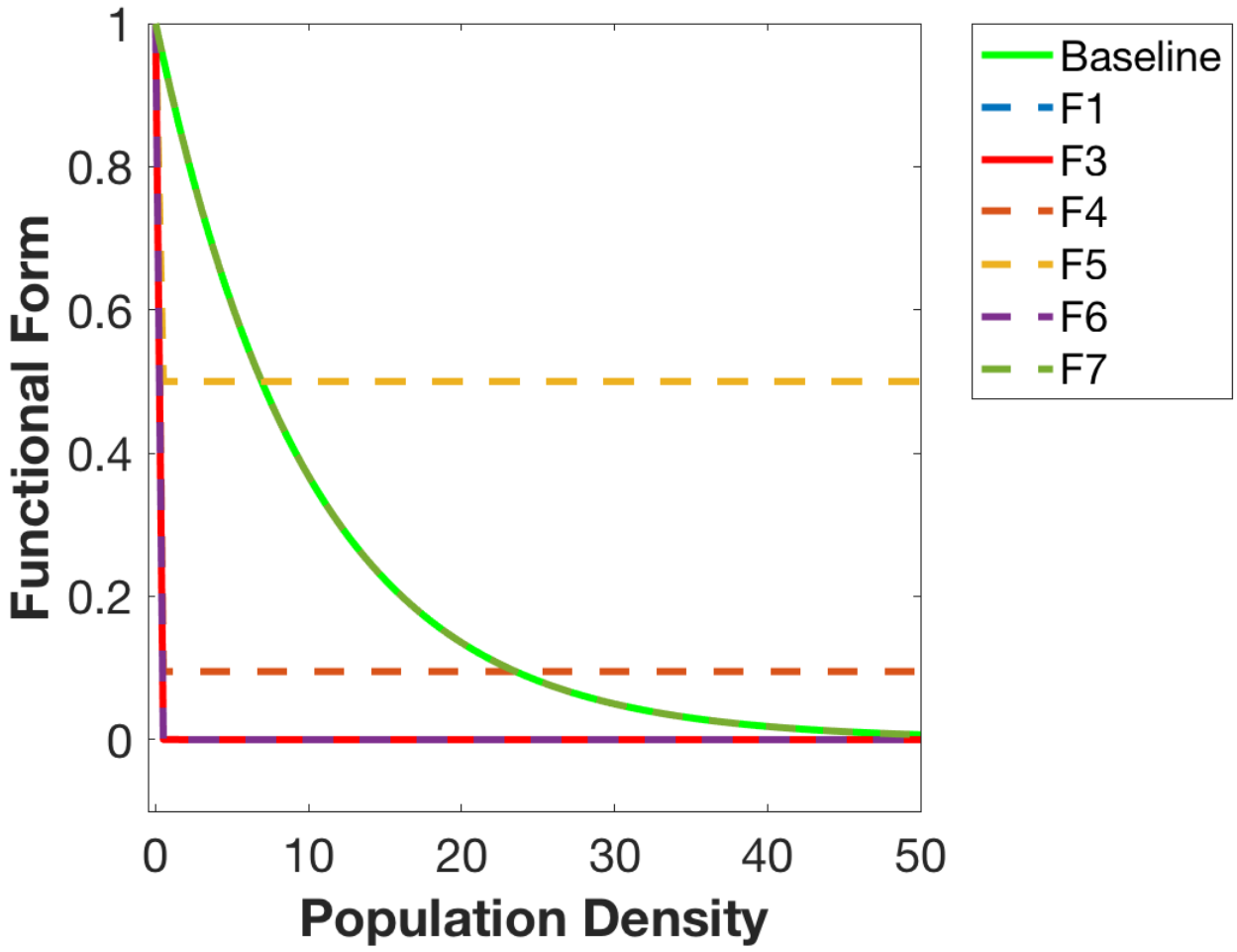

Figure 2.3: The fitted functional forms in Table 2.2 to the baseline function $f_2(N)$. We used constrained optimization (for $a, b > 0$ and minimized over the norm of the error.

We fit each functional form to the baseline by constrained optimization (i.e. $a, b > 0$ and minimize error over the L_2 norm. To achieve this, we treat the Ricker function, i.e. $f_2(N)$ as the 'data' by discretizing 1000 points (over a population density from 0 to 100) of the function and used the matlab function *fmincon* to fit the parameter values for each of the other funcitonal forms such that the L_2 norm of the difference between the 'data', i.e. discretized Ricker function, and the given functional form is minimized.

Many of the a and b values are essentially zero and perhaps biologically unfeasible but they serve as a baseline for mathematical comparison. We also include extensive analysis about literature values from [3].

While introducing the seven functional forms we briefly stated that ideally $f(N) = 1$, when $N = 0$ and $f(N) \to 0$, when $N \to \infty$. This behavior is consistent with data provided in

[3] and follows the trend that population dynamics exhibit different qualitative behavior at high and low levels with respect to some sort of upper bound or carrying capacity.

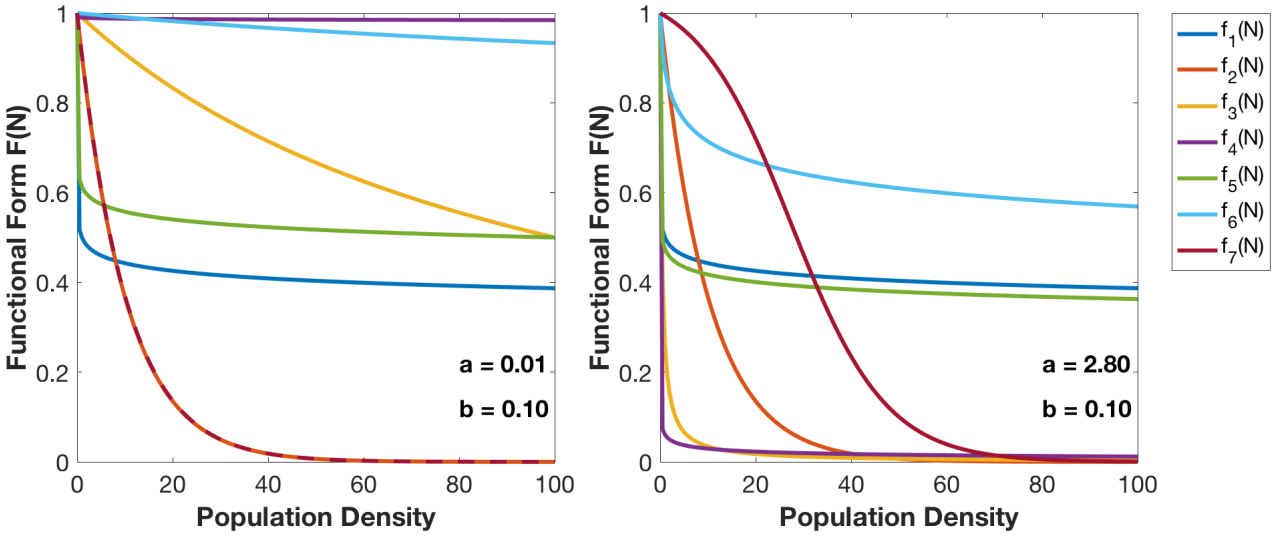

(a) Functional forms plotted against population density for $b = 0.1$ and $a < 1$.

(b) Functional forms plotted against population density for $b = 0.1$ and $a > 1$.

Figure 2.4: The plot on the left demonstrates the functional forms plotted for the literature based values of $a = 0.01$ and $b = 0.1$ [3]. We also include the plot for $a > 1$ on the right as the authors of [3] discuss scenarios in which $a, b > 1$ but do not plot such.

However, in Figure 2.4(a) not all of the functions are monotonically decreasing. The functional form $f_1(N) = N^{-b}$ does not appear on the plot in Figure 2.4 due to the fact that as $N \to 0$, $f_1(N) \to \infty$. We also observe that many of the functional forms do not converge to zero as the the population density increases to 100 individuals.

Much of this behavior can be explained with the fact that $a, b < 1$. In particular the use of the literature value of $a = 0.01 \approx 0$ makes the functional forms $f_7(N)$ and $f_2(N)$ essentially the same (hence why they are plotted on top of one another. The authors of [3] discuss regimes in which both $a, b > 1$, though do not fit it to any data they had at the time. For our purposes here, we often fix $a = 2.8$ and $b = 0.1$ as what we call the 'literature' or 'literature based' parameters as they are taken from [3, 17].

In order to compare each of these functional forms (in a model) in Chapter 4, we also need to analyze how they interact for the fitted parameter choices.

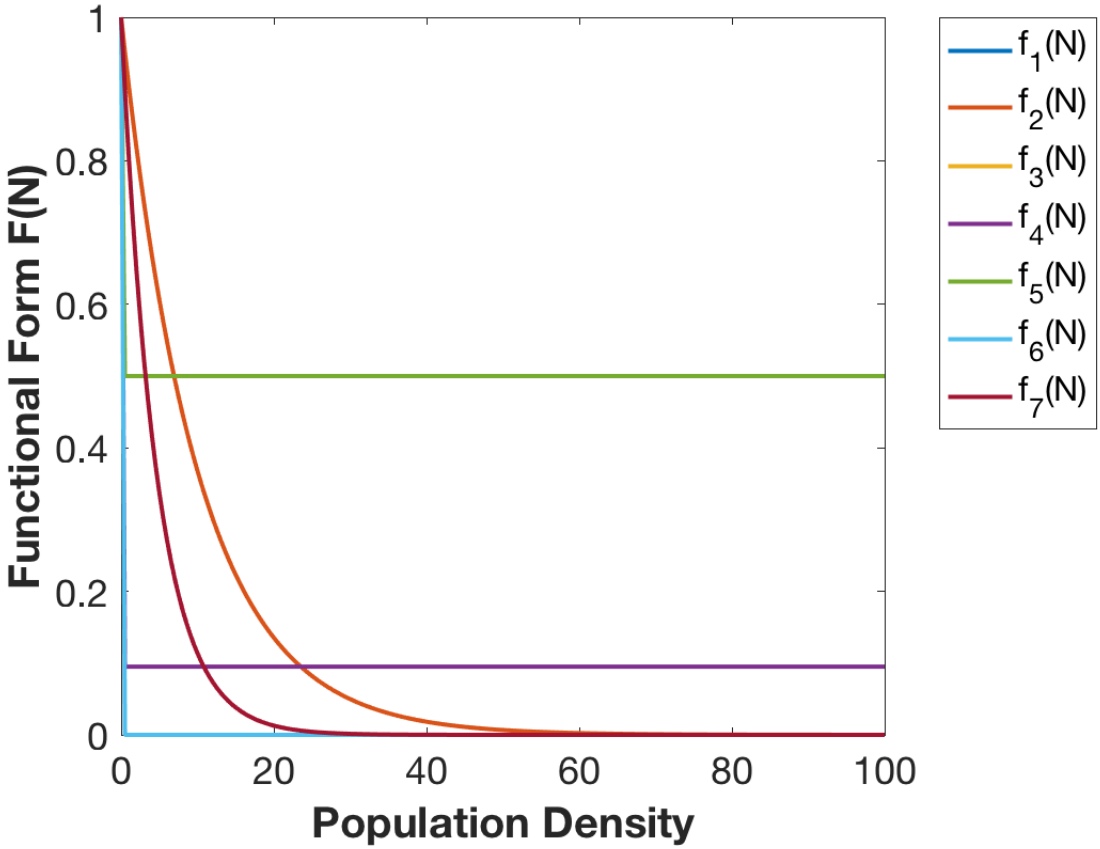

Figure 2.5: The functional forms given in Table 2.2 with optimal parameter choices.

For visual aid we include Figure 2.5 to demonstrate how the shift in parameters can lead to drastically different population density trends. Each particular value of a and b is taken from Table 2.2. Although the functional forms were fitted to the baseline $f_2(N)$, they don't necessarily follow the same behavior. For example, we see that $f_7(N)$ does exhibit similar behavior to $f_7(N)$ while all others do not. In fact, many of the other forms lie on top of each other as they tend to zero rather rapidly for the fitted forms in Table 2.2.

2.4 Functional Forms for the Simplest Model

In this section, we analyze and compare how each of the seven functional forms in Table 2.2 behave on their own (i.e. their impact as population density changes) and in the simplest model setting expressed in the previous section as:

$$N_{t+1} = N_t f(N_t). \tag{2.3}$$

Each particular functional form has either one or two parameters which we call a and b to incorporate a scaling effect of the population. For example, in the particular form study previously, given by:

$$f_5(N) = \frac{1}{1 + (aN)^b};$$

we have the parameter a which plays a role in increasing the population as $n \to 0$, and the parameter b plays a role in decreasing/stabilizing the population as $N \to \infty$. Previous work has referred to these parameters as 'scaling parameters' and we often do the same, while exploring the choice of values and implications they have [4]. For example, below in Figure 2.4 we take the values induced via [3] which are data driven. In Chapter 4, we will see that the choice of a and b produce different dynamics and have different biological implications. Particularly, we propose the use of the functional form given by $f_5(N)$ and $f_7(N)$ to an existing infectious disease model that exhibits interesting bifurcation behavior.

As before in Section 2.2 we can see that the population at time $t+1$ is denoted as N_{t+1} is a function bounded by the population size at the previous time step, i.e. N_t.

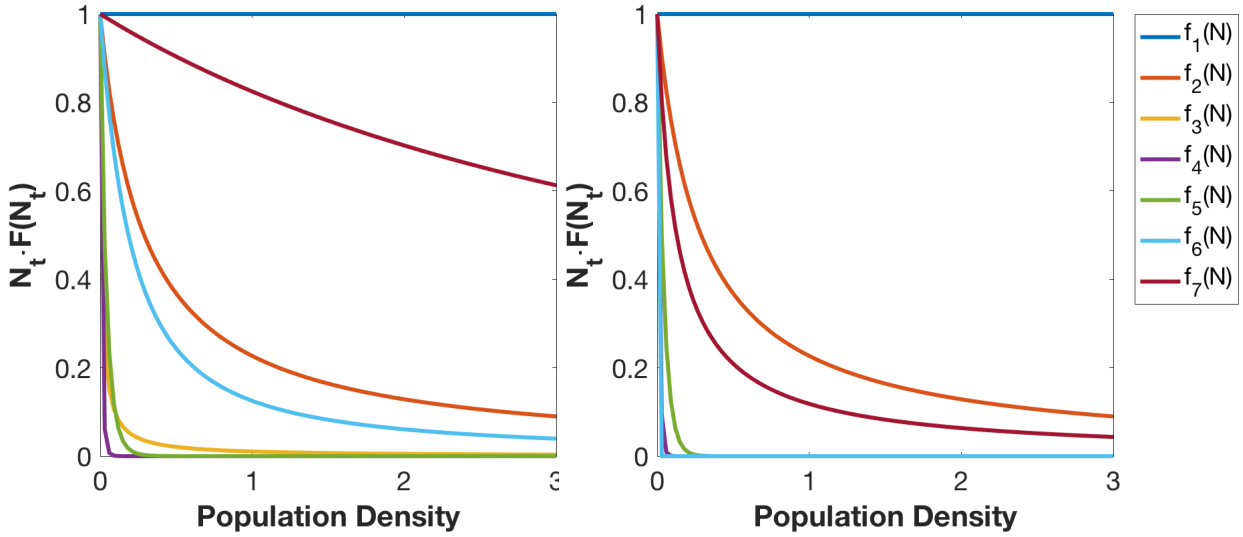

(a) The simplest model population density for the literature parameters.

(b) The simplest model population density for the fitted parameters.

Figure 2.6: The plot on the left demonstrates the simplest model plotted for the literature based values of $a = 2.8$ and $b = 0.1$ [3]. The plot on the right demonstrates the simplest model plotted for the fitted parameter values in Table 2.2.

Above in Figure 2.6 we take $N_t \in [0, 1]$ to be the population density and plot the simple model. We see that as population density increases nearly all of the models tend to zero with the obvious exception of $f_1(N_t) = N_t \cdot N_t^{-b}$ which will always be one. Although the differences seem minor here, we see that there is a noticeable shift in the order of which

models tend to zero when comparing the literature based values and the fitted values. This important distinction could potentially explain behavior observed later in Chapter 4.

2.4.1 Functional Forms tending to zero

We saw in the previous section that the simplest model and the functional forms themselves either tend to zero or tend to a single point. As we discussed earlier, we desire forms that tends toward zero as the iterations become arbitrarily large. In this section we analyze the behavior of each form and how it approaches zero. Below, we discuss the behavior of the functional forms against the iteration number to analyze how quickly each form tends to zero. We provide figures for both the literature based and fitted parameters.

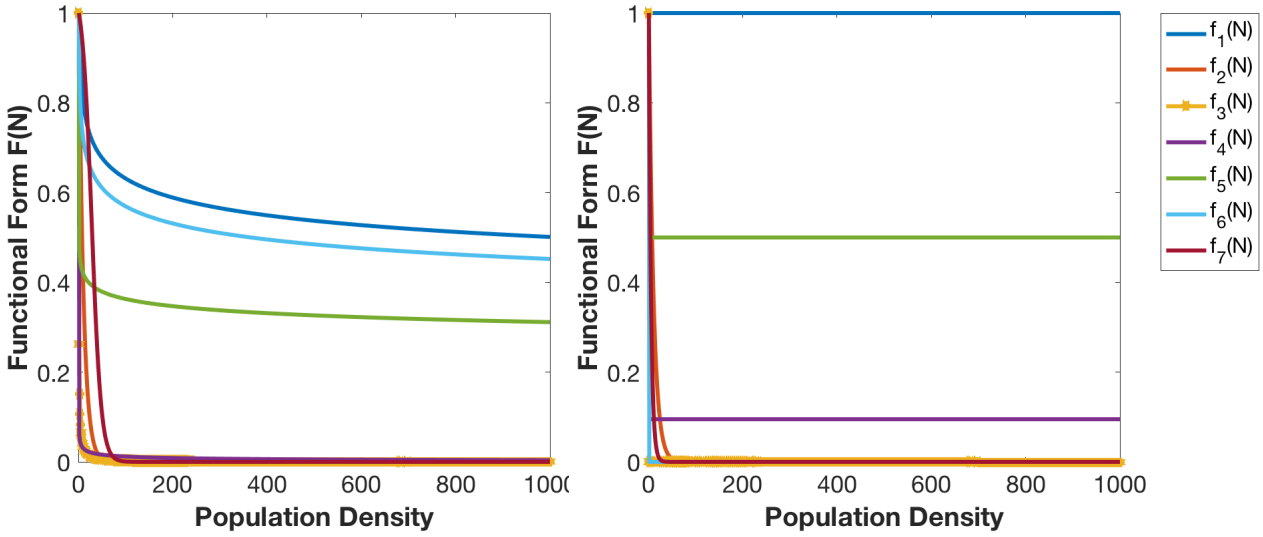

(a) The functional forms tending to zero for the literature parameters.

(b) The functional forms tending to zero for the fitted parameters.

Figure 2.7: The plot on the left demonstrates the functional forms against much larger population density for the literature based values of $a = 2.8$ and $b = 0.1$ [3]. The plot on the right demonstrates the functional forms against the same population density for the fitted parameter values in Table 2.2.

For example, in Figure 2.7 we see that even after 1000 iterations, not all of the functions have truly approached zero. Some, such as f_2 and f_7, settle near zero relatively quickly (within several hundred iterations), whereas others tend toward some number within an epsilon of zero (f_1 and f_3). Interestingly, we also see that a handful of functional forms do not tend to zero with large population density. In particular, for the choice of literature based parameters, forms $f_1(N)$, $f_5(N)$ and $f_6(N)$ do not; whereas for the choice of the fitted parameters $f_1(N)$, $f_4(N)$ and $f_5(N)$ do not.

2.5 Summary

In this chapter, we introduced the concept of biological density dependence and the sensitive dependence of parameter choices various functional forms have. Each functional form has a particular biological meaning and could be suitable for different situations [3]. Although some of the functional forms have one scaling parameter whereas others have two; we discuss the differences of each form in terms of their traditional curves and what we refer to as 'the simplest population model'. These examples demonstrate that minute differences of parameter choices lead to drastically different results in both the functional forms and the model. Additionally, we performed constrained optimization to obtain fitted parameter values for each of the functional forms in order to get another method of comparing their behavior to a common choice [4, 17]. In the following chapter we introduce a model from infectious disease biology and discuss the role of density dependence in its current state.

Chapter 3

The Infectious Salmon Anemia virus (ISAv) Model

3.1 Role of density dependence in bifurcations

In a previous chapter, through Table 2.2 we saw functional forms to incorporate density dependence from Bellows [3]. Clearly the trends and nuances of each of these functional forms play a critical role in qualitative dynamical behavior. This section serves to explore how density dependence plays a role in bifurcation analysis, with several examples in mind. In particular, I explore a case in which authors use a Ricker recruitment function [4], which is a well studied functional form [2, 17], to incorporate density dependence in infection recruiting. I review some analysis performed by [4] to lay ground work for alternative recruitment functions. Although there is a plethora of interesting biological behavior and of course the model is derived from a physical process, the scope of this thesis currently serves to analyze the mathematical behavior of this model. In particular, we explore biological concepts such as density dependence, infection recruitment, among others; however, the underlying motivation for this thesis is mathematical. In the discussion section (i.e. Chapter 6) we provide some insight into the validity of the model and discuss interpretations, though we note that open biological questions still remain.

3.2 Infectious salmon anemia virus model

An application of interest is given by Infectious salmon anemia virus (ISAv); a viral disease from *Orthomyxoviridae* which has drastically reduced populations of salmon worldwide [4, 24, 34, 35]. In addition to economic losses [4, 24] this infectious disease is noted as one of the most dangerous diseases of fish populations, as no treatments currently exist. We model

the population dynamics of infection in the salmon population.

Model

We utilize the model derived by van den Dreissche and Yakubu [4]. In the model, the salmon population is divided by disease status: susceptible (S_t) or infected (I_t); and the total salmon population follows $N_t = S_t + I_t$. Because the infected salmon do not recover it was chosen to use an *SI* epidemic model with no recovery class [4]. Infected salmon are also able to shed virus, and the free virus population is given by V_t. The model assumes that a proportion of susceptible salmon become infected, a proportion of infected salmon die, and susceptible salmon reproduce into their own class. The ISAv model is given by:

$$\begin{aligned} S_{t+1} &= rS_t\,\mathbf{g}(\mathbf{S_t}) + \hat{d}S_t\Big(\theta\Phi_I(I_t) + \hat{\theta}\Phi_V(V_t)\Big), \\ I_{t+1} &= \hat{d}\Big(S_t\big(\theta\widehat{\Phi_I}(I_t) + \hat{\theta}\widehat{\Phi_V}(V_t)\big) + \hat{\mu}I_t\Big), \\ V_{t+1} &= \widehat{d_v}(V_t + \delta I_t). \end{aligned} \tag{3.1}$$

In the subsequent sections we describe each of the terms and parameters. All parameter names and typical values (or ranges) are found in Table 3.1 [4]. A schematic of the model is given in Figure 3.1.

Table 3.1: Parameter and Function Descriptions for the ISAv model.

Symbol	**Biological Description**	**Value**	**Range**
b	Scaling parameter for density dependence	0.1	$[0, 1]$
r	Intrinsic growth rate	e^4	$(0, 160]$
β_I	Poisson constant for infection transmission from infectious salmon	0.056	$[0, 1]$
β_V	Poisson constant for infection transmission from virus	0.01	$[0, 1]$
θ	Fraction of salmon that come into contact with infected salmon	0.6	$[0, 1]$
$\hat{\theta}$	Fraction of salmon that come into contact with the virus	$1 - \theta$	
$\hat{d}$	Probability of survival of salmon	0.5	$[0, 1]$
$\widehat{d_v}$	Fraction of virus that persists	0.8	$[0, 1]$
$\widehat{\mu}$	Fraction of infectious salmon that survive	0.3	$[0, 1]$
δ	Virus shed at a given time step.	0.2	$[0, 1]$
$\Phi_I(I_t)$	Probability that susceptible salmon do not become infected via contact with infected salmon		$[0, 1]$
$\Phi_V(V_t)$	Probability that susceptible salmon do not become infected via contact with the virus		$[0, 1]$

Reproduction

Since infected salmon cannot reproduce, only susceptible salmon can reproduce and be recruited to the infected class. In the original model [4, 17, 24], susceptible salmon reproduce via a Ricker function defined by:

$$g(S_t) = e^{-bS_t}. \tag{3.2}$$

While the authors had biological motivation to choose this particular function, this thesis aims to explore other suitable alternatives for $g(S_t)$. In Equation 3.2, b is a scaling parameter to incorporate density dependence [4]. We note here that for each choice of $g(S_t)$, we have a factor of rS_t on the outside where $r > 0$ is the intrinsic growth rate.

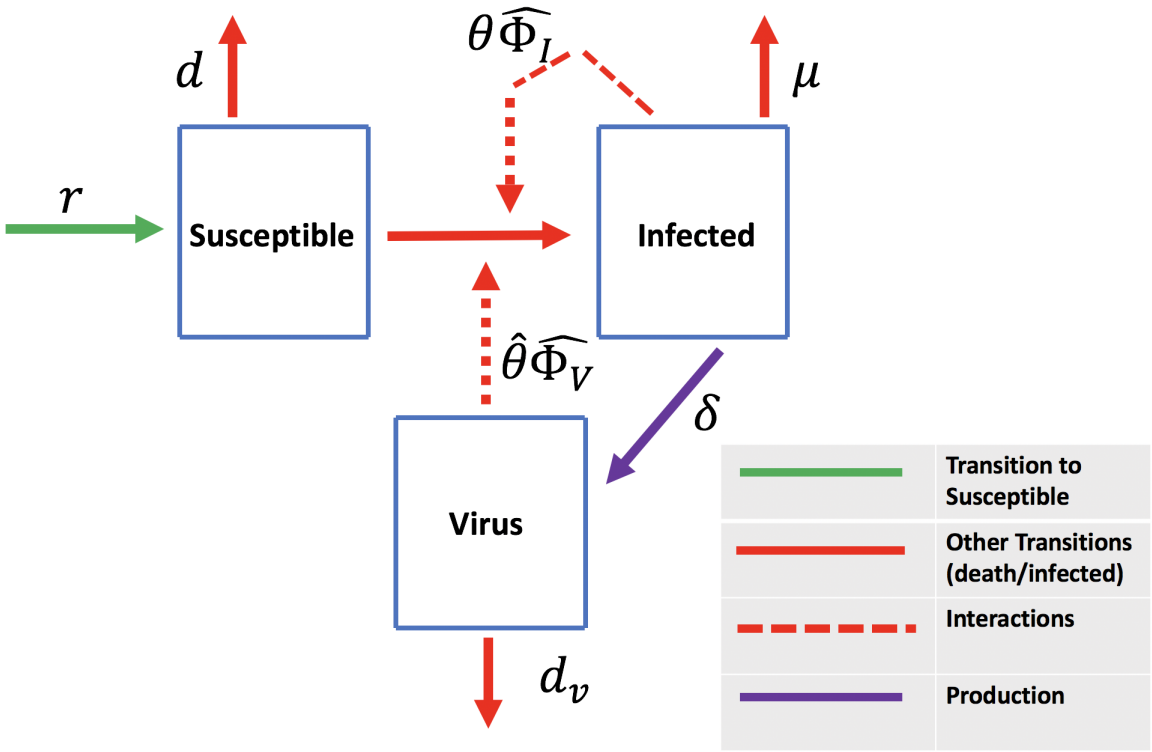

Figure 3.1: Schematic of the ISAv model. The pool of susceptible salmon can die, remain in the susceptible or move to the infected class at the next time step. However, infected salmon remain infected (or die) since there is no recovery class and no immunity. We also note that the interaction between the viral population and the susceptible and infectious population is not a transfer. The parameter $\widehat{\theta}$ describes the relationship between the populations. Namely, $\widehat{\theta}$ is the fraction of salmon that become infected because they came in contact with the virus directly (if the event even happened, which is governed by the probability via $\widehat{\Phi}_V$). $\widehat{d}_v$ is the constant fraction of the virus that persists.

Mortality

We assume that some fraction of the salmon (both susceptible and infected) die of natural causes unrelated to infection at a given time step. We denote this fraction as d, and often refer (in the model) to the fraction of those that survive via $\hat{d} = 1 - d$. Similarly, we assume a constant fraction of disease-induced mortality for infectious salmon via $\mu \in (0, 1)$, though refer in the model to $\widehat{\mu} = 1 - \mu$ for the infectious salmon that survive. Finally, we also take into account the proportion of virus cleared at a given time step $d_v \in (0, 1)$ and refer to $\widehat{d}_v = 1 - d_v$ as the proportion of virus that is not cleared in a given time step.

Infection

The model, as written, assumes that all susceptible salmon that do not die due to natural causes contact infected salmon or virus. The fraction of susceptible salmon that contact infected salmon is given by $\theta \in [0, 1]$. The probability of these salmon becoming infected in a given time step is given as:

$$\widehat{\Phi}_I(I_t) = (1 - \Phi_I(I_t)). \tag{3.3}$$

where $\Phi_I(I_t)$ is defined below.

Similarly, at each time step the remaining susceptible salmon $\widehat{\theta} = 1 - \theta$ come in contact with virus [4] with a probability of infection given by:

$$\widehat{\Phi}_V(V_t) = (1 - \Phi_V(V_t)); \tag{3.4}$$

where $\Phi_V(V_t)$ is defined below.

Φ_I, Φ_V are referred to as 'escape functions' due to their expression of 'avoiding' the virus either from other salmon or contact with free virus. These functions are given by:

$$\Phi_I, \Phi_V : \mathbb{R}_+ \mapsto [0, 1]$$

which are nonlinear, decreasing, and smooth. These functions obey a probability distribution chosen specifically for the ISAv model. In particular, the authors choose these functions to obey Poisson processes, via:

$$\begin{aligned} \Phi_I(I_t) &= e^{-\beta_I I_t}, \\ \Phi_V(V_t) &= e^{-\beta_V V_t} \end{aligned} \tag{3.5}$$

and allow $\beta_j > 0$ to be transmission constants for $j \in \{I, V\}$.

3.2.1 Proof of Boundedness

For biological realism, it is important to know that at a given time step either the viral or infected population will not exponentially grow. This prohibits population explosion of the virus which would cause susceptible salmon to die out unreasonably fast.

The boundedness theorem in this section shows that the infected population is naturally governed by the number of susceptible salmon at a given time step.

Theorem 3.2.1: *For the given ISAv model,* $\forall t \in \{1, 2, ...N\}$ *and* $\forall (S_t, I_t, V_t) \in \mathbb{R}^3_+$*, there is no population explosion provided* $(S_0, I_0, V_0) \in \mathbb{R}^3_+$.

Proof:
We begin by only considering the susceptible salmon. From the model, we know that:

$$S_{t+1} = rS_t e^{-bS_t} + \hat{d}S_t\bigg(\theta\Phi_I(I_t) + \hat{\theta}\Phi_V(V_t)\bigg).$$

Factoring out the common term S_t gives us:

$$S_{t+1} = S_t\left(re^{-bS_t} + \hat{d}(\theta\Phi_I(I_t) + \hat{\theta}\Phi_V(V_t)\right).$$

Now, since $\Phi_I(I_t) \leq 1$ and $\Phi_V(V_t) \leq 1$ as they are probabilities; and $\theta + \hat{\theta} = 1$ by definition, we can observe that:

$$S_{t+1} \leq S_t\big(re^{-bS_t} + \hat{d}(1)\big),$$

and using the definition of $\hat{d}$, we get:

$$S_{t+1} \leq S_t\big(re^{-bS_t} + 1 - d\big).$$

Hence the susceptible population at time $t + 1$ is bounded by a factor of the susceptible salmon present at the previous time step.

Now, the same process can be followed to obtain similar results for the infected class. Namely, we find that:

$$I_{t+1} \leq (1 - d)S_t + (1 - d)(1 - \mu)I_t.$$

Similarly, the infected salmon at time $t + 1$ are bounded by a factor of both the previous time step's susceptible and infected populations. As all populations are bounded, there is no population explosion.
□

This theorem gives us sufficient conditions that population explosion does not happen, i.e. solutions do not 'blow up'. However, the theorem does not give any conditions about cascading into chaotic-like behavior, which we will explore in later sections. Additionally, the theorem characterizes the concept that the next time step's infected and susceptible classes are governed by the population of each at the previous time step.

3.3 Equilibrium Solutions and Stability for the ISAv Model

3.3.1 Absence of Infection

Fixed Points

In the absence of infection, we take $I_t = V_t = 0$, and are only left with our first equation from the model:

$$S_{t+1} = rS_te^{-bS_t} + \hat{d}S_t\big(\theta\Phi_I(I_t) + \hat{\theta}\Phi_V(V_t)\big).$$

Since $I_t = V_t = 0$, then we know that $\Phi_I = \Phi_V = 1$. Furthermore, using the fact that $\theta + \widehat{\theta} = 1$, we are left with:

$$S_{t+1} = rS_t e^{-bS_t} + \hat{d}S_t.$$

However, in the following sections as we propose alternatives to the Ricker recruitment functions, this leads to the general expression:

$$\begin{aligned} S_{t+1} &= rS_t g(S_t) + \hat{d}S_t, \\ &= rS_t g(S_t) + (1-d)S_t. \end{aligned} \tag{3.6}$$

Hence, to find fixed points of the generic model in the absence of infection we wish to solve $S_{t+1} = S_t$. This is achieved by (note the shift to d instead of $\hat{d}$ here):

$$rS^* g(S^*) = S^* d, \tag{3.7}$$

where S^* denotes the fixed point of Equation 3.6.

Thus, in the case of the Ricker recruitment function, we see that Equation 3.6 becomes:

$$rS^* e^{-bS^*} = S^* d.$$

We find two fixed points, S^*. The first, $S^* = 0$ is trivial, and we ignore it moving forward. Solving for $S^* \neq 0$, we can arrive at the expression:

$$S^* = \frac{\ln(\frac{r}{d})}{b}. \tag{3.8}$$

Stability

We focus on the stability of the fixed point given by:

$$S^* = \frac{\ln(\frac{r}{d})}{b}.$$

In the absence of infection, the ISAv model is strictly governed by the equation:

$$S_{t+1} = rS_t e^{-bS_t} + \hat{d}S_t.$$

Taking the derivative of both sides gives:

$$\frac{\partial S_{t+1}}{\partial S_t} = re^{-bS_t} - brS_t e^{-bS_t} + \widehat{d}.$$

Substituting in the expression for S^*, we obtain:

$$\begin{aligned} \left.\frac{\partial S_{t+1}}{\partial S_t}\right|_{S^*} &= re^{-b\frac{\ln(r/d)}{b}} - br\frac{\ln(r/d)}{b}e^{-b\frac{\ln(r/d)}{b}} + \widehat{d} \\ &= 1 - \ln\left(\frac{r}{d}\right). \end{aligned} \tag{3.9}$$

Now, we can see that Equation 3.9 is bounded in magnitude by 1, indicating stability when:

$$\begin{aligned} &\left|1 - \ln\left(\frac{r}{d}\right)\right| \leq 1 \\ \iff &-2 \leq -\ln\left(\frac{r}{d}\right) \leq 0 \\ \iff &1 \leq R_d \leq e^2 \end{aligned} \tag{3.10}$$

Thus we know that the Equilibrium given by Equation 3.8 is stable when $R_d \in [1, e^2]$. In the subsections below, we explore some numerical results that are consistent with this in the absence of infection.

Liapunov Exponent in the Absence of Infection

The Liapunov Exponent is a metric for analyzing chaotic behavior in a system [8]. We define the Liapunov Exponent as:

$$\lambda(\vec{x}_0) = \lim_{t\to\infty} \frac{1}{t} \ln\left[\rho\Big(\prod_{k=0}^{t-1} J(\vec{x}_0)\Big)\right],$$

where $J(\vec{x}_0)$ is the Jacobian evaluated at the given point.

Now, in the absence of infection, we have $I_t = V_t = 0$, and so our Jacobian for the ISAv model simplifies to:

$$J = \begin{bmatrix} re^{-bS_t} - bre^{-bS_t} + \widehat{d}\,\theta + \widehat{d}\,\widehat{\theta} & -\theta\widehat{d}\,\beta_I S_t & -\widehat{\theta}\,\widehat{d}\,\beta_V S_t \\ 0 & \widehat{d}\,S_t\,\theta\,\beta_I + \widehat{d}\,\widehat{\mu} & \widehat{d}\,S_t\,\widehat{\theta}\,\beta_V \\ 0 & \widehat{d}_v\delta & \widehat{d}_v \end{bmatrix} \tag{3.11}$$

We can use the Jacobian to derive results about potential presence of chaotic behavior. In the following section we numerically demonstrate this.

Numerical Appearance of Chaotic Behavior

We numerically examine the Liapunov exponent as we vary both the intrinsic growth rate r and the probability of death d in the absence of infection. In this case, the system is reduced to:

$$S_{t+1} = rS_te^{-bS_t} + \widehat{d}S_t,$$

and the scaling parameter b has no effect on the stability (see Equation 3.10). In particular $\forall b \in [0,1]$ given the standard parameters of r and d the susceptible population remains in a stable two-cycle.

In Figures 3.2 and 3.3, we include the bifurcation diagram for the intrinsic growth rate r and the probability of death d in the absence of infection, i.e. when the model is reduced to Equation 3.6. We omit the bifurcation plot for the scaling parameter b as it doesn't impact the stability.

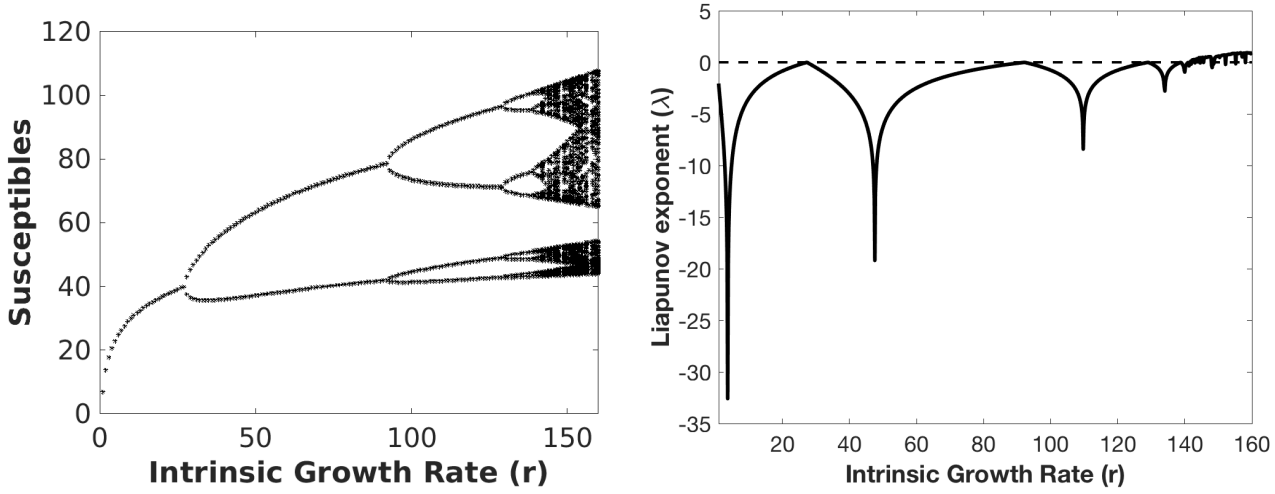

(a) Numerical bifurcation plot

(b) Liapunov exponent

Figure 3.2: Qualitative behavior of the ISAv model in the absence of infection as the intrinsic growth rate, r, is varied in $r \in (0, 160]$ for fixed values of $d = \widehat{d} = 0.5$, and $b = 0.1$. $S(0) = 150$.

To create Figures 3.2 and 3.3, we eliminate transient behavior by running the model in both plots for $N = 5000$ time steps before plotting any behavior.

The left hand plot of the bifurcation exhibits what appears to be chaotic behavior when r is large. The Liapunov exponent for a fixed initial condition of $S_0 = 150$ suggests chaotic behavior is exhibited when r is large; i.e. we see that λ goes above0 for certain r. Although this does not prove that in the absence of infection the model can become chaotic, it supports results for standalone initial conditions.

Similarly, in Figure 3.3, the probability of death is denoted by d and is bounded, $d \in [0,1]$. The notation in the equation uses $\widehat{d}$, the probability of survival. Thus we see that for high values of the probability of death (i.e. low probability of survival) we observe behavior that appears to be chaotic. For the particular initial condition of $S_0 = 150$, we calculate the behavior of the Liapunov exponent as d is varied and we see that it becomes positive as the probability of death is high.

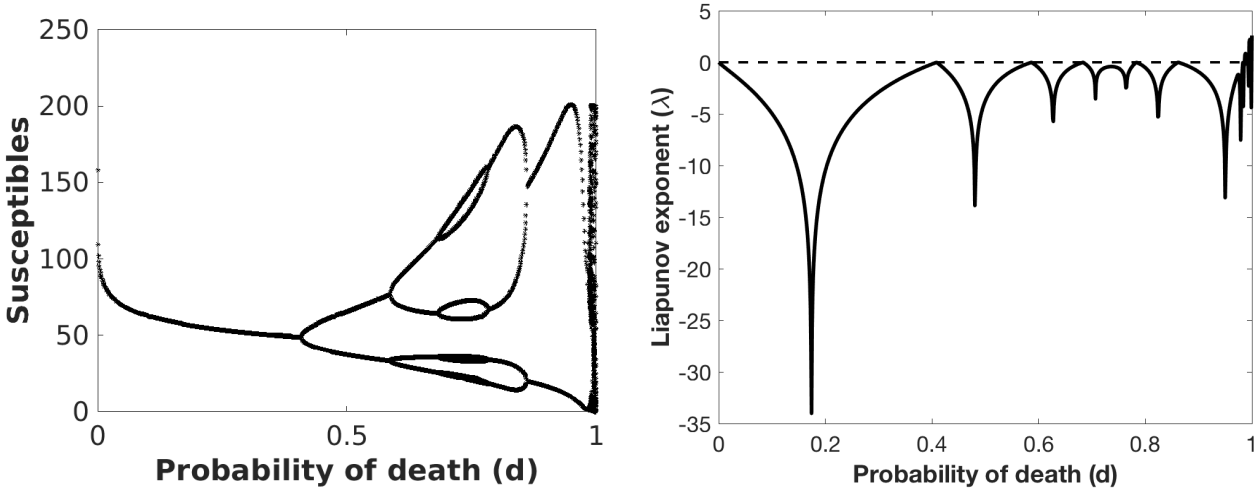

(a) Numerical bifurcation plot (b) Liapunov exponent

Figure 3.3: Qualitative behavior of the ISAv model in the absence of infection as the probability of death, d, is varied in $d \in [0, 1]$ for fixed values of $r = e^4$, and $b = 0.1$. $S(0) = 150$.

Similar to the case of the intrinsic growth rate r, although this does not prove true chaotic behavior for all initial conditions, it confirms numerical speculations that the model seems to be chaotic in the absence of infection.

Bifurcations along two parameters

Here we introduce some interesting two-parameter bifurcation results; specifically, we vary both the intrinsic growth rate, r, and the probability of death, d, simultaneously. As done previously, we eliminate transient behavior by running the model for 5000 time steps (at each pair of r, d). As we cannot plot the behavior itself after long time, we count the number of unique values the population takes over the last 100 time steps – representative of the cycle length. We see in Figure 3.4 that as long as $R_d \leq e^2$ we have a 'one cycle', i.e. a single stable fixed point. Upon inspection of the model it is not immediately clear how parameter combinations beyond that region will translate to cyclic behavior.

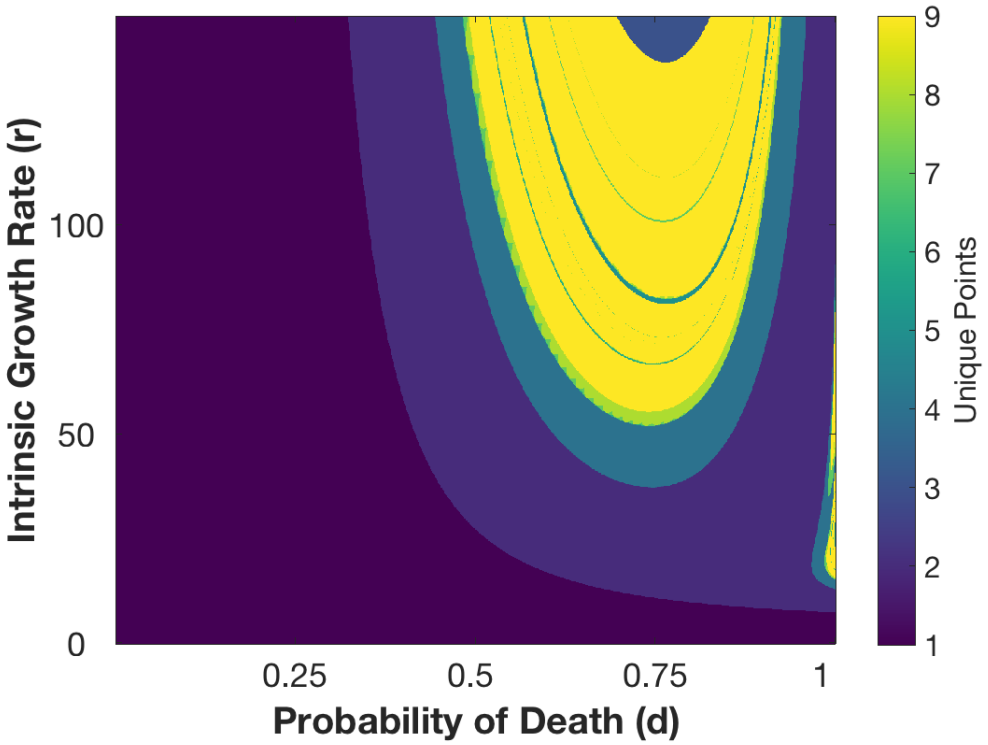

Figure 3.4: Unique values of the ISAv model in the absence of infection as the intrinsic growth rate and probability of death are varied. Here, $r \in [1, 150]$, $d \in (0, 1)$, and $b = 0.1$ with $S(0) = 150$.

We vary the intrinsic growth rate $r \in [1, 150]$, and the probability of death $d \in (0, 1)$ with 1000 equidistant points creating the mesh.

Figure 3.4 demonstrates that we see period doubling behavior cascading into what could potentially be chaotic (i.e. more than eight cycles) but with small 'rest' regions that produce low cyclic behavior. For visual purposes we denoted anything over eight unique as 'nine'. It is still largely unanswered as to what is biologically responsible for these regions of low complexity, or particular combinations of the intrinsic growth rate and probability of death that lead to smaller unique value counts in a region of apparent chaotic behavior.

3.3.2 Calculating R_0 for the ISAv model

R_0 for one-cycle system

Here, we find the explicit expression for the basic reproductive number R_0 when there is a single stable fixed point, i.e. $k = 1$. Using the general framework of Section 1.3, we recall

that:

$$\tilde{\mathcal{T}} = T_2 T_1$$
$$\tilde{\mathcal{F}} = (F_2 + T_2)(F_1 + T_1) - \tilde{\mathcal{T}}.$$

Now, using the equilibrium point given by $S^* = (\frac{\ln(R_d)}{b}, 0, 0)$, we can substitute in and obtain:

$$\tilde{\mathcal{F}} = \begin{bmatrix} -\frac{\ln(R_d)}{b}\hat{d}\theta{\Phi_I}'(0) & -\frac{\ln(R_d)}{b}\hat{d}\theta{\Phi_I}'(0) \\ 0 & 0 \end{bmatrix} \tag{3.12}$$
$$\tilde{\mathcal{T}} = \begin{bmatrix} \hat{d}\hat{\mu} & 0 \\ \hat{d_v}\delta & \hat{d_v} \end{bmatrix},$$

and so the expression for R_0 takes the form:

$$R_0 = \rho\Big(\tilde{\mathcal{F}}(I - \tilde{\mathcal{T}})^{-1}\Big), \tag{3.13}$$

where I is the identity matrix. The authors of [4] this it one step further and express that: $R_0 = R_{0I} + R_{0V}$ where each $R_{0I,V}$ are given by:

$$R_{0I} = \frac{-\hat{d}\ \ln(R_d)\theta{\Phi_I}'(0)}{b(1 - \hat{d}\hat{\mu})}, \tag{3.14}$$
$$R_{0V} = \frac{-\hat{d}\hat{d_v}\delta\ \ln(R_d)\hat{\theta}{\Phi_V}'(0)}{b\hat{d_v}(1 - \hat{d}\hat{\mu})}.$$

In Chapter 5 we will use these expressions to discuss interesting bifurcation behavior not previously studied for the ISAv model.

R_0 for two-cycle

Here, we calculate an implicit form for R_0 when the DFE is in a stable two-cycle. As mentioned before, in the absence of infection, the model becomes:

$$S_{t+1} = rS_t\, g(S_t) + \hat{d}S_t,$$

where in this particular example we take $g(S_t) = e^{-bS_t}$. The analytical expression of the 2-cycle takes the form:

$$S_{t+2} = rS_{t+1}e^{-bS_{t+1}} + \hat{d}S_{t+1}, \tag{3.15}$$

where $S_{t+1} = rS_t e^{-bS_t} + \hat{d}S_t$.

There is no closed form expression to solve this analytically. We will show that the behavior of R_0 via the Next Generation Matrix Method will indicate the stability of the two-cycle.

Next Generation Matrix Method for the 2-cycle

In Section 1.3, we introduced the Next Generation Matrix Method. Using similar notation to that in Section 1.3.2, we obtain that new infections to infected compartments and transitions in infected compartments are respectively given by:

$$F_j = \begin{bmatrix} -\hat{d}z_{j\infty}\theta\Phi'_I(0) & -\hat{d}z_{j\infty}\hat{\theta}\Phi'_V(0) \\ 0 & 0 \end{bmatrix},$$
$$T_j = \begin{bmatrix} \hat{d}\hat{\mu} & 0 \\ \hat{d}_v\delta & \hat{d}_v \end{bmatrix},$$

where $z_{j\infty}$ denote the points in the j-cycle.

Here, we take $j = 2$ for the two-cycle, which leaves us with:

$$F_1 + T_1 = \begin{bmatrix} -\hat{d}z_{1\infty}\theta\Phi'_I(0) + \hat{d}\hat{\mu} & -\hat{d}z_{1\infty}\hat{\theta}\Phi'_V(0) \\ \hat{d}_v\delta & \hat{d}_v \end{bmatrix}, \tag{3.16}$$
$$F_2 + T_2 = \begin{bmatrix} -\hat{d}z_{2\infty}\theta\Phi'_I(0) + \hat{d}\hat{\mu} & -\hat{d}z_{2\infty}\hat{\theta}\Phi'_V(0) \\ \hat{d}_v\delta & \hat{d}_v \end{bmatrix}.$$

Using the results from Section 1.3.2, particularly that:

$$\tilde{\mathcal{T}} = T_kT_k...T_1,$$
$$\tilde{\mathcal{F}} = (F_k + T_k)(F_{k-1} + T_{k-1})...(F_1 + T_1) - \tilde{\mathcal{T}},$$

we get:

$$\tilde{\mathcal{T}} = T_2T_1, \tag{3.17}$$
$$\tilde{\mathcal{F}} = (F_2 + T_2)(F_1 + T_1) - \tilde{\mathcal{T}}.$$

Now, we are concerned with $\rho\big(\tilde{\mathcal{F}}(I - \tilde{\mathcal{T}})^{-1}\big)$, and so we see that:

$$(I - \tilde{\mathcal{T}})^{-1} = \begin{bmatrix} \frac{1}{1-\hat{d}^2\hat{\mu}^2} & 0 \\ \frac{\delta\hat{d}\hat{\mu}\hat{d}_v + \hat{d_v}^2\delta}{\left(1-\hat{d}^2\hat{\mu}^2\right)\left(1-\hat{d_v}^2\right)} & \frac{1}{1-\hat{d_v}^2} \end{bmatrix},$$
$$\tilde{\mathcal{F}} = \begin{bmatrix} f_{11} & f_{12} \\ -\hat{d}\hat{d}_v\delta\theta\Phi_I'(0)z_{1\infty} & -\hat{d}\hat{d}_v\delta\hat{\theta}\Phi_V'(0)z_{1\infty} \end{bmatrix},$$

again where I is the identity matrix, $(\cdot)^{-1}$ denotes the usual matrix inverse, and the expressions for f_{11} and f_{12} are given [4] by:

$$f_{11} = \hat{d}^2\theta^2(\Phi_I{}'(0))^2 z_{1\infty}z_{2\infty} - \hat{d}^2\hat{\mu}\Phi'_I(0)(z_{1\infty}+z_{2\infty}) - \hat{d}\hat{d}_v\delta\hat{\theta}\Phi_V{}'(0)z_{2\infty},$$
$$f_{12} = \hat{d}^2\theta\Phi_I{}'(0)\hat{\theta}z_{1\infty}z_{2\infty} - \hat{d}^2\hat{\mu}\Phi'_V(0)\hat{\theta}z_{1\infty} - \hat{d}\hat{d}_v\hat{\theta}\Phi'_V(0)z_{2\infty}.$$

As we do not have closed form solutions for $z_{1\infty}$ and $z_{2\infty}$, we do not have an explicit formula for R_0. However, we can use this analytical expression (for a fixed set of parameter choices and thus for fixed $z_{j\infty}, j \in \{1,2\}$) to explore interesting bifurcations for parameters that do not change the fixed points.

3.3.3 Stability Analysis in the Presence of Infection

Derived earlier in Equation 3.1, the full ISAv model is given by:

$$f(S_t,V_t,I_t) = S_{t+1} = rS_t\,\mathbf{g}(\mathbf{S_t}) + \hat{d}S_t\big(\theta\Phi_I(I_t) + \hat{\theta}\Phi_V(V_t)\big),$$
$$g(S_t,V_t,I_t) = I_{t+1} = \hat{d}\bigg(S_t\big(\theta\widehat{\Phi_I}(I_t) + \hat{\theta}\widehat{\Phi_V}(V_t)\big) + \hat{\mu}I_t\bigg),$$
$$h(S_t,V_t,I_t) = V_{t+1} = \widehat{d_v}(V_t + \delta I_t),$$

where $\mathbf{g}(\mathbf{S_t}) = e^{-bS_t}$. Recall from Equation 1.11 in the Section 1.2.4 that the Liapunov exponent for a system of discrete differential equations is defined as:

$$\lambda(\vec{x}_0) = \lim_{t\to\infty}\frac{1}{t}\ln\left[\rho\bigg(\prod_{k=0}^{t-1}J(\vec{x}_0)\bigg)\right].$$

where $J(\cdot)$ is the Jacobian of the system. Thus, we can define the Jacobian for the ISAv model as:

$$J = \begin{bmatrix} \dfrac{\partial f}{\partial S} & \dfrac{\partial f}{\partial I} & \dfrac{\partial f}{\partial V} \\ \dfrac{\partial g}{\partial S} & \dfrac{\partial g}{\partial I} & \dfrac{\partial g}{\partial V} \\ \dfrac{\partial h}{\partial S} & \dfrac{\partial h}{\partial I} & \dfrac{\partial h}{\partial V} \end{bmatrix}.$$

Thus, substituting in the partials from the full ISAv model in the presence of infection, we obtain:

$$J = \begin{bmatrix} re^{-bS_t} - bre^{-bS_t} + \widehat{d}(\theta e^{-\beta_I I_t} + \widehat{\theta} e^{-\beta_V V_t}) & -\theta\, \widehat{d}\, \beta_I S_t e^{-\beta_I I_t} & -\widehat{\theta}\, \widehat{d}\, \beta_V S_t e^{-\beta_V V_t} \\ \widehat{d}\, \theta(1 - e^{-\beta_I I_t}) + \widehat{d}\, \widehat{\theta}(1 - e^{-\beta_V V_t}) & \widehat{d}\, \theta\, S_t\, \beta_I e^{-\beta_I I_t} + \widehat{d}\widehat{\mu} & \widehat{d}\, S_t\, \widehat{\theta}\, \beta_V e^{-\beta_V V_t} \\ 0 & \widehat{d}_v \delta & \widehat{d}_v \end{bmatrix} \tag{3.18}$$

As all of the parameters are known, (see Table 5.1), we can derive some numerical results about the Liapunov exponent here.

Bifurcation along the Intrinsic Growth Rate

Similar to the case in the absence of infection, we varied the intrinsic growth rate as the bifurcation parameter and found interesting numerical results. We eliminated transient dynamics by running each simulation for 5000 time steps and varying $r \in [0, 150]$ by a step size of 0.5. For each fixed value of r, we se the initial conditions to be $S_0 = 150$, $I_0 = 20$, $V_0 = 30$.

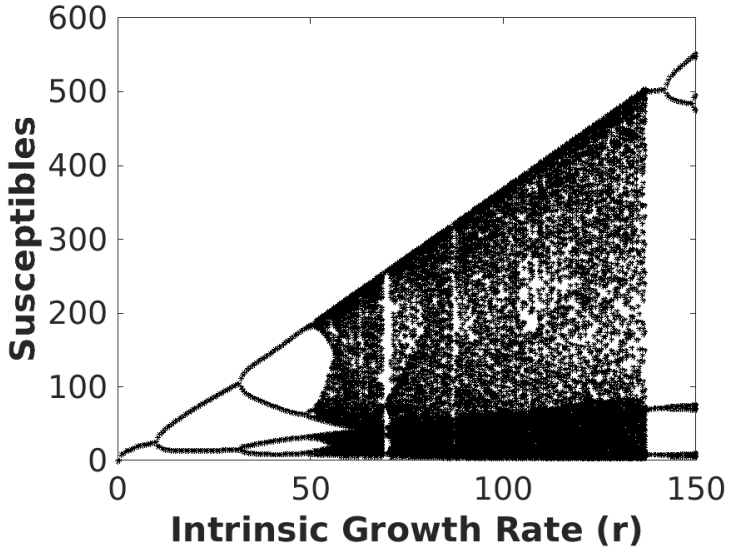

Figure 3.5: Bifurcation plot for the intrinsic growth rate r as the bifurcation parameter against susceptible salmon. We vary $r \in [0, 150]$ with fixed initial conditions of $S_0 = 150$, $I_0 = 20$, $V_0 = 30$.

The bifurcation structure above in Figure 3.5 is extremely interesting as it appears to be

period doubling cascading into chaotic behavior. In the following subsection we derive some results about the Liapunov exponent which add further evidence of chaotic behavior.

Liapunov Exponents

In Section 1.2.4, we introduced the Liapunov exponent as a metric for determining chaotic behavior of a dynamical system. In Figure 3.6, we plot the Liapunov exponent and the L^∞ norm as the intrisinc growth rate, r, is varied. To create Figure 3.6, we eliminate transient dynamics by running the model for 5000 time steps before starting our Liapunov calculation for 16 iterations.

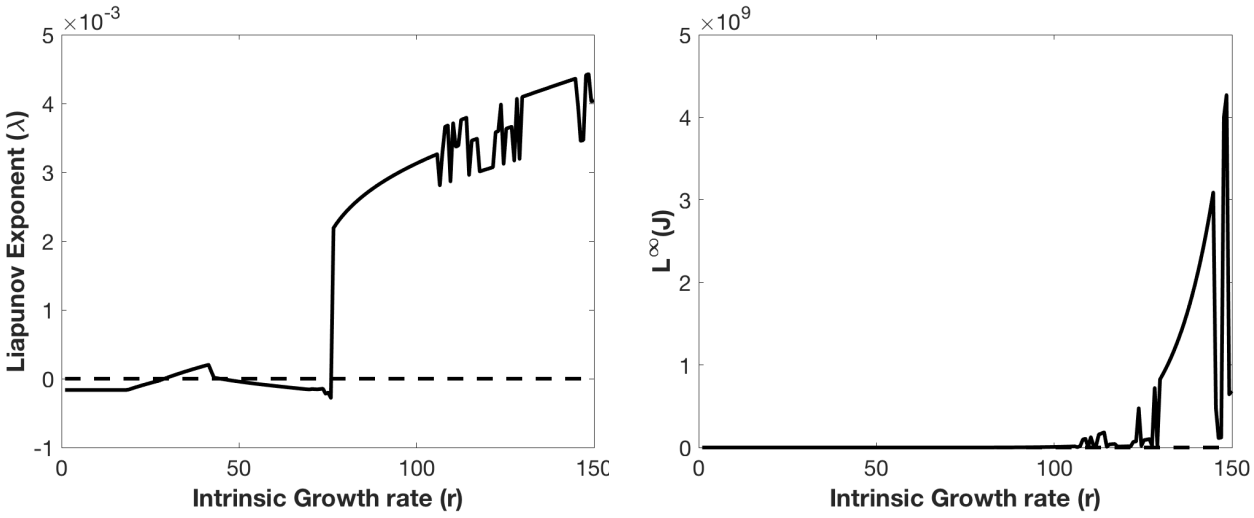

(a) Liapunov exponent (b) L^∞ norm for the Jacobian of the ISAv model

Figure 3.6: Liapunov exponent as intrinsic growth rate r is varied in $(0, 150]$ for a fixed initial condition of $S_0 = 150$, $I_0 = 20$, $V_0 = 30$. All other parameters are found in Table 3.1.

We see that this echoes the same results found in Figure 3.4; i.e. for a fixed probability of death of $d = 0.50$ there is a regime in which the system is stable ($\lambda < 0$) and a region in which the system appears to be chaotic ($\lambda > 0$). To add further evidence we also provide the L^∞ norm at each step also to show that it bounds the Liapunov exponent above. We see that $L^\infty(J) = 0$ when $\lambda < 0$ and grows large when $\lambda > 0$.

Bifurcations and Liapunov Exponent for the Probability of Death

We repeat the same process (of both the Bifurcation and Liapunov exponent calculation) now with a fixed intrinsic growth rate of $r = 100$ and vary the probability of death, d, with the same initial conditions and transient elimination.

The results in Figure 3.7 are also consistent with those in Figure 3.4. For example, we choose this nontypical value of $r = 100$ so that it demonstrates the changing behavior in the presence of infection which is consistent with the unique value count behavior demonstrated below in the subsection. Although we compare qualitative results, i.e. similarity of how sensitive the (r, d) space is demonstrated in Figure 3.4, we produce the same plot in the presence of infection.

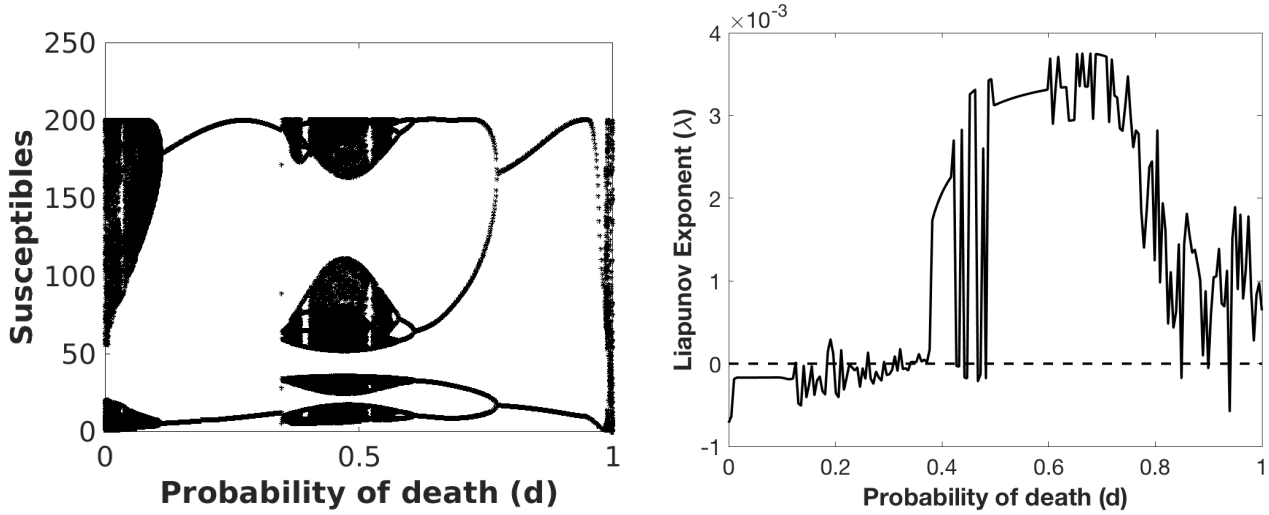

(a) Bifurcation Plot (b) Liapunov Exponent

Figure 3.7: The left hand side indicates a numerical bifurcation plot for the ISAv model in the presence of infection as the probability of death is varied from $[0, 1]$ against susceptible salmon. The right hand side indicates the calculation of the Liapunov exponent for the same set of conditions. In both cases, the initial conditions are fixed at $S_0 = 150$, $I_0 = 20$, $V_0 = 30$.

Bifurcations along two parameters with Infection

Similar to the case of no infection, we eliminate transient dynamics by running the simulation for 5000 time steps before analyzing unique value count behavior (for each pair of (r, d)). We see some structure as before, though it seems that there is a much larger region which could be potential chaotic behavior (i.e. more than nine unique values). We use the same initial conditions with the Liapunov exponent calculations given above in Figures 3.7 and 3.6 which aids to the argument chaotic behavior is ocurring (i.e. see fixed value of $r = 100$ as d is varied with respect to Figure 3.7).

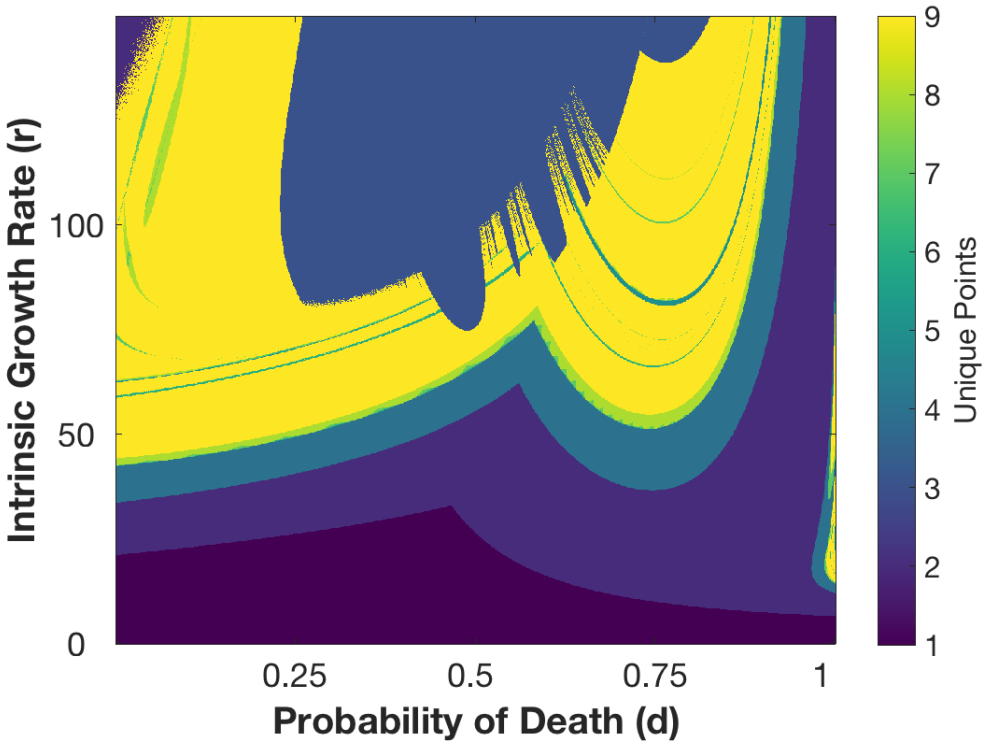

Figure 3.8: Unique values of the ISAv model in the presence of infection as the intrinsic growth rate and probability of death are varied. Here, $r \in [1, 150]$, $d \in (0, 1)$, and $b = 0.1$ with $S_0 = 150$, $I_0 = 20$, and $V_0 = 30$.

Although this is only evidence for a single initial condition of $S_0 = 150$, $I_0 = 20$, and $V_0 = 30$, it provides strong evidence of chaotic behavior which is useful as a base line comparison for alternative models proposed in Chapter 4.

3.4 Summary

This Chapter has introduced the ISAv model [4], derived analysis about the basic reproductive number, and stability criterion. We repeat some analysis from [4] and use classical results such as [19] to demonstrate for a fixed initial condition (both in the absence and presence of infection) chaotic behavior is occurring as the Liapunov exponent is strictly positive for particular choices of the intrinsic growth rate r and the probability of death d. Additionally, we provide insight into what the (r, d) space looks like in terms of number of unique values (a potential metric for cycle behavior) as we vary r and d simultaneously. While the number of unique values does not necessarily equal the cycle count, it aids to the explanation of chaotic behavior and sensitive dependence of both initial conditions and parameter choices.

Chapter 4

Alternate Versions of the ISAv Model

In Chapter 3, we examined the original ISAv model with the Ricker density dependent function. This model exhibited interesting bifurcation structures as we varied the intrinsic growth rate and probability of death. We examined this behavior both in the absence and presence of infection.

In this chapter, we repeat this analysis for various other functional forms for density dependence introduced in Section 2.2. Additionally, we analyze the bifurcation structures of a modification of the ISAv model with no free virus population (i.e. only susceptible and infected salmon).

We derive stability criterion for two functional forms and compare and contrast the bifurcation structures for all seven functional forms for the key parameters highlighted above. We also discuss results about the Liapunov exponent for the models with substituted functional forms to show they exhibit chaotic behavior for a fixed set of initial conditions.

4.1 Functional forms for density dependence

We focus on two functional forms introduced in Section 2.2: $f_5(N) = \frac{1}{1+(aN)^b}$ and (the normalized) $f_7(N) = \frac{1}{c+e^{bN-a}}$, where N is population size and $a, b \in \mathbb{R}$. We examine these functional forms with parameters taken from the literature [3] and from fitting the Ricker function. We will see that these two forms are largely representative of the different qualitative behavior exhibited by the other forms (which are included in the Section 2.2).

4.1.1 Functional Form $\mathbf{f_5(N)}$

As given in Equation 3.1, we have the generic ISAv model:

$$\begin{aligned} S_{t+1} &= rS_t\mathbf{g}(\mathbf{S_t}) + \hat{d}S_t\big(\theta\Phi_I(I_t) + \hat{\theta}\Phi_V(V_t)\big), \\ I_{t+1} &= \hat{d}\Bigg(S_t\big(\theta\widehat{\Phi_I}(I_t) + \hat{\theta}\widehat{\Phi_V}(V_t)\big) + \hat{\mu}I_t\Bigg), \\ V_{t+1} &= \widehat{d_v}(V_t + \delta I_t), \end{aligned}$$

where previously the $\mathbf{g}(\mathbf{S_t})$ was the Ricker recruitment function. We recall the functional form which we denoted $f_5(N)$ in Section 2.2, given as:

$$f(N) = \frac{1}{1\ + (aN)^b},$$

which can be written in terms of the ISAv model as:

$$\mathbf{g}(\mathbf{S_t}) = \frac{1}{1\ + (aS_t)^b}. \tag{4.1}$$

In Section 4.2.1, we derive stability conditions for the susceptible salmon population in the absence of infection with the functional form given in Equation 4.1.

4.1.2 Functional Form $\mathbf{f_7(N)}$

Similar to the previous section, we propose using the functional form from Section 2.2 (Table 2.2) which we call $f_7(N)$. This particular form is given by:

$$f(N) = \frac{1}{c + e^{bN-a}},$$

which in terms of the ISAv model can be rewritten as:

$$\mathbf{g}(\mathbf{S_t}) = \frac{1}{c + e^{bS_t-a}}, \tag{4.2}$$

again where $c = 1-e^{-a}$ is the scaling parameter to make the functional form start at 1 when the population is 0.

In Section 4.2, we discuss stability criterion both in the presence and absence of infection for the functional form.

4.2 Stability analysis for modified functional forms for density dependence

We examine the stability of the ISAv model with the modified functional forms in the absence of infection. We will see that although similar (relative to mathematical properties discussed in Section 1.1.2) they produce drastically different dynamics and bifurcation structures.

4.2.1 Stability in the Absence of Infection for $\mathbf{f_5(N)}$

In the absence of infection, i.e. $I_t = V_t = 0$, the ISAv model reduces to:

$$S_{t+1} = rS_t\,\mathbf{g}(\mathbf{S_t}) + \widehat{d}S_t.$$

Note that the functional form for density dependence does not alter the infected salmon or viral populations. In Section 3.2, we derived stability conditions in the absence of infection with the Ricker density dependent function (See Equation 3.10). Similarly, using the f_5 we obtain the eqation:

$$S_{t+1} = \frac{rS_t}{1\ + (aS_t)^b} + \widehat{d}S_t.$$

Therefore, setting $S_t = S_{t+1} = S^*$, we see that:

$$\begin{aligned} S^* &= \frac{rS^*}{1\ + (aS^*)^b} + \widehat{d}S^* \\ \iff (1-\widehat{d}) &= \frac{r}{1\ + (aS^*)^b} \\ \iff R_d - 1 &= (aS^*)^b \\ \iff \qquad S^* &= \frac{(R_d-1)^{1/b}}{a}, \end{aligned} \tag{4.3}$$

where $R_d = \frac{r}{d}$. This gives a closed form expression for the fixed point in the absence of infection with the functional form, f_5. This will be locally asymptotically stable if the following conditions hold:

$$\begin{aligned} &|S^*| \leq 1 \\ \iff &\left|\frac{(R_d-1)^{1/b}}{a}\right| \leq 1 \\ \iff &(-a)^b + 1 \leq R_d \leq a^b + 1. \end{aligned} \tag{4.4}$$

In general the biological relevant choices of r and d will lead to the expression derived in Equation 4.4 not being satisfied. In particular, with a value of $b < 1$, we see that

the population becomes arbitrarily large (though not necessarily unbounded) leading to interesting dynamic behavior that may not necessarily be attributed to chaos.

In order to think about this critically, we show numerical examples similar to that of Figure 3.4 in which we vary r and d simultaneously to analyze unique value counts with the new functional form. First we examine the population dynamics that exhibit arbitrarily large populations.

Numerical Results

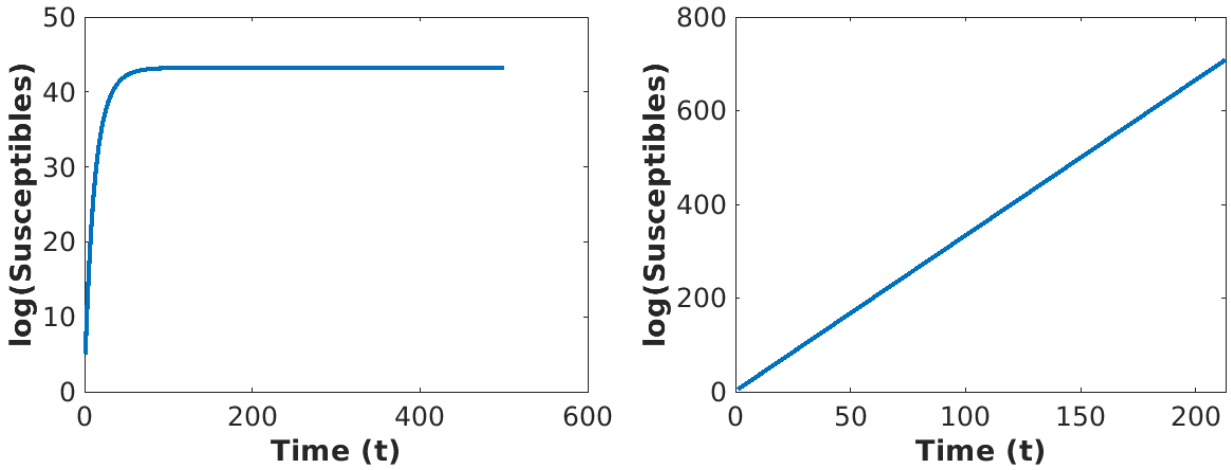

(a) $a = 2.8$, and $b = 0.1$.

(b) $a = 1.99$, and $b = 1.67 \times 10^{-9}$.

Figure 4.1: The dynamics of the ISAv model with the functional form given by $f_5(N)$ from Section 2.2 to incorporate density dependence. Both populations become arbitrarily large with the fitted parameters (right) leading to arguably unbounded population levels.

Clearly we see that in the absence of infection with the use for the functional form $f_5(N)$ as the density dependence function, the susceptible population grows arbitrarily large.

We also vary the probability of death and intrinsic growth rate simultaneously. In Figure 4.2 we vary both the probability of death and intrinsic growth rate, similar to Section 3.3.3, and count the number of population values we observe.

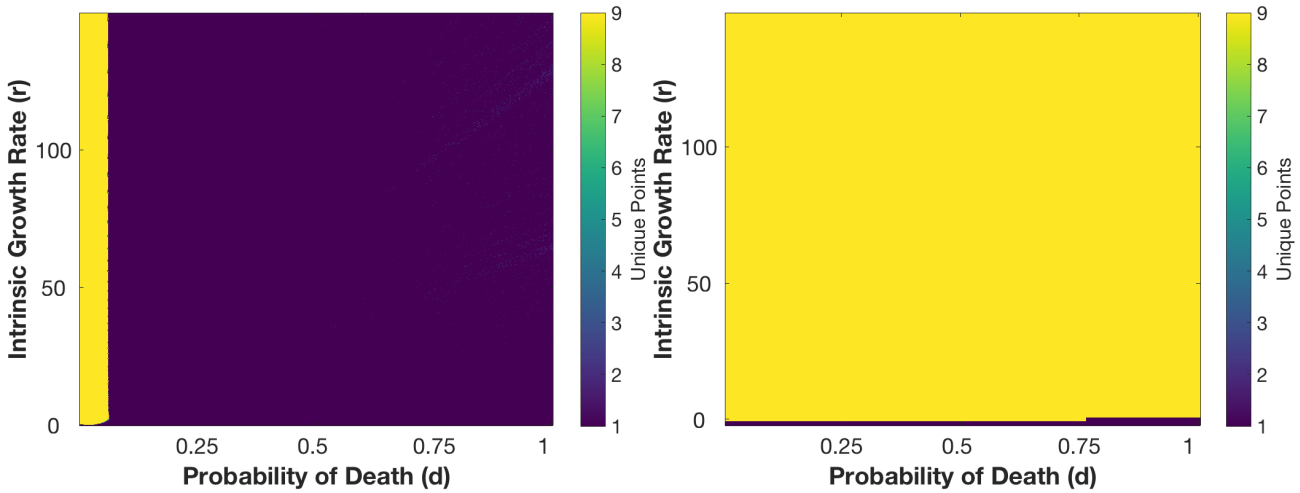

(a) $a = 2.8$, and $b = 0.1$.

(b) $a = 1.99$, and $b = 1.67 \times 10^{-9}$.

Figure 4.2: The unique value behavior of the ISAv model in the absence of infection with $f_5(N)$ as the density dependence. In this plot, we take the literature values from [3, 4] against the fitted values from our curve fitting in Section 2.3.

In Figure 4.2(a) we fix $b = 0.1$ as before, and take $a = 2.8$ [3]. We see that for low probability of death we observe a behavior with cycle length greater than nine. Although this situation may not be biologically feasible, it is certainly different than the structure observed in the original ISAv model in the absence of infection (see Figure 3.4). We also see that much of the region is a single unique value, this corresponds to the dynamics tendining to zero. In particular, the susceptible salmon population goes to zero as the probability of death becomes arbitrarily high for this set of parameters.

In contrast, when we fit parameters to observe behavior similar to the Ricker function from Section 3.2, the behavior is very different. In Figure 4.2(b) there is a small window of the intrinsic growth rate r just greater than one such that we have a single stable fixed point (i.e. where Equation 4.4 is satisfied). In general, most of the behavior appears to be of more unique values.

Although it is tempting to attribute this to potentially chaotic behavior, Figure 4.1 yields a different explanation. In the case of the literature parameters [3, 4] (left both plots) we see that the population becomes arbitrarily large and settles at a single fixed point. However, for the fitted parameters from Section 2.3, (right both plots), the population continually grows to arguably unbounded levels, hence producing a unique value at each time step (causing Figure 4.2(b) to be completely yellow).

Liapunov Exponent

The behavior of unique values in the absence of infection for the ISAv model with $f_5(N)$ as the functional form for density dependence can be attributed to the large growing population (and in particular $b < 1$). We omit the use of Liapunov exponents in this case as they do not show the evidence of chaos, and it is likely not occurring.

4.2.2 Stability in the Presence of Infection for $f_5(N)$

We derived the Jacobian for the original ISAv model, specifically in Equation 3.18. By substituting in the functional form f_7, given by Equation 4.1, the only entry of the Jacobian matrix that changes is $J(1,1) = \frac{\partial f}{\partial S}$. This gives the Jacobian matrix as:

$$J = \begin{bmatrix} \frac{r[1+(a^b - ba^{b-1})S_t^b]}{[1+(aS_t)^b]^2} + \widehat{d}(\theta e^{-\beta_I I_t} + \widehat{\theta} e^{-\beta_V V_t}) & -\theta\, \widehat{d}\, \beta_I S_t e^{-\beta_I I_t} & -\widehat{\theta}\, \widehat{d}\, \beta_V S_t e^{-\beta_V V_t} \\ \widehat{d}\, \theta(1 - e^{-\beta_I I_t}) + \widehat{d}\, \widehat{\theta}(1 - e^{-\beta_V V_t}) & \widehat{d}\, \theta\, S_t\, \beta_I e^{-\beta_I I_t} + \widehat{d}\widehat{\mu} & \widehat{d}\, S_t\, \widehat{\theta}\, \beta_V e^{-\beta_V V_t} \\ 0 & \widehat{d}_v \delta & \widehat{d}_v \end{bmatrix} \tag{4.5}$$

We use this to numerically examine stability.

Numerical Results

Similar to the case of no infection for this functional form, we see that the population becomes arbitrarily large.

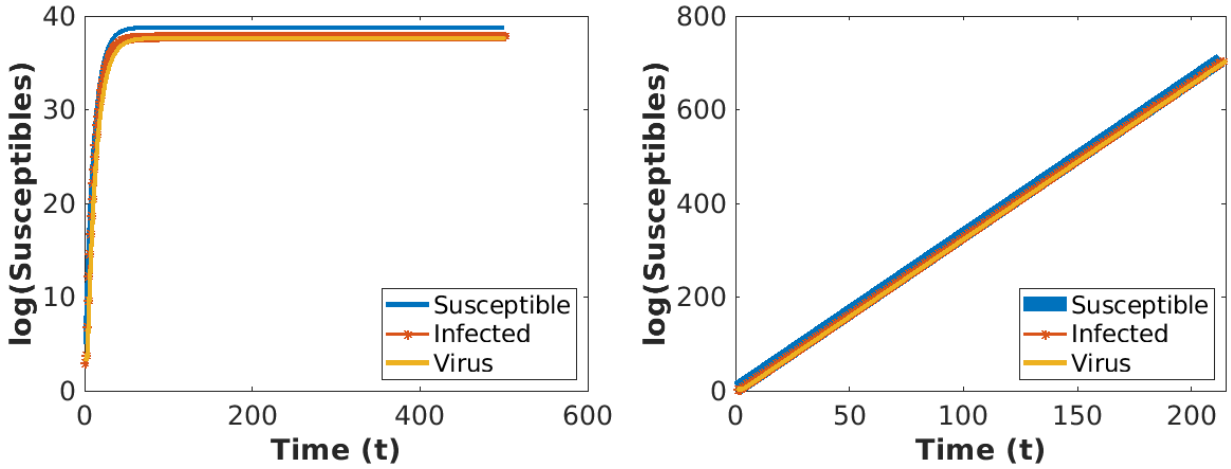

(a) $a = 2.8$ and $b = 0.1$.

(b) $a = 1.99$, and $b = 1.67 \times 10^{-9}$.

Figure 4.3: Population dynamics for the modified ISAv model with $f_5(N)$ as the density dependence function in the presence of infection with both literature-based and fitted parameter sets.

In particular, we see that in Figure 4.3(b) (i.e. the fitted parameters) the population is plotted on a log scale and becomes increasing large as soon as the first fifty time steps. This likely leads to the number of unique value results we explore below.

We vary both the probability of death and the intrinsic growth rate simultaneously. We see strikingly similar results to that of the ISAv model with $f_5(N)$ as the density dependent function in the absence of infection. In particular, the literature-based parameters exhibit mostly stable regimes or low unique value counts for nearly all of the (r, d) space considered. However, this corresponds to the susceptible salmon population tending to a (nonzero) fixed point as the population does not die off.

As we move to the fitted parameters we see the behavior changes drastically and nearly all of the parameter space exhibits many different values across 1000 iterations.

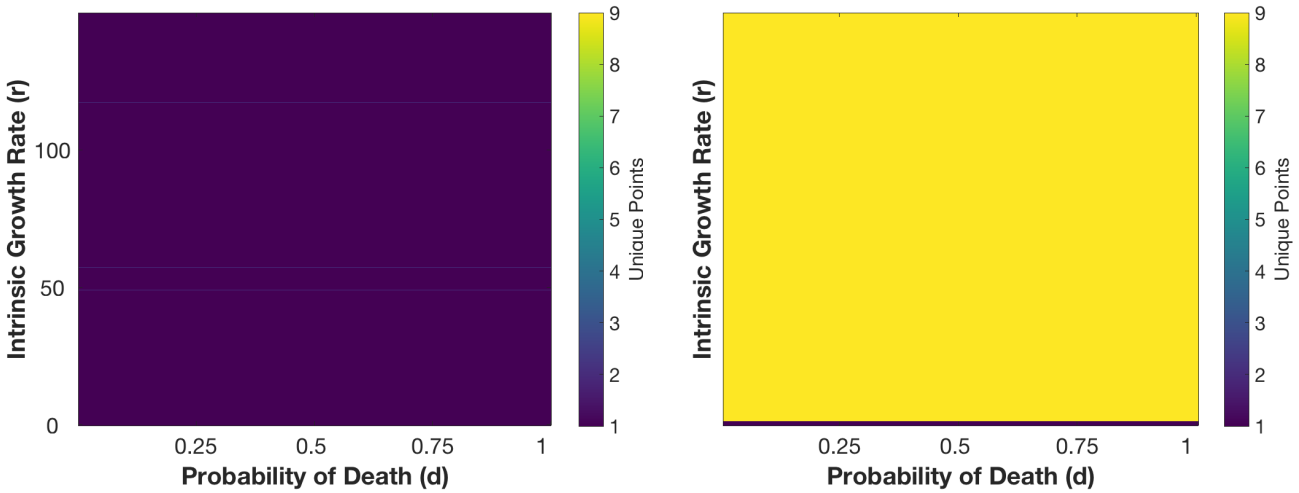

(a) $a = 2.8$ and $b = 0.1$. (b) $a = 1.99$, and $b = 1.67 \times 10^{-9}$.

Figure 4.4: Long time behavior for the modified ISAv model with $f_5(N)$ as the density dependence function in the presence of infection with both literature-based and fitted parameter sets.

As with the case of the $f_5(N)$ function used for density dependence in the absence of infection, unique value behavior is observed due to the unboudedness of the model (particularly with $b < 1$) and not necessarily because of chaotic behavior.

Liapunov Exponent

The Liapunov exponent for this functional form is omitted as chaotic behavior is not ocurring.

4.2.3 Stability in the Absence of Infection for $\mathbf{f_7(N)}$

We now consider the use of the functional form $f_7(N)$. In the absence of infection, we set $I_t = V_t = 0$, and the ISAv model becomes:

$$S_{t+1} = rS_t\,\mathbf{g}(\mathbf{S_t}) + \widehat{d}S_t.$$

Substituting in the functional form $f_7(N)$, in terms of the ISAv model notation gives:

$$S_{t+1} = \frac{rS_t}{c + e^{bS_t - a}} + \widehat{d}S_t,$$

again where $c = 1 - e^{-a}$ is the scaling parameter described previously.

In order to derive stability criterion, we set $S_t = S_{t+1} = S^*$, and see this expression becomes:

$$S^* = \frac{rS^*}{c + e^{bS^* - a}} + \widehat{d}S^*.$$

Now, rearranging and solving for S^*, leaves us with the (nontrivial) fixed point in the absence of infection as:

$$S^* = \frac{\ln(R_d - c) + a}{b}, \tag{4.6}$$

where $R_d = \frac{r}{d}$. Now, in order to determine when this fixed point is stable, we examine the stability condition:

$$\begin{aligned} & |S^*| \leq 1 \\ \iff & |\ln(R_d - c) + a| \leq b \\ \iff & e^{-b-a} + c \leq R_d \leq e^{b-a} + c. \end{aligned} \tag{4.7}$$

This is a particularly narrow range given that in general the choices for a, b are taken from narrow ranges also.

Numerical Results

In the case of the ISAv model with $f_7(N)$ for the density dependent function form, we observe interesting bifurcation structure as we vary the intrinsic growth rate r and the probability of death d simultaneously.

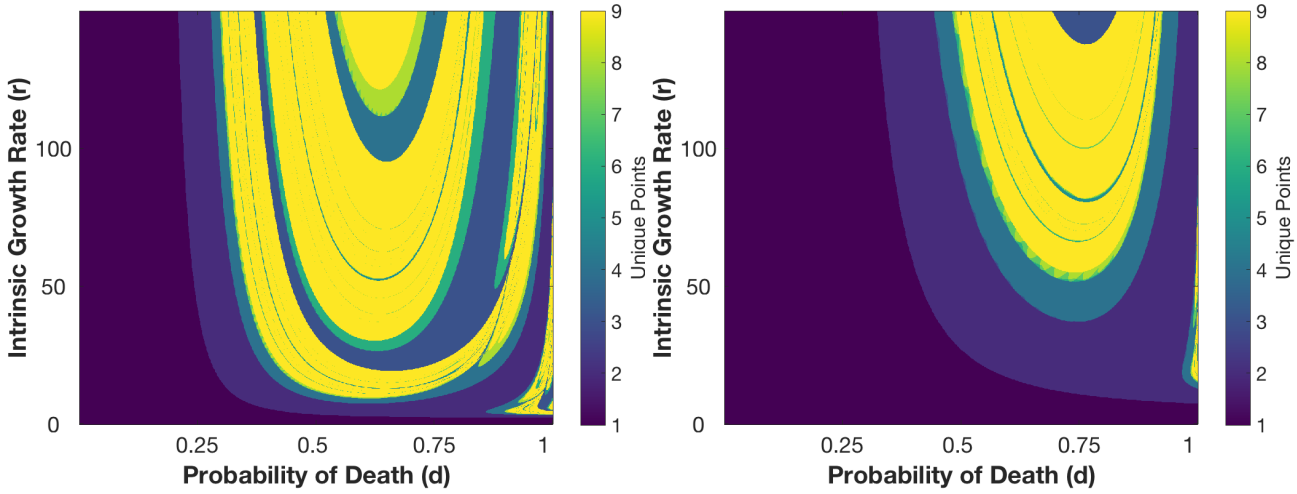

(a) $a = 2.8$, and $b = 0.1$.

(b) $a = 8.9 \times 10^{-3}$, and $b = 0.218$.

Figure 4.5: The long term behavior of the ISAv model in the absence of infection with $f_7(N)$ as the density dependent functional form. The figure compares the literature values from [3, 4] against the fitted values from Section 2.3.

We obtain Figure 4.5 by computing the number of unique values after 5000 time steps for each combination of (r, d) with a 1000×1000 mesh.

Specifically, in Figure 4.5(a) we observe clear cut regions where the long term behavior changes. Although qualitatively similar to Figure 4.5(b), the fited parameter set gives much larger regions where lower counts of unique values are observed. We see relatively similar structure (under both parameter sets) to the original Ricker recruitment function in the ISAv model (see Figure 3.4). In fact, we see extremely similar behavior in Figure 4.5(b) to that of the the original Ricker function which is expected, as the parameters were fitted to the Ricker function itself.

We examine the Liapunov exponents to further provide evidence for chaos.

Liapunov Exponents

As with the original ISAv model we calculate the Liapunov exponent by the formula defined in Section 1.2.4, and by eliminating the transient dynamics, i.e. running for 5000 time steps befor examining behavior.

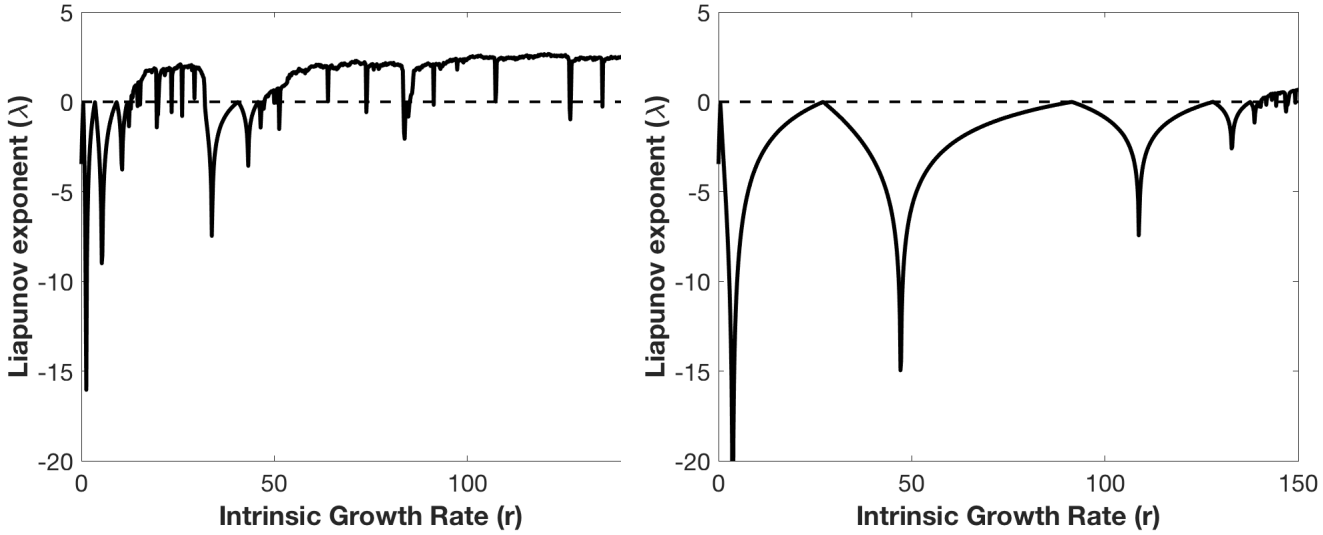

(a) Literature-based parameters $a = 2.8$ and $b = 0.1$.

(b) Fitted parameters $a = 8.9 \times 10^{-3}$, and $b = 0.218$.

Figure 4.6: The Liapunov exponent for the ISAv model with the functional form $f_7(N)$ as the intrinsic growth rate, r is varied for both literature-based and fitted parameters. $S_0 = 150$, $I_0 = 20$ and $V_0 = 30$. We fix the probability of death at $d = 0.50$.

Figure 4.6 demonstrates behavior consistent with that observed in the previous section (see Figure 4.5). In particular, we see that the literature-based parameter choices (left) produce

a larger region in which the Liapunov exponent is positive, indicating unstable behavior for these fixed initial conditions. On the other hand, we see that the fitted parameters produce a smaller region in which the Liapunov exponent is positive. This is consistent with the results seen in Figure 4.5. We omit the plots for the Liapunov exponent for a fixed value of the intrinsic growth rate r as we vary the probability of death d; these results tell the same story in consistency with the discussion above.

4.2.4 Stability in the Presence of Infection for $\mathbf{f_7(N)}$

Stability Criterion

As in Section 4.2.1, we see that the substitution of a modified functional form for density dependence only effects the first Jacobian entry $J(1,1) = \frac{\partial f}{\partial S}$. The new Jacobian given by substituting the functional form $f_7(N)$ is:

$$J = \begin{bmatrix} \frac{r[c+(1-bS_t)e^{bS_t-a}]}{(c+e^{bS_t-a})^2} + \widehat{d}(\theta e^{-\beta_I I_t} + \widehat{\theta} e^{-\beta_V V_t}) & -\theta\, \widehat{d}\, \beta_I S_t e^{-\beta_I I_t} & -\widehat{\theta}\, \widehat{d}\, \beta_V S_t e^{-\beta_V V_t} \\ \widehat{d}\, \theta(1 - e^{-\beta_I I_t}) + \widehat{d}\, \widehat{\theta}(1 - e^{-\beta_V V_t}) & \widehat{d}\, \theta\, S_t\, \beta_I e^{-\beta_I I_t} + \widehat{d}\widehat{\mu} & \widehat{d}\, S_t\, \widehat{\theta}\, \beta_V e^{-\beta_V V_t} \\ 0 & \widehat{d}_v \delta & \widehat{d}_v \end{bmatrix} \tag{4.8}$$

Numerical Results

Here we present the unique value count behavior for the ISAv model with $f_7(N)$ as the density dependence function in the susceptible population. We created a 1000×1000 mesh of (r, d) values and eliminated transient dynamics for 5000 time steps. We use the fixed initial condition of $S_0 = 150$, $I_0 = 20$, and $V_0 = 30$.

Figure 4.7 demonstrates the long term behavior for varied intrinsic growth rate and probability of death for the literature-based parameters and fitted parameters. In Figure 4.7(b), the use of the fitted parameter values demonstrates strikingly similar behavior to that of no infected population (see Figure 4.5). However, we see that the literature-based parameters in the presence of infection produce a much larger region in (r, d) space in which nine or more values are found. This indicates chaotic behavior is possible; we show some examples of the Liapunov exponent below that confirm this for a fixed initial condition.

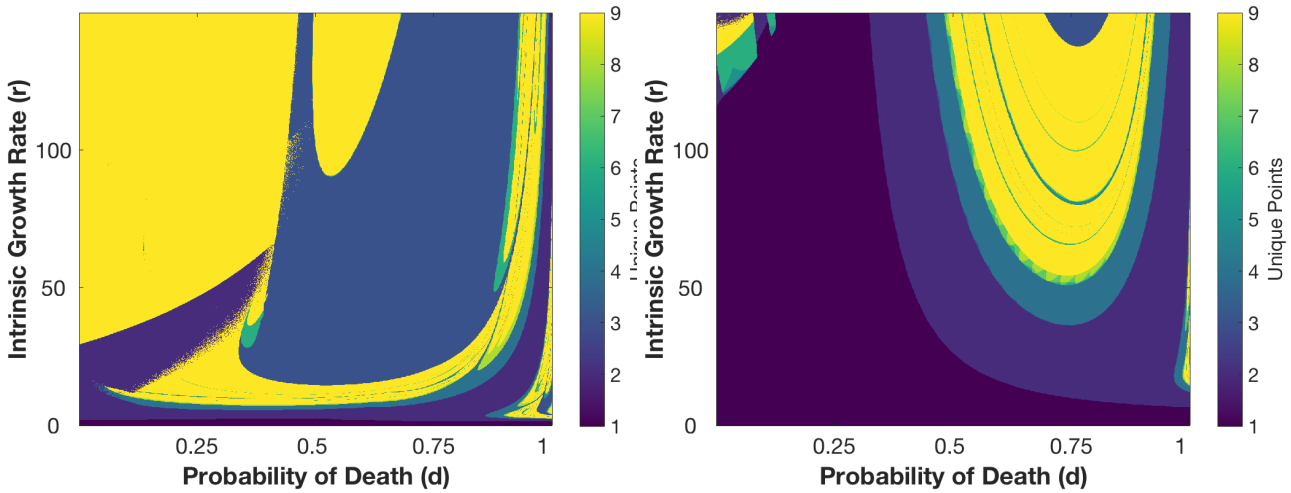

(a) $a = 2.8$, and $b = 0.1$.

(b) $a = 8.9 \times 10^{-3}$, and $b = 0.218$.

Figure 4.7: The long term behavior of the ISAv model in the presence of infection with $f_7(N)$ as the density dependent functional form. The figure compares the literature values against the fitted values from Section 2.3. The initial conditions are taken to be $S_0 = 150$, $I_0 = 20$, and $V_0 = 30$

Liapunov Exponents

We present the Liapunov exponent calculation for the varied intrinsic growth rate in the presence of infection with $f_7(N)$ as the density dependent function. We see that in Figure 4.8, unstable behavior is occurring as the Liapunov exponent becomes positive. This is further evidence that chaos is occurring for this fixed set of initial conditions.

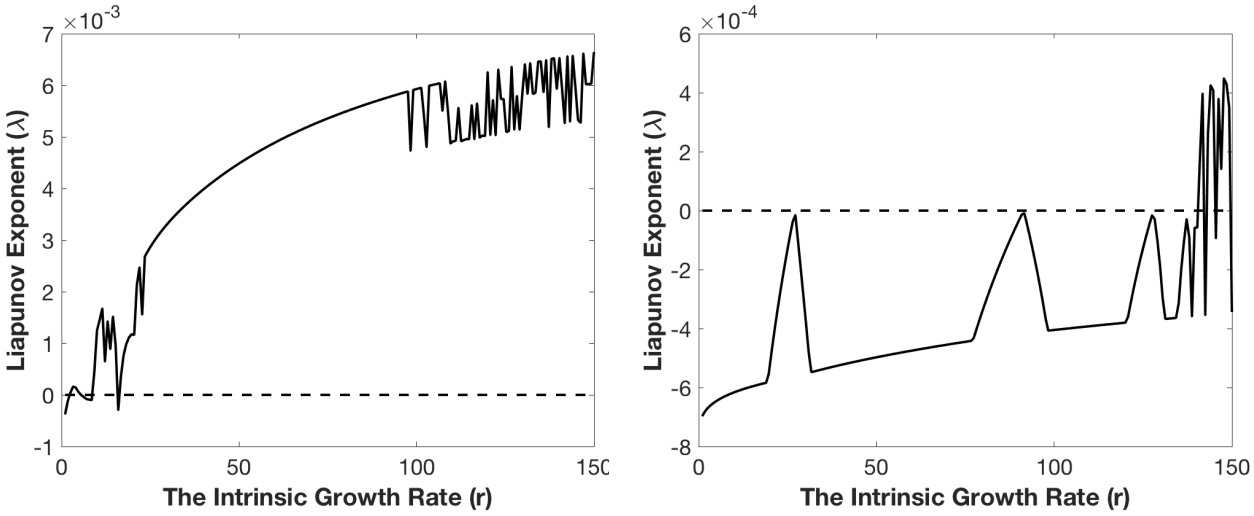

(a) Liapunov exponent $a = 2.8$ and $b = 0.1$.

(b) Liapunov Exponent $a = 8.9 \times 10^{-3}$, and $b = 0.218$.

Figure 4.8: Liapunov exponent from the ISAv model with $f_7(N)$ as the density dependent functional form as the intrinsic growth rate is varied for a fixed initial condition of $S_0 = 150$, $I_0 = 20$, $V_0 = 30$.

We perform the same analysis for varying the intrinsic growth rate r. We eliminate transient behavior of 5000 time steps and vary $r \in [1, 150]$ and find that with the literature parameters $\big($Figure 4.8(a) $\big)$ [3], there is a large region of chaotic behavior for a fixed value of $d = 0.5$. This is consistent with the results seen in Figure 4.7(a) above. Similarly, in the case of the fitted parameters, we see that there is chaotic behavior (i.e $.\lambda > 0$ as $r \to 150$) which is also consistent with Figure 4.7(b) above.

4.3 The ISAv Model without Virus Population

Here, we examine the model in the absence of the viral population; i.e. just include the susceptible and infected salmon. Consider setting the viral population to zero: $V_0 = 0$; and the fraction of salmon infected via contact with the virus to zero: $\widehat{\theta} = 0$. This leaves us with the following model:

$$\begin{aligned} f = S_{t+1} &= r S_t \, \mathbf{g}(\mathbf{S_t}) + \widehat{d} S_t \theta \Phi_I(I_t) \\ g = I_{t+1} &= \widehat{d}\big(S_t \theta \Phi_I(I_t)\big) + \widehat{\mu} I_t \end{aligned} \tag{4.9}$$

Stability Criterion

In the case of the original ISAv model which uses the Ricker function, Equation 4.9 becomes:

$$\begin{aligned} f = S_{t+1} &= rS_t e^{-bS_t} + \widehat{d}S_t\theta\Phi_I(I_t) \\ g = I_{t+1} &= \widehat{d}\big(S_t\theta\Phi_I(I_t)\big) + \widehat{\mu}I_t. \end{aligned} \tag{4.10}$$

Now, to find the fixed points of the system, we must satisfy:

$$\begin{aligned} f = S_{t+1} &= rS_t e^{-bS_t} + \widehat{d}S_t\theta\Phi_I(I_t) \\ g = I_{t+1} &= \widehat{d}\big(S_t\theta\Phi_I(I_t)\big) + \widehat{\mu}I_t. \end{aligned} \tag{4.11}$$

Computing both of the fixed points (in terms of the infecteds and susceptibles) we can obtain:

$$\begin{aligned} S^* &= \frac{\ln(r\hat{d}\theta) - \beta_I I^*}{b}, \\ \ln(\mu I^*) + \beta_I &= \ln(\hat{d}S^*\theta), \end{aligned}$$

which is in terms of the other fixed points. There is no closed form expression that exists for the fixed points explicitly in terms of parameters. However, we can still use this version of the fixed point expression to our advantage.

We compute the Jacobian in the absence of viral population by:

$$J = \begin{bmatrix} \frac{\partial f}{\partial S} & \frac{\partial f}{\partial I} \\ \\ \frac{\partial g}{\partial S} & \frac{\partial g}{\partial I} \end{bmatrix}$$

Substituting in each component, this becomes:

$$J = \begin{bmatrix} r\mathbf{g}(\mathbf{S_t}) + rS_t\mathbf{g}'(\mathbf{S_t}) + \widehat{d}\theta e^{-\beta_I I_t} & -\beta_I \widehat{d}S_t\theta e^{-\beta_I I_t} \\ \\ \widehat{d}\theta e^{-\beta_I I_t} & -\beta_I \widehat{d}S_t\theta e^{-\beta_I I_t} + \widehat{\mu} \end{bmatrix} \tag{4.12}$$

Here we consider the general ISAv model with the Ricker recruitment function, i.e. $f_2(N)$. Thus, the Jacobian is reduced to:

$$J = \begin{bmatrix} re^{-bS_t} - bre^{-bS_t} + \widehat{d}\theta e^{-\beta_I I_t} & -\beta_I \widehat{d} S_t \theta e^{-\beta_I I_t} \\ \widehat{d}\theta e^{-\beta_I I_t} & -\beta_I \widehat{d} S_t \theta e^{-\beta_I I_t} + \widehat{\mu} \end{bmatrix} \tag{4.13}$$

Numerical Results

We examine the bifurcation structure along the intrinsic growth rate and probability of death simultaneously by varying both and counting the number of unique values after transient dynamics. We see relatively similar qualitative behavior to previous versions of the model, in that there are several clear cut regions where low dimensional behavior is observed. However, there are areas that seem much more sensitive to exact combinations of (r, d).

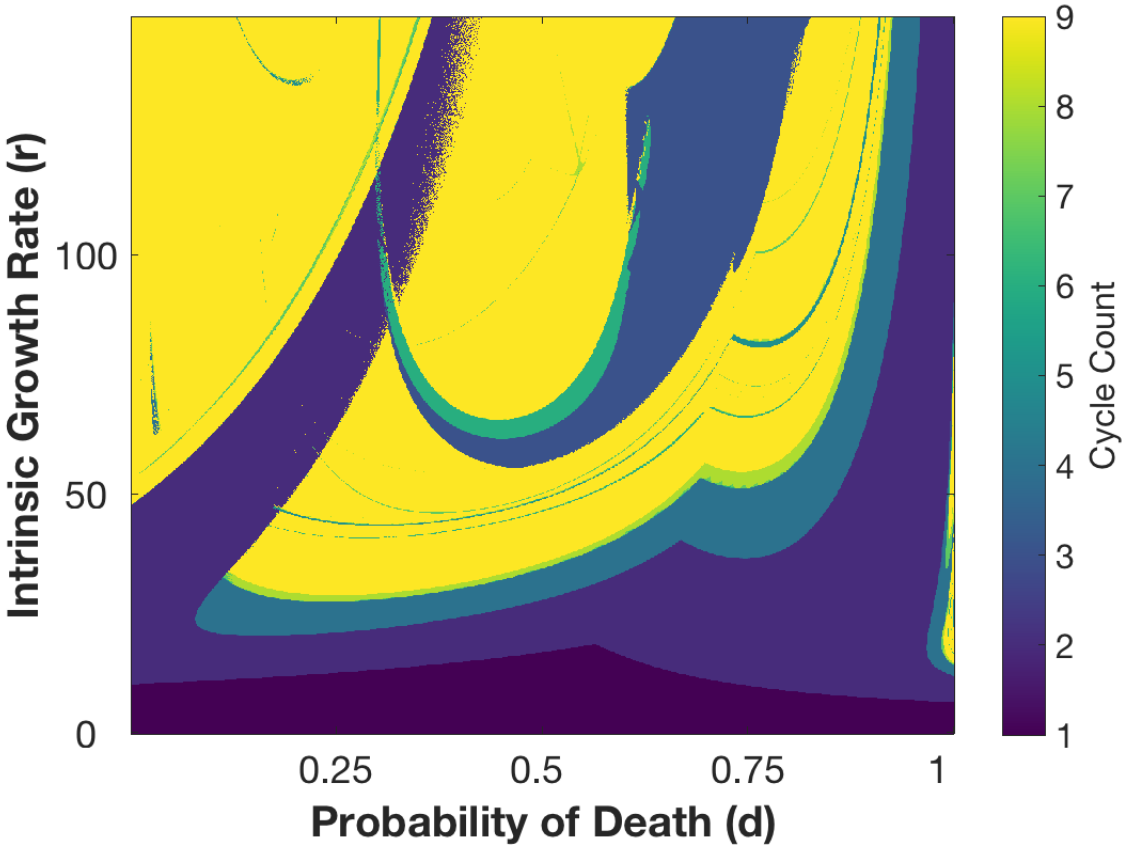

Figure 4.9: The long term behavior for the ISAv model with no viral compartment and the Ricker function as the density dependent function. $S_0 = 150$, $I_0 = 50$

We generate Figure 4.9 by eliminating transient behavior for 5000 time steps and varying

r and d simultaneously for an initial condition of $S_0 = 150$, $V_0 = 20$. We observe behavior that appears to be chaotic which we is consistent with our calculations for the Liapunov exponent.

Liapunov Exponents

We eliminate transient behavior by allowing the dynamics to run for 5000 time steps, and vary a single parameter (r) in order to calculate the Liapunov exponent. We note here that we choose the same initial conditions of $S_0 = 150$, and $I_0 = 25$.

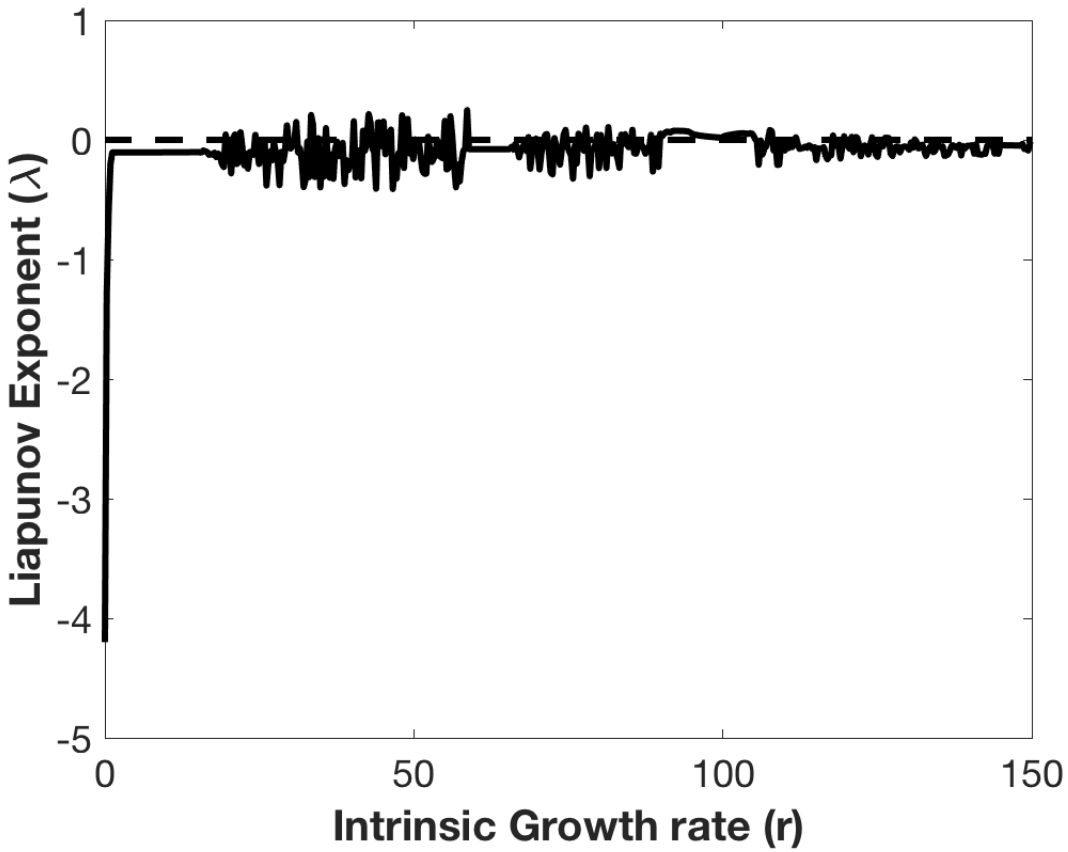

Figure 4.10: Liapunov exponent for the ISAv model in the absence of viral population with initial conditions $S_0 = 150$, $I_0 = 50$. We vary the intrinsic growth rate from $r \in [0, 150]$ for a fixed value of $d = 0.9$.

This is consistent with Figure 4.9. We take a different value of the probability of death than usual, (namely $d = 0.9$) to demonstrate the oscillation of the Liapunov exponent about the horizontal axis and sensititivty of (r, d) combinations. However, it is not entirely surprising

as we saw chaotic behavior in a population of susceptible salmon with no infected salmon or viral population.

4.4 Other Functional Forms

We saw in the Section 4.2 that the Ricker recruitment function and the functional form $f_7(N)$ gave interesting bifurcation diagrams along both the intrinsic growth rate (r) and the probability of death (d). The functional form $f_5(N)$ served as a baseline for 'uninteresting' bifurcation behavior along both parameters in both the absence and presence of infection.

In this section we present similar numerical results for the each of the other five functional forms given in Section 2.3, both in the absence and presence of infection, as well as with literature-based and fitted parameter sets. Most of the functional forms, though mathematically similar to Ricker and $f_7(N)$, do not exhibit similar bifurcation structures. However, we demonstrate that after fitting each of these functional forms (as described in Section 2.3), the fitted parameter choices cause the entire biologically relevant (r, d) space to become all uniquely valued. This is due to the fact that the functions grow arbitrarily large with the fitted parameter choice, much like $f_5(N)$ did in Section 4.2. For brevity, we omit the plots of the dynamics for each of the functional forms and only include the unique value counting plots.

In particular, we discuss the numerical results for functional forms f_1, f_3, f_4, and f_6 since forms f_5 and f_7 were discussed above and form f_2 is the original Ricker recruitment function. Table 4.1 gives the fitted values for a and b obtained via curve fitting described in Section 2.3. However, we also analyze each of the functional forms with literature-based parameters. In particular we take $a = 2.8$ [3] and $b = 0.1$ [3, 4].

In each of the following sections we omit the calculation of the Jacobian and the Liapunov exponents for each of the functional forms given here. We only provide the long term behavior as r and d are varied as baselines for comparison to the results discussed in other sections throughout this chapter.

Table 4.1: Functional Forms to Incorporate Density Dependence.

Function number	$f(N)$	Sign of $\frac{df^2}{dN^2}$	Fitted a	Fitted b	Reference
$f_1(N)$	N^{-b}	+	**X**	1.496×10^{-7}	[27]
$\mathbf{f_2(N)}$	$\mathbf{e^{-bN}}$	+	**X**	**0.1**	[7, 12, 17, 25, 26]
$f_3(N)$	$\frac{1}{1+aN}$	+	9.578×10^4	**X**	[8, 30]
$f_4(N)$	e^{-aN^b}	+,-	2.353	8.936×10^{-8}	[3]
$f_5(N)$	$\frac{1}{1+(aN)^b}$	+,-	1.9949	1.6668×10^{-9}	[31]
$f_6(N)$	$\frac{1}{(1+aN)^b}$	+	10	10	[32, 33]
$f_7(N)$	$\frac{1}{(c+e^{bN-a})}$	+,-	8.9473×10^{-7}	0.1	[9, 28, 29]

Functional Forms in the Absence of Infection with Literature-based Parameters

Figure 4.11 demonstrates the long term behavior for each functional form as the density dependent function in the ISAv model when $I_t = V_t = 0$. Functional forms f_1 and f_6 provide similar behavior to that of f_5 in the absence of infection with literature-based parameters. Namely, we see a small region of higher unique value count for extremely small probability of death; and stable behavior otherwise. We can think of the literature parameters as a 'lights off' scenario in which the majority of (r, d) space exhibits simple, stable behavior. This tiny region of 'lights on' space leads to arbitarily growing populations which has been confirmed with the dynamics.

We also observe that the other functional forms exhibit stable behavior for essentially all combinations of r and d in the space.

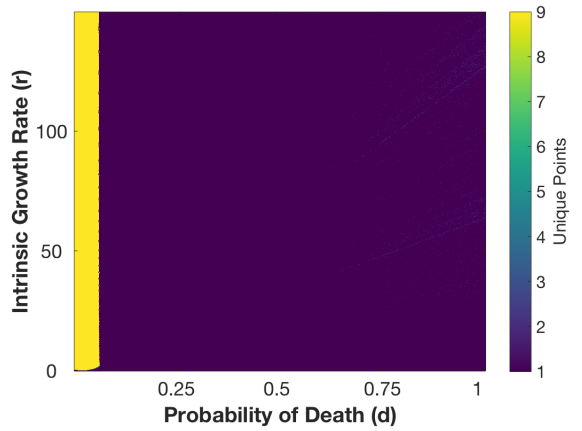

(a) The functional form $f_1(N)$.

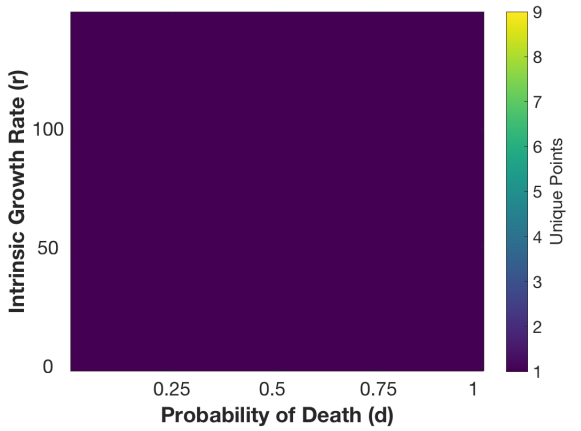

(b) The functional form $f_3(N)$.

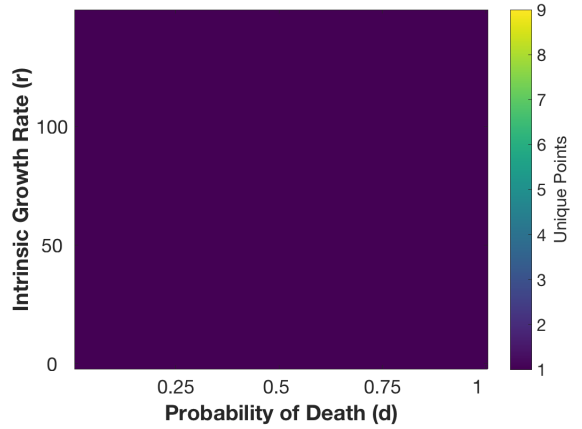

(c) The functional form $f_4(N)$.

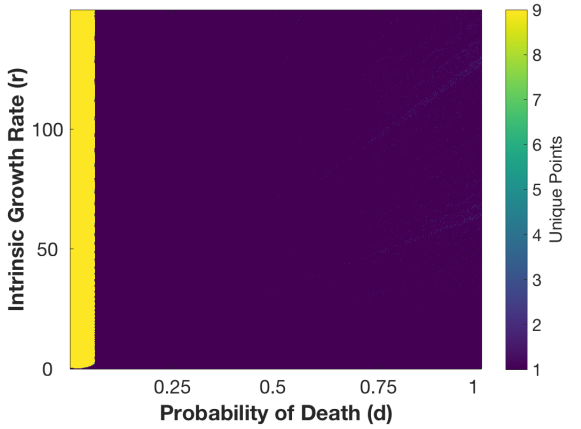

(d) The functional form $f_6(N)$.

Figure 4.11: The long term behavior for the ISAv model with the functional forms given by $f_{1,3,4,6}(N)$ to incorporate density dependence in the absence of infection with literature-based parameters. Parameter values can be found in Table 4.1

Functional Forms in the Presence of Infection with Literature-based Parameters

Similar to the case above in the absence of infection, we see that adding infection to the system with literature based parameters leaves nearly all of the relevant (r, d) space exhibiting stable behavior.

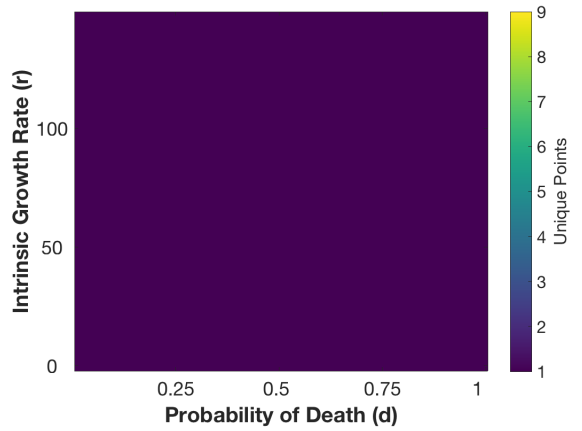

(a) The functional form $f_1(N)$.

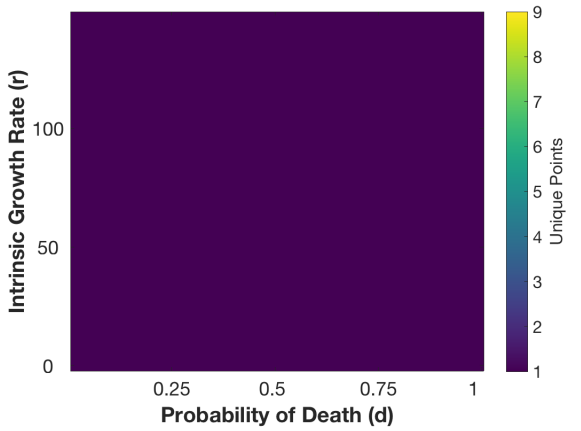

(b) The functional form $f_3(N)$.

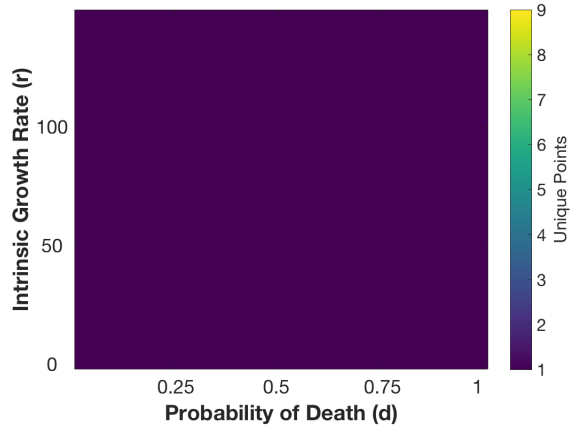

(c) The functional form $f_4(N)$.

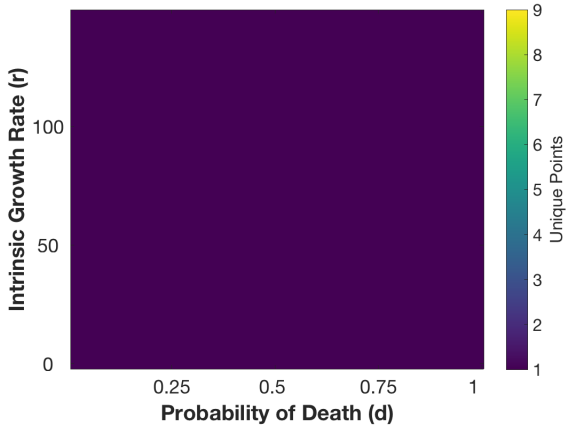

(d) The functional form $f_6(N)$.

Figure 4.12: The long term behavior for the ISAv model with the functional forms given by $f_{1,3,4,6}(N)$ to incorporate density dependence in the presence of infection with literature-based parameters. See Table 2.2.

Functional Forms in the Absence of Infection with fitted Parameters

We see that functional forms $f_1(N)$ and $f_4(N)$ exhibit the 'lights on' scenario in which the majority (or all) of the biologically relevant (r, d) space exhibit more than nine unique values. Unfortunately the functional forms $f_3(N)$ and $f_6(N)$ do not exhibit anything other than stable behavior. Examining simulations of the dynamics confirm that functional forms $f_1(N)$ and $f_4(N)$ have populations that grow arbitrarily large and do not actually exhibit chaotic behavior.

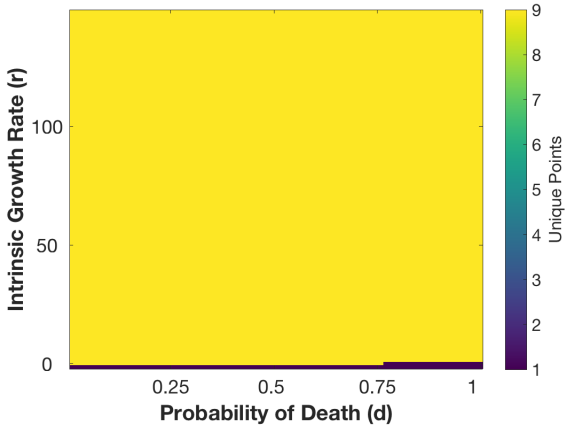

(a) The functional form $f_1(N)$.

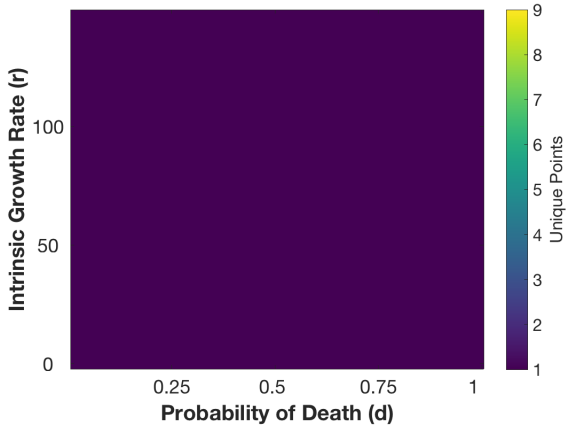

(b) The functional form $f_3(N)$.

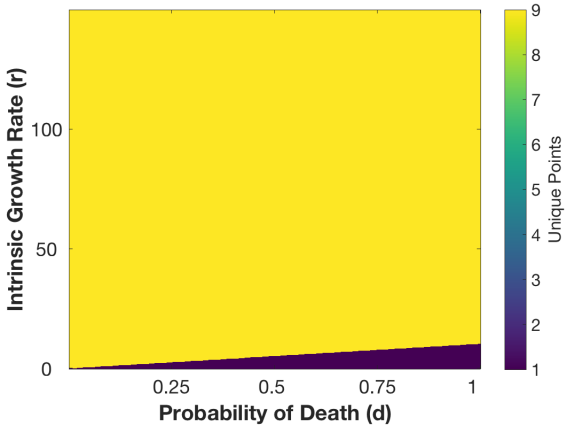

(c) The functional form $f_4(N)$.

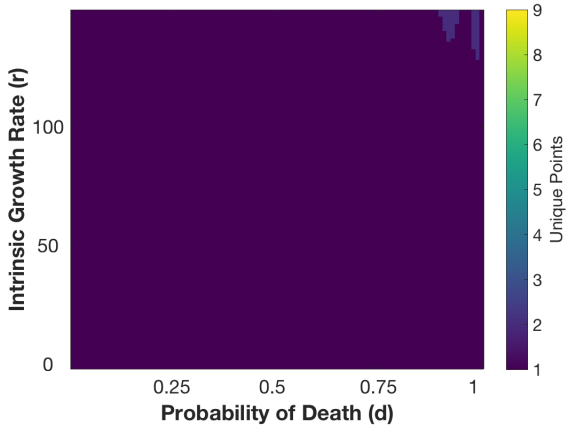

(d) The functional form $f_6(N)$.

Figure 4.13: The cycle count behavior for the ISAv model with the functional forms given by $f_{1,3,4,6}(N)$ to incorporate density dependence in the absence of infection with the optimal parameters.

Functional Forms in the Presence of Infection with fitted Parameters

We see in this section that adding infection to the system (as in the case with literature-based parameters) largely leaves the qualitative behavior of the cycle counts unchanged. In particular, $f_1(N)$ and $f_4(N)$ still exhibit unique value counts for nearly all choices of r and d whereas $f_3(N)$ and $f_6(N)$ exhibit stable behavior. This was also confirmed by simulating the dynamics that there is no chaotic behavior occuring; the population continually grows.

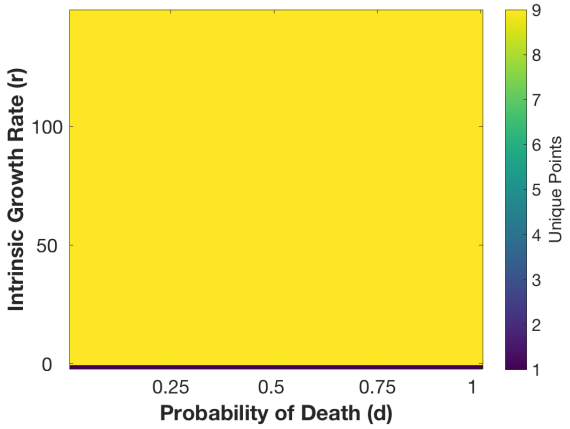

(a) The functional form $f_1(N)$.

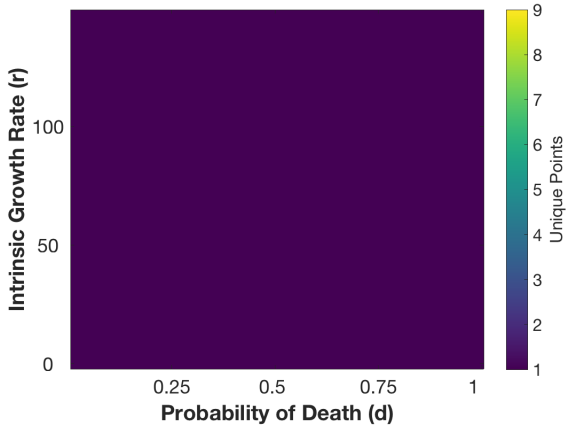

(b) The functional form $f_3(N)$.

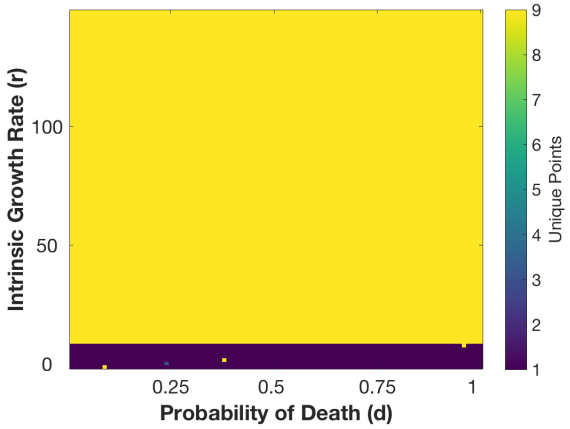

(c) The functional form $f_4(N)$.

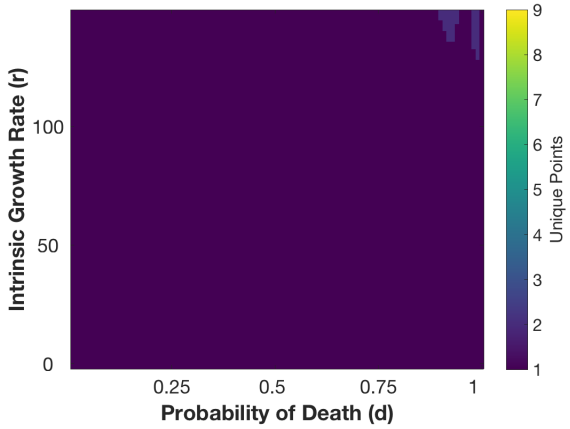

(d) The functional form $f_6(N)$.

Figure 4.14: The long term behavior for the ISAv model with the functional forms given by $f_{1,3,4,6}(N)$ to incorporate density dependence in the presence of infection with the optimal parameters.

4.5 Summary

Each of these plots in Figures 4.11- 4.14 served as important baseline metrics for behavior exhibited elsewhere. In particular we saw in the case of the original Ricker recruitment function and the functional form $f_7(N) = \frac{1}{c+e^{bN-a}}$ we exhibit interesting unique value count behavior which was shown to be chaotic for fixed initial conditions (in the absence and presence of infection). This chapter has shown that mathematically similar functional forms can exhibit drastically different dynamics, even when they are fitted (via polynomial interpolation) to the 'baseline' Ricker function. In Chapter 5 we begin thinking about bifurcation structures beyond that of only the intrinsic growth rate and probability of death.

Chapter 5

Numerical Bifurcation Examples of the ISAv Model

In Chapter 4 we analyze the bifurcation structures along both the intrinsic growth rate (r) and the probability of death (d) both in the presence & absence of infection, and with various functional forms in the susceptible population of salmon to incorporate density dependence. The choices of analyzing r and d are natural as they appear in the fixed points and their stability.

In this chapter, we return to the definition of the basic reproductive number described in Section 1.3. The basic reproductive number, denoted R_0 is the number of secondary infection cases at a given time step based on previous infection cases. In Section 3.3.2, we derived an analytical expression for the basic reproductive number for parameter choices that keep the model in a stable two-cycle regime.

Here, we vary the basic reproductive number (which is an expression of other parameters) by varying each parameter in the original ISAv model. For brevity, we leave this analysis in the case of other functional forms for future work.

It is important to recognize here that although the majority of Chapter 4 was focused on the intrinsic growth rate and probability of death, each of the other parameters plays a key role in the basic reproductive number and brings their own unique bifurcation structure to the model as they are varied. Many of these parameters do not appear in the model when there is no infection or virus (i.e. $I_0 = V_0 = 0$) and so the analysis in the absence of infection is omitted.

5.1 Behavior of R_0 in the Presence of Infection

As we recall from Chapter 3, the parameters r and d both change the fixed point of the ISAv model, i.e. the expression for R_d, or the components of cycles, $z_{j\infty}$. Here, we observe what appears to be chaos for the parameters that do not change the fixed points $\{z_{1\infty}, z_{2\infty}\}$. In particular the following parameters are varied (as they all appear in the expression of R_0 derived in the previous chapter): δ, μ, d_v, θ, as well as the transmission constants β_I, and β_V. We will take standard fixed values of various parameters which are given below here in Table 5.1. We examine a single bifurcation parameter and fix the other parameters with respect to those below unless specifically stated [4].

Table 5.1: Common fixed values for parameters unless otherwise stated.

Parameter	**Biological Description**	**Fixed Value**
b	Scaling parameter for the population size.	0.1
r	Intrinsic growth rate.	e^4
β_V	Poisson constant for infection transmission from the viral population.	0.01
β_I	Poisson constant for infection transmission from the infected salmon.	0.056
θ	Fraction of salmon that become infected via contact with infected salmon.	0.6
$\hat{d}$	Probability of survival.	0.5
$\widehat{d_v}$	The constant fraction of virus that persists.	0.8
$\widehat{\mu}$	The fraction of ISA infectious salmon that survive.	0.3
δ	The virus shed at a given time step.	0.2

In each of the following sections, we plot the bifurcation diagram by solving the dynamics for 5000 time steps (i.e. getting rid of any transient behavior), and plot the last 100 time steps for the desired bifurcation parameter specified. Unless otherwise stated, it can be assumed that all non-bifurcation parameters take the constant values given in Table 5.1.

5.2 The Fraction of Infected Salmon that Survive

As noted in Table 3.1, recall that $\hat{\mu}$ is the fraction of infected salmon that survive. Therefore, $1 - \hat{\mu} = \mu$ is the fraction of infected salmon that do not survive. In Figure 5.1, we vary $\mu \in [0, 1]$. The plot on the left depicts a bifurcation diagram for a fixed transmission probability constant of $\beta_I = 0.046$, whereas the plot on the right depicts $\beta_I = 0.056$. The authors from [4] have marked β_I as a parameter that plays a large role in the dynamics and

stability as well. In a later section we vary both transmission constants β_I and β_V. For each bifurcation plot, we vary the parameter described in the range denoted on the plot, and we calculate the basic reproductive number and plot it against the number of individuals infected.

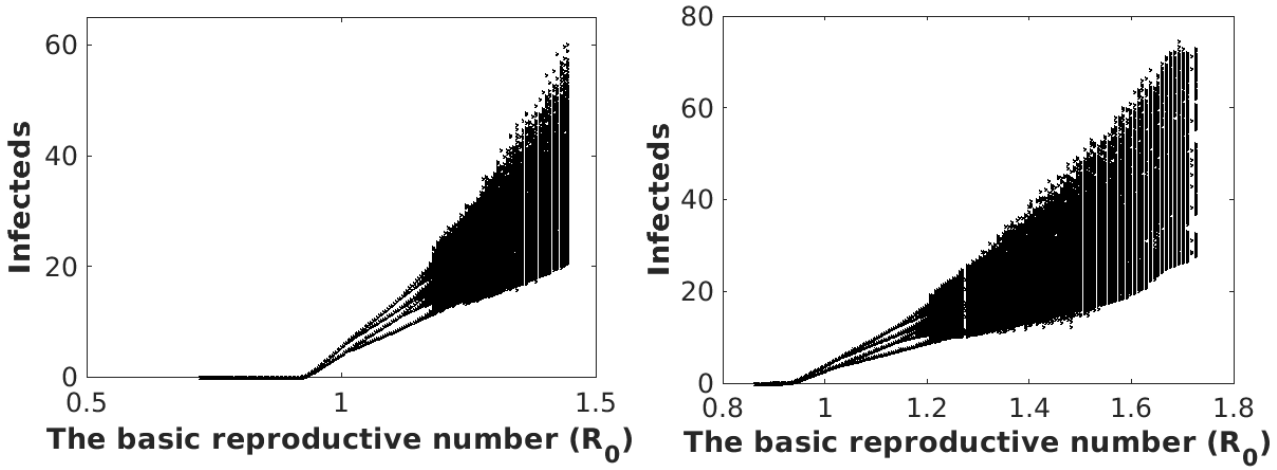

(a) $\beta_I = 0.046$. (b) $\beta_I = 0.056$.

Figure 5.1: The bifurcation diagram as we vary the fraction of infected salmon that survive, μ, for different transmission constants. We take the initial conditions of $S_0 = 150$, $I_0 = 20$, and $V_0 = 30$.

As we see in Figure 5.1, the value of the transmission constant (β_I) doesn't alter the structure of the bifurcation appearing here. At the critical value of $R_0 = 1$, we see the appearance of stable infected populations. As R_0 increases, we see period-doubling bifurcations, that lead to regions that appear chaotic. Note that $\mu \notin [0, 1]$ is outside the realm of biological relevance (as it is a probability) which explains the abrupt end in both plots as well as slight difference in the axes. It does appear that as $\mu \to 1$ (the fraction of infected salmon that are dying) behavior appears to be chaotic. Most notably, R_0 is significantly greater than 1 which means most salmon do not die due to disease.

5.3 The Fraction of Salmon that become infected via contact

Recall that in Table 3.1, we define θ as the fraction of salmon that become infected via contact with an infected salmon. Therefore $\hat{\theta} = 1 - \theta$ is the fraction of salmon that become infected via contact with the virus directly. Both of these fractions are intertwined with the functions $\widehat{\Phi_I}$: the probability that susceptible salmon become infected via contact with the

infected salmon; and $\widehat{\Phi_V}$: the probability that salmon become infected via contact with the virus. Therefore, the $\widehat{\Phi}$ functions govern the probability contact happens and θ (or $\widehat{\theta}$) are the fraction affected presuming the event from $\widehat{\Phi}$ happens.

We vary $\theta \in [0, 1]$ as the bifurcation parameter and fix both $\beta_I = 0.046$ and $\beta_I = 0.056$.

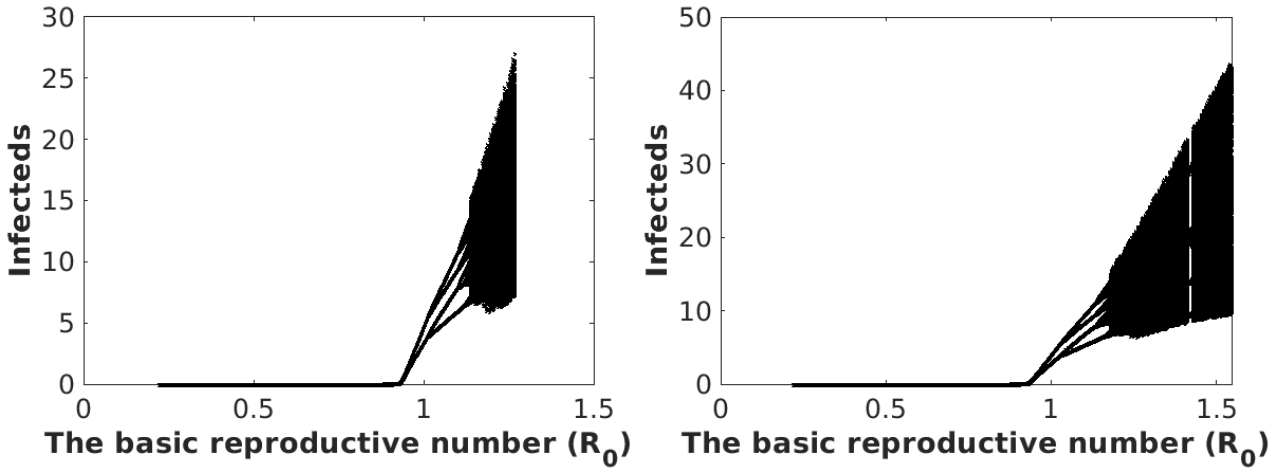

(a) A bifurcation diagram for the parameter θ as we fix $\beta_I = 0.046$.

(b) A bifurcation diagram for the parameter θ as we fix $\beta_I = 0.056$.

Figure 5.2: The bifurcation diagram as we vary the fraction of salmon that become infected via contact with other salmon, or the virus itself. In particular we vary $\theta \in [0, 1]$ for fixed infection transmission constants. We take initial conditions of $S_0 = 150$, $I_0 = 20$, $V_0 = 30$.

Similar to the case of the earlier section when we varied μ, we see in Figure 5.2 that as we increase the fraction of salmon that contact infected salmon, i.e. θ (as opposed to contact with the virus i.e. $\widehat{\theta}$) we obtain persistent infection at $R_0 = 1$ and what appears to be numerical evidence of cascading into chaotic behavior as R_0 increases. However it is not as evident as the points are more dense throughout. Again, since θ is bounded by 1, we do not bring these plots outside of the biological realm of significance.

5.4 Virus Shedding

Recall from the model given in Equation 3.1 that the virus shedding at a given time step only appears in the infected population, via:

$$V_{t+1} = \widehat{d_v}(V_t + \delta I_t).$$

The authors bound $\delta \in [0, 1]$, though as it is defined as the virus shed (at a given time step) per infected individual it need not be bounded in this way. Though there may be biologically

feasible bounds, we currently stay within the realm of $[0, 1]$ as given by the literature [4]. In Figure 5.3, the structure is strikingly similar to other bifurcation behavior in this chapter, namely the period doubling bifurcations we see above in the case of μ and θ.

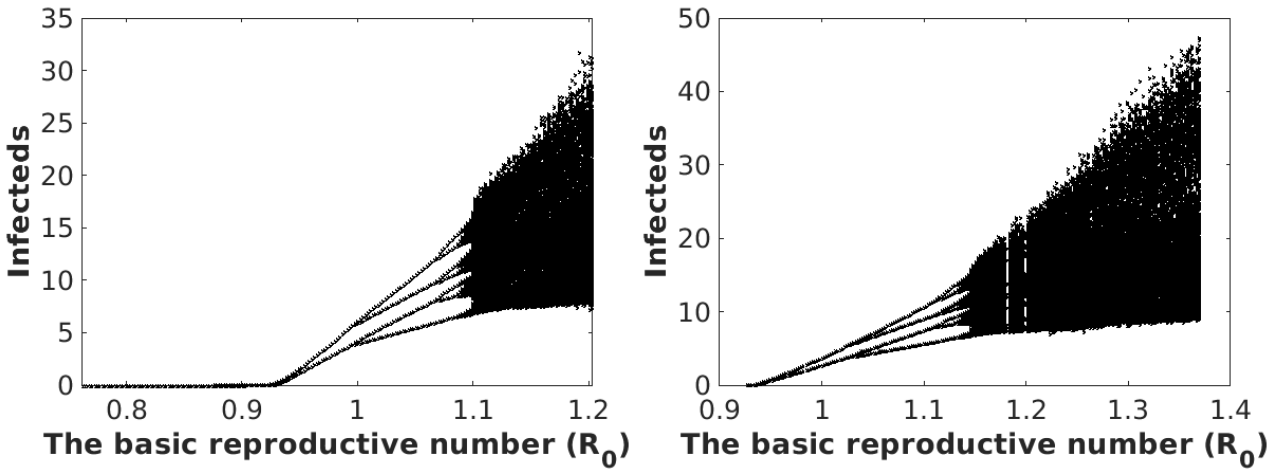

(a) $\beta_I = 0.046$. (b) $\beta_I = 0.056$.

Figure 5.3: The bifurcation diagram as we vary the virus shed at a given time step from $\delta \in [0, 1]$ for fixed infection transmission constants. We take initial conditions of $S_0 = 150$, $I_0 = 20$, $V_0 = 30$.

As evident in Figure 5.3, we observe an infected population appearing at $R_0 = 1$, and what appears to be period doubling to chaotic behavior (with some sort of density structure) as R_0 increases. We see that the transmission constant β_I does not affect the qualitative structure of the bifurcation diagram but opens up the range of the apparent chaotic behavior.

5.5 The Constant Fraction of the Virus that persists

As mentioned in Table 3.1, $\hat{d_v}$ is the fraction of the virus that persists at each time step. In this section we use $d_v = 1 - \hat{d_v}$ as the bifurcation parameter: the fraction of the virus that is lost. We take $d_v \in [0, 1]$ for fixed values of $\beta_I = 0.046$ and $\beta_I = 0.056$. In Figure 5.4 we see that the basic reproductive number R_0 gets large for both values of the transmission constant (β_I). Although these bifurcation diagrams have different qualitative behavior than the previous ones, we do see some structure for large R_0 values. Particularly in the case of the lower transmission constant it seems the k-cycle takes k extremely large. The bifurcation plot associated with the higher transmission constant has bounded regions in which the behavior lies (Figure 5.4(b)).

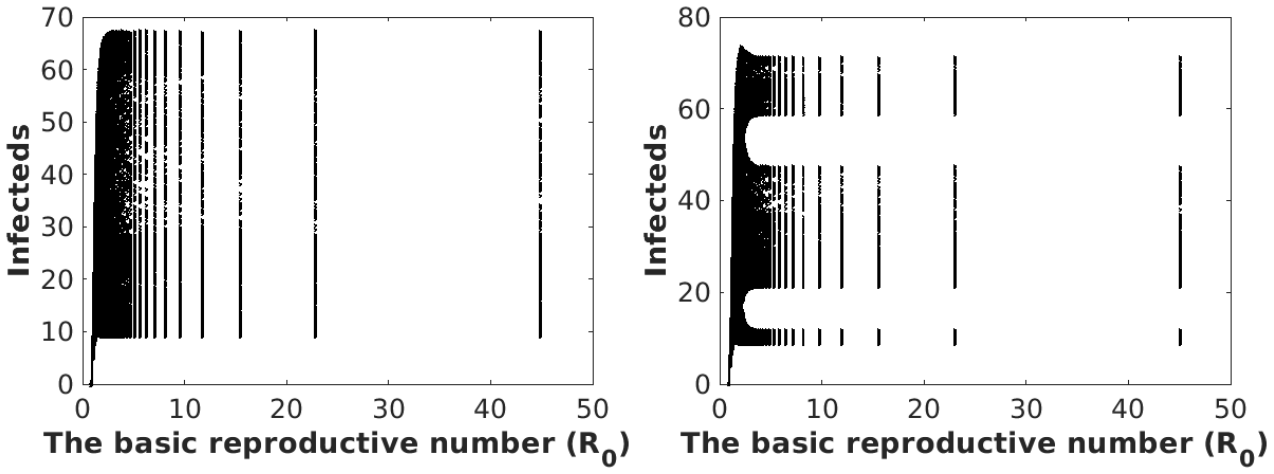

(a) $\beta_I = 0.046$. (b) $\beta_I = 0.056$.

Figure 5.4: The bifurcation diagram as we vary the fraction of the virus that does not survive, $d_v \in [0, 1]$ for two infection transmission constants. We take the fixed initial condition of $S_0 = 150$, $I_0 = 20$, $V_0 = 30$.

Although for very small R_0 we see behavior that could be interpreted as chaotic, the full pictures in Figure 5.4 reveal much more structure leading us to believe that the population cycle is large but bounded (and hence not chaotic).

As mentioned in the caption for Figure 5.4, we vary $d_v \in [0, 1]$, though we do so with 1000 points. The interesting structure we see gives the visual misrepresentation that and R_0 value of 30 does not exist. This is not necessarily the case. With the current mesh size and the probability bounds, there is not a particular value of d_v such that $R_0 = 30$. This can also be explained by the fact that the other parameters are fixed in the values from Table 5.1.

5.6 Infection Transmission Constants

Recall from Equation 3.5, we have that:

$$\Phi_I(I_t) = e^{-\beta_I I_t}, \tag{5.1}$$

$$\Phi_V(V_t) = e^{-\beta_V V_t},$$

where Φ_I and Φ_V are the probability that susceptible salmon do not become infected with the infected salmon and actual virus respectively [4]. In this section we vary both of the transmission constants β_I and β_V which allow the Φ functions to follow Poisson distributions. As β_I has been a particular parameter of interest in previous sections, we vary it completely from $[0, 1]$ as well as provide an in depth view next to it below in Figure 5.5.

Poisson Constant for Infection Transmission from Infected Salmon

We vary β_I, the transmission constant that represents the fraction of infection that is transmitted from salmon that are infected. The authors from [4] state that they vary this parameter and plot R_0, and achieve similar results to Figure 5.5(a). As we do not know how they varied R_0, it is difficult to precisely replicate the behavior they observe. Interestingly, in Figure 5.5(b) we see that bringing the infection transmission constant β_I all the way to one actually resumes behavior of a stable four-cycle. This behavior has not been observed in the ISAv model and has not been previously documented in infectious disease modeling.

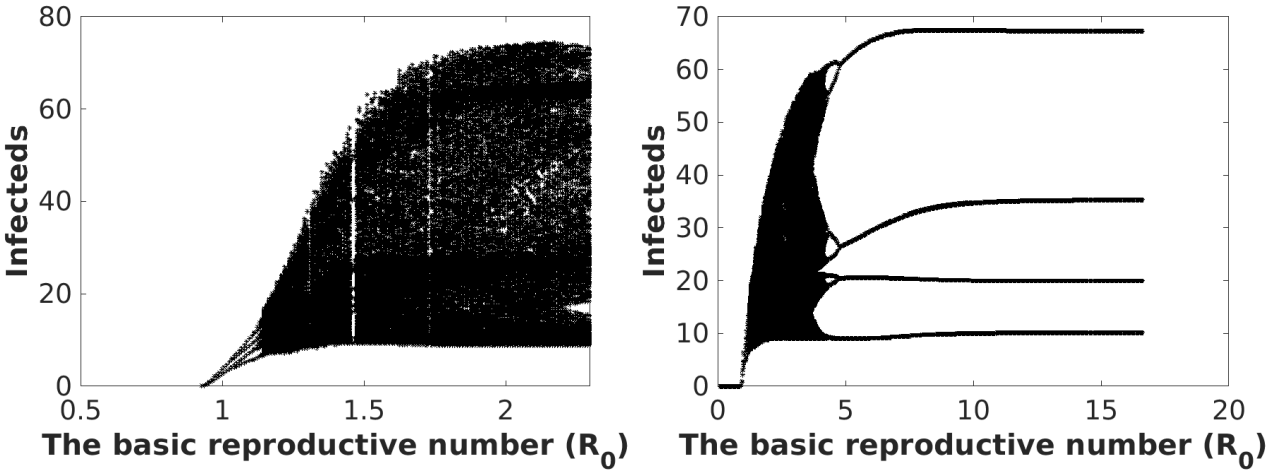

(a) The bifurcation diagram for R_0 for $\beta_I \in [0, 0.1]$.

(b) The bifurcation diagram for R_0 for $\beta_I \in [0, 1]$.

Figure 5.5: The bifurcation diagram for the infection transmission constant from infected salmon varied in $\beta_I \in [0, 1]$ which exhibits potentially chaotic behavior returning to a four cycle. We take initial conditions of $S_0 = 150$, $I_0 = 20$, $V_0 = 30$.

Poisson Constant for Infection Transmission from the Virus

We take $\beta_V \in [0, 1]$ for fixed $\beta_I = 0.056$. We recall that β_V is the transmission constant from the contact of the virus directly. We see behavior that could potentially be described as chaotic below.

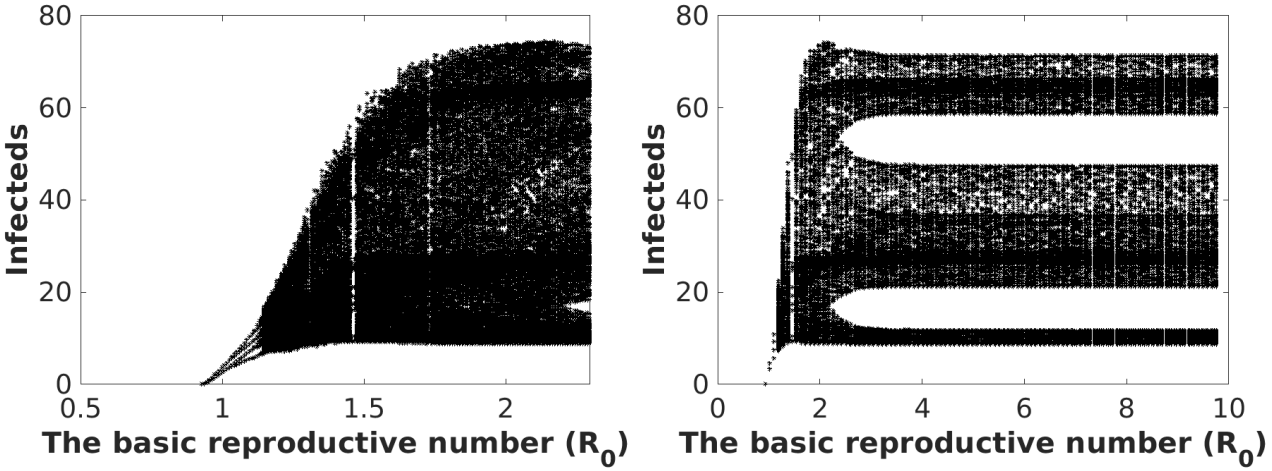

(a) The bifurcation diagram for R_0 for $\beta_V \in [0, 0.1]$.

(b) The bifurcation diagram for R_0 for $\beta_V \in [0, 1]$.

Figure 5.6: The bifurcation diagram for the infection transmission constant from the virus itself with two zoomed in regions which exhibit potentially chaotic behavior. We take initial conditions of $S_0 = 150$, $I_0 = 20$, $V_0 = 30$.

Figure 5.6(a) provides a zoomed in version of Figure 5.6(b). Interestingly, bringing β_v all the way to 1 we see that there is some structure and the values live in four regions. This is previously unexplored and not well understood.

5.7 Summary

In this section we explore bifurcations for parameters beyond the intrinsic growth rate and the probability of death. We demonstrate interesting bifurcation structure that in many cases (i.e. in the case of μ, θ and δ) is period doubling that appears to cascade into chaotic behavior [4, 14, 15]. On the other hand, parameters such as $\hat{d}_v$, and the infection transmission constants β_I and β_V do not have as clear cut structure. For example, virus death $\hat{d}_v$ and the transmission constant from virus passed through contact with the virus directly β_V demonstrate what appears to be chaotic behavior that settles into bounded regions. On the other hand, the transmission constant from virus passed through contact with infected individuals β_I shows apparent chaotic behavior which settles back into a four cycle. This sort of behavior in both cases is not previously well understood and is a major finding in the ISAv model.

On the other hand, open questions still remain. The authors of [4] provide a figure similar to Figure 5.5(a), though do not provide axes. Numerical and analytical evaluations have been performed and bifurcations are consistently beginning immediately before $R_0 = 1$ which is not entirely consistent with previous theory. This will be explored in future work.

Chapter 6

Discussion and Conclusion

The scope of this thesis was to address the question of how density dependence influences dynamical systems modeling by taking a case example and demonstrating mathematically similar functional forms of density dependence lead to drastically different dynamics. Though the question of how to characterize density dependence is still broad and remains open, this work has shown that the slight alteration in functional form can lead to potentially unintended modeling behavior. Beyond the choice of functional form, for the ISAv model we studied, we saw that the parameterization also played a key role in qualitative behavior and suggests that the question of how to mathematically characterize the role of density dependence has further layers to it.

In Chapter 1, we discussed and repeated analysis of classical results such as the logistic growth map in a single dimensional biological system [4, 18, 19, 20, 21, 22]. In Chapter 3 we introduced the Infected Salmon Anemia virus model, well studied in [4, 34, 35, 24] which is an infectious disease model that incorporates density dependence through the Ricker function. We rederived results from [4] and went beyond to demonstrate what appears to be chaotic behavior for particular parameters, as well as show unexplored parameters induce similar behavior. Though structurally similar [3] (i.e. concavity and monotonically decreasing), many of the functional forms we introduced in Chapter 2 proved to exhibit drastically different bifurcation behavior when used in the ISAv model explored in Chapter 4.

Density dependence is an important role in the population modeling world as it guarantees dynamical system behavior is a function of current/previous population size (as well as various other parameters and factors). Our results demonstrated that for a fixed model there is extreme sensitivity to functional form choice as well as parameterization. Further, incorrect choices can lead to biologically unfeasible results of unbounded population sizes (see behaviors in Chapters 4 and 5).

Although chaos is thought of colloquially as wildly unpredictable behavior, we discussed the rigorous definition in that it boils down to sensitivity of initial conditions. In particular,

two initial conditions that are extremely close together could (and do) take wildly different trajectories as time approaches infinity. The Liapunov exponent is used to prove behavior is occuring [8, 15]; and we used this metric for various choices of the density dependence function(s) described in this thesis (Table 2.1).

The Ricker recruitment function [3, 4, 17] has been used in various biological models for both population and within host infectious disease models. We treated the Ricker recruitment function as a "baseline" functional form (see Section 2.3). Though each of the seven functional forms introduced in Chapter 2 have original parameters discussed in [3], we also fit each form to the Ricker recruitment function as means to compare each function. This allowed us to compare mathematical behavior, though biological scaling parameters may have been placed on the back burner.

Beyond the goal of choosing the correct functional form, a key theme we wanted to emphasize was the parameterization of each form. We briefly mentioned before that we pulled values discussed from the literature [3], as well as fit each functional form to the Ricker function to obtain parameters. Much of unbounded behavior we described above was observed with the use of fitted parameters as they tended to bring exponents (in the denominator) that were close to zero, which led to the populations growing exceptionally large. With respect to both the absence and presence of infection, many of the functional forms exhibited stable regions that covered most of the (r, d) space. Open questions still remain as to if these functional forms are correctly parameterized and a possible direction to take this question would be to fit each of the forms to data. However, we can say that in the case of the ISAv model (and perhaps in general other infectious disease models) that parameterization should be a key concern to obtain biologically feasible results. Potential solutions to remediate unboundedness and biological infeasibility include gathering more data and careful literature examination before model construction.

The basic reproductive number is an important metric for the spreading of infection and can produce different bifurcation behavior depending on the particular parameter varied [18, 19, 20, 21]. For example, parameters such as the fraction of infected salmon that die (μ), the fraction of salmon infected via contact with infecteds (θ), and the virus shed (δ) produced a bifurcation in the number of infected individuals that appears to exhibit period doubling into chaotic behavior [2, 14, 15, 20]. While this is a common bifurcation structure [17], the use of these parameters yield interesting results such as the importance of the basic reproductive number. In fact, most of these parameters were not been previously explored in the context of the ISAv model [4].

On the other hand, we saw that other parameters such as the infection transmission constants (denoted $\beta_{I,V}$) , and the viral death (d_v) do not produce as common bifurcation structures. The viral death (d_v) and infection transmission constant from the virus (β_V) exhibited what appears to be chaotic behavior (near $R_0 \in [1, 1.5]$) for the small parameter range of β_V taken from [4] (See Figures 5.4,5.6). However, expanding beyond this range showed bounded regions that exhibit what could be chaotic behavior in a given region.

The infection transmission constant from the infected individuals (β_I) was shown to have apparent chaotic behavior locally around $R_0 \in [1, 2.5]$ also, and in fact this was a major finding of [4]. However, bringing the infection transmission constant all the way to 1 (i.e. $R_0 \in [1, 20]$) showed that behavior returns to a stable four cycle; something not previously well understood in infectious disease biology (See Figure 5.5).

The role each of these key parameters play was important to the overall question as to whether chaotic behavior is truly occuring in the ISAv model. Though we showed examples of bifurcations in which behavior appears to chaotic, as well as positive Liapunov exponents, it remains to be proven that chaos is occuring.

One possible method of doing this is bounding the spectral radius with a matrix norm [5]. We demonstrated this was possible in the case of the original ISAv model (in the presence of infection) with the Ricker function as the intrinsic growth rate r was varied. The L^∞ norm bounded the Liapunov exponent from above when we observed what appeared to be stable 1 and 2 cycle behavior.

Unfortunately, much of this analysis failed for varying the probability of death as well as for substituted functional forms. This can be explained for the functional forms that became unbounded by the simple fact that they were not chaotic; just unbounded. However, it remains to be shown that for the Ricker function and the functional form we denote $f_7(N)$ that behavior is truly chaotic for all initial conditions. Questions such as these still linger about the ISAv model and lead to the complicated analysis of density dependence in infectious disease modeling.

In fact, it is not immediately clear if the ISAv model as currently writtens is the most appropriate choice for this salmon population. For example, the $\Phi_I(I_t)$ and $\Phi_V(V_t)$ functions represented the probability that salmon who come into contact with the infected salmon and virus respectively do not become infected. However, each of the salmon come in contact with either the infecteds or virus, and the fraction that actually receive the infection is governed by the parameters θ and $\hat{\theta}$. Aside from clarity of notation, it is not entirely supported that this scenario of 'everyone contacting someone' is the correct or biologically relevant scenario [33, 34, 35]. The biological literature for infectious salmon anemia virus has been garnering more attention through the publication of recent work such as [4, 24] which exhibit interesting dynamics.

It may be possible that there exists a mathematical model that can characterize the biology of the infectious salmon anemia virus in a more simplistic manner. As mentioned previously, available data would be a vital tool for fitting funcitonal forms for density dependence; or simply for population dynamics. The virus has several other implications simply beyond the biological death of the species.

While mathematically interesting, complex and not fully understood, the ISAv model has many avenues it can be explored with and applied. For example, we suggested using the population model in the absence of the virus (with many functional forms) as well as fitting

the ideal functional form to data if it exists. We demonstrated that in the case of the Ricker function for density dependence, we still observed interesting and complicated dynamics. Additionally, we saw that with the susceptible population alone there are complex dynamics not completely understood. This suggests that a lower order model could potentially be of use until the biology is completely determined from a model. We also propose adding a fraction of susceptible salmon that do not come into contact with the infected salmon nor the viral population (if the viral population exists in the model).

Apart from potential biological and economic impacts, health and global warming concerns are rapidly increasing every year [36]. Modeling dynamical systems in the realm of biology is becoming an increasingly important and vital tool. This work serves as a key factor in thinking critically about using the correct choice of density dependence in biological modeling, analyzing systems that become chaotic and return to stable behavior, and simply demonstrating chaotic scenarios that are not 'all or nothing' scenarios such as in the logistic growth map where chaotic regimes are for clearly defined parameter spaces. Though we cannot characterize how to correctly identify the most suitable functional form choice for any dynamical systems model (or even infectious disease model for that matter), we have demonstrated that mathematically similar functions can significantly alter the qualitative and quantitative analysis of a given system.

The ISAv model is one of many infectious disease models that are currently garnering attention through the mathematical modeling community. We use it as a case study to demonstrate main points of the thesis described above, though it is possible counter examples to these points can arise. In other words, for a particular system, density dependence may simply have no role in qualitative behavior. We argue that though these cases likely exist, the biological and mathematical community should rigorously vet the use of such models when applying them to a physical scenario. Several of the global threats we mentioned above indicate why this is of utmost important; as well as the simple fact that models exist to provide insight to misunderstood phenomena.

Many questions about generic density dependence remain open, though this work has provided a tool kit for which authors can consider the fine tuning of model choices. It is our hope that this thesis lays the groundwork for future directions about the role of density dependence in generic biological modeling.

Bibliography

[1] E. N. Lorenz, "Empirical orthogonal functions and statistical weather prediction," 1956.

[2] R. M. May, "Simple mathematical models with very complicated dynamics," *Nature*, vol. 261, no. 5560, pp. 459–467, 1976.

[3] T. Bellows, "The descriptive properties of some models for density dependence," *The Journal of Animal Ecology*, pp. 139–156, 1981.

[4] P. van den Driessche and A.-A. Yakubu, "Demographic population cycles and $\mathscr{R}_0$ in discrete-time epidemic models," *Journal of Biological Dynamics*, pp. 1–22, 2018.

[5] J. W. Demmel, *Applied numerical linear algebra*, vol. 56. Siam, 1997.

[6] J. Gleick, *Chaos: Making a new science*. Open Road Media, 2011.

[7] R. M. May, "Biological populations obeying difference equations: stable points, stable cycles, and chaos," *Journal of Theoretical Biology*, vol. 51, no. 2, pp. 511–524, 1975.

[8] E. C. Pielou *et al.*, *An Introduction to Mathematical Ecology*. New York, USA, Wiley-Inter-science, 1969.

[9] M. B. Usher, "Developments in the Leslie matrix model.," *Mathematical Models in Ecology*, pp. 29–60, 1972.

[10] P. Verhulst, "La loi daccroissement de la population," *Nouv. Mem. Acad. Roy. Soc. Belle-lettr. Bruxelles*, vol. 18, no. 1, 1845.

[11] P. Verhulst, "Deuxième mémoire sur la loi d'accroissement de la population.," *Mémoires de l'académie royale des sciences, des lettres et des beaux-arts de Belgique*, vol. 20, pp. 1–32, 1847.

[12] R. M. May and G. F. Oster, "Bifurcations and dynamic complexity in simple ecological models," *The American Naturalist*, vol. 110, no. 974, pp. 573–599, 1976.

[13] L. Cook, "Oscillation in the simple logistic growth model," *Nature*, vol. 207, no. 4994, p. 316, 1965.

[14] J. L. Massera, "Contributions to stability theory," *Annals of Mathematics*, pp. 182–206, 1956.

[15] T.-Y. Li and J. A. Yorke, "Period three implies chaos," *The American Mathematical Monthly*, vol. 82, no. 10, pp. 985–992, 1975.

[16] S. N. Elaydi, *Discrete chaos: with applications in science and engineering*. Chapman and Hall/CRC, 2007.

[17] W. E. Ricker, "Stock and recruitment," *Journal of the Fisheries Board of Canada*, vol. 11, no. 5, pp. 559–623, 1954.

[18] J. C. Blackwood and L. M. Childs, "An introduction to compartmental modeling for the budding infectious disease modeler," *Letters in Biomathematics*, vol. 5, no. 1, pp. 195–221, 2018.

[19] L. J. Allen and P. Van den Driessche, "The basic reproduction number in some discrete-time epidemic models," *Journal of Difference Equations and Applications*, vol. 14, no. 10-11, pp. 1127–1147, 2008.

[20] J. H. O. Diekkman and J. Metz, "On the definition and computation of the basic reproduction ratio $\mathcal{R}_0$ in models for infectious diseases in heterogeneous populations," *Journal of Mathematical Biology*, vol. 28, no. 4, pp. 365–382, 1990.

[21] J. M. Cushing and O. Diekmann, "The many guises of $\mathcal{R}_0$ (a didactic note)," *Journal of Theoretical Biology*, vol. 404, pp. 295–302, 2016.

[22] J. M. Cushing and Z. Yicang, "The net reproductive value and stability in matrix population models," *Natural Resource Modeling*, vol. 8, no. 4, pp. 297–333, 1994.

[23] P. Van den Driessche and J. Watmough, "Reproduction numbers and sub-threshold endemic equilibria for compartmental models of disease transmission," *Mathematical biosciences*, vol. 180, no. 1-2, pp. 29–48, 2002.

[24] P. van den Driessche and A.-A. Yakubu, "Disease extinction versus persistence in discrete-time epidemic models," *Bulletin of Mathematical Biology*, pp. 1–35, 2018.

[25] A. Macfadyen, "Animal Ecology: Aims and Methods," tech. rep., 1963.

[26] R. May, G. Conway, M. Hassell, and T. Southwood, "Time delays, density-dependence and single-species oscillations," *The Journal of Animal Ecology*, pp. 747–770, 1974.

[27] G. Varley and G. Gradwell, "Key factors in population studies," *Journal of Animal Ecology*, vol. 29, no. 2, pp. 399–401, 1960.

[28] G. Ullyett, "Competition for food and allied phenomena in sheep-blowfly populations," *Philosophical Transactions of the Royal Society of London. Series B, Biological Sciences*, vol. 234, no. 610, pp. 77–174, 1950.

[29] C. Pennycuick, R. Compton, and L. Beckingham, "A computer model for simulating the growth of a population, or of two interacting populations," *Journal of Theoretical Biology*, vol. 18, no. 3, pp. 316–329, 1968.

[30] J. G. Skellam, "Random dispersal in theoretical populations," *Biometrika*, vol. 38, no. 1/2, pp. 196–218, 1951.

[31] J. M. Smith and M. Slatkin, "The stability of predator-prey systems," *Ecology*, vol. 54, no. 2, pp. 384–391, 1973.

[32] M. Hassell, "Density-dependence in single-species populations," *The Journal of Animal Ecology*, pp. 283–295, 1975.

[33] M. P. Hassell, J. H. Lawton, and R. May, "Patterns of dynamical behaviour in single-species populations," *The Journal of Animal Ecology*, pp. 471–486, 1976.

[34] K. Falk, E. Namork, E. Rimstad, S. Mjaaland, and B. H. Dannevig, "Characterization of infectious salmon anemia virus, an orthomyxo-like virus isolated from Atlantic salmon (*Salmo salar L.*)," *Journal of Virology*, vol. 71, no. 12, pp. 9016–9023, 1997.

[35] E. Milliken and S. S. Pilyugin, "A model of infectious salmon anemia virus with viral diffusion between wild and farmed patches," *Discrete & Continuous Dynamical Systems-Series B*, vol. 21, no. 6, 2016.

[36] J. A. Patz, P. R. Epstein, T. A. Burke, and J. M. Balbus, "Global climate change and emerging infectious diseases," *Journal of American Medical Association*, vol. 275, no. 3, pp. 217–223, 1996.